Large-angle production of charged pions with 3–12.9 GeV/*c* incident protons on nuclear targets

M. G. Catanesi,[1] E. Radicioni,[1] R. Edgecock,[2] M. Ellis,[2,*] F. J. P. Soler,[2] C. Gößling,[3] S. Bunyatov,[4] A. Krasnoperov,[4] B. Popov,[4,†] V. Serdiouk,[4] V. Tereschenko,[4] E. Di Capua,[5] G. Vidal-Sitjes,[5,‡] A. Artamonov,[6,§] S. Giani,[6] S. Gilardoni,[6] P. Gorbunov,[6,§] A. Grant,[6] A. Grossheim,[6,∥] A. Ivanchenko,[6,¶] V. Ivanchenko,[6,**] A. Kayis-Topaksu,[6,††] J. Panman,[6] I. Papadopoulos,[6] E. Tcherniaev,[6] I. Tsukerman,[6,§] R. Veenhof,[6] C. Wiebusch,[6,‡‡] P. Zucchelli,[6,§§] A. Blondel,[7] S. Borghi,[7] M. C. Morone,[7,∥∥] G. Prior,[7,¶¶] R. Schroeter,[7] C. Meurer,[8] U. Gastaldi,[9] G. B. Mills,[10,***] J. S. Graulich,[11,†††] G. Grégoire,[11] M. Bonesini,[12,‡‡‡] F. Ferri,[12] M. Kirsanov,[13] A. Bagulya,[14] V. Grichine,[14] N. Polukhina,[14] V. Palladino,[15] L. Coney,[16,***] D. Schmitz,[16,***] G. Barr,[17] A. De Santo,[17] F. Bobisut,[18] D. Gibin,[18] A. Guglielmi,[18] M. Mezzetto,[18] J. Dumarchez,[19] U. Dore,[20] D. Orestano,[21] F. Pastore,[21] A. Tonazzo,[21] L. Tortora,[21] C. Booth,[22] L. Howlett,[22] G. Skoro,[22] M. Bogomilov,[23] M. Chizhov,[23] D. Kolev,[23] R. Tsenov,[23] S. Piperov,[24] P. Temnikov,[24] M. Apollonio,[25] P. Chimenti,[25] G. Giannini,[25] J. Burguet-Castell,[26] A. Cervera-Villanueva,[26] J. J. Gómez-Cadenas,[26] J. Martín-Albo,[26] P. Novella,[26] M. Sorel,[26] and A. Tornero[26]

(HARP Collaboration)

[1]*Sezione INFN, Bari, Italy*
[2]*Rutherford Appleton Laboratory, Chilton, Didcot, United Kingdom*
[3]*Institut für Physik, Universität Dortmund, Dortmund, Germany*
[4]*Joint Institute for Nuclear Research, JINR Dubna, Russia*
[5]*Università degli Studi e Sezione INFN, Ferrara, Italy*
[6]*CERN, Geneva, Switzerland*
[7]*Section de Physique, Université de Genève, Genève, Switzerland*
[8]*Institut für Physik, Forschungszentrum Karlsruhe, Karlsruhe, Germany*
[9]*Laboratori Nazionali di Legnaro dell' INFN, Legnaro, Italy*
[10]*Los Alamos National Laboratory, Los Alamos, New Mexico, USA*
[11]*Institut de Physique Nucléaire, UCL, Louvain-la-Neuve, Belgium*
[12]*Sezione INFN Milano Bicocca, Milano, Italy*
[13]*Institute for Nuclear Research, Moscow, Russia*
[14]*P. N. Lebedev Institute of Physics (FIAN), Russian Academy of Sciences, Moscow, Russia*
[15]*Università "Federico II" e Sezione INFN, Napoli, Italy*
[16]*Columbia University, New York, USA*
[17]*Nuclear and Astrophysics Laboratory, University of Oxford, Oxford, United Kingdom*
[18]*Università degli Studi e Sezione INFN, Padova, Italy*
[19]*LPNHE, Universités de Paris VI et VII, Paris, France*
[20]*Università "La Sapienza" e Sezione INFN Roma I, Roma, Italy*
[21]*Università degli Studi e Sezione INFN Roma Tre, Roma, Italy*
[22]*Department of Physics, University of Sheffield, Sheffield, United Kingdom*
[23]*Faculty of Physics, St. Kliment Ohridski University, Sofia, Bulgaria*
[24]*Institute for Nuclear Research and Nuclear Energy, Academy of Sciences, Sofia, Bulgaria*
[25]*Università degli Studi e Sezione INFN, Trieste, Italy*
[26]*Instituto de Física Corpuscular, IFIC, CSIC and Universidad de Valencia, Valencia, Spain*

Measurements of the double-differential $\pi^{\pm}$ production cross section in the momentum range $100 \leqslant p \leqslant 800$ MeV/*c* and angle range $0.35 \leqslant \theta \leqslant 2.15$ rad in proton-beryllium, proton-carbon, proton-aluminium, proton-copper, proton-tin, proton-tantalum, and proton-lead collisions are presented. The data were taken with the large-acceptance HARP detector in the T9 beam line of the CERN PS. The pions were produced by proton beams in a momentum range from 3 to 12.9 GeV/*c* hitting a target with a thickness of 5% of a nuclear interaction length. Tracking and identification of the produced particles was performed by using a small-radius cylindrical Time Projection Chamber (TPC) placed inside a solenoidal magnet. Incident particles were identified by an elaborate system of beam detectors. Results are obtained for the double-differential cross sections $d^2\sigma/(dpd\theta)$ at six incident proton beam momenta [3, 5, 8, and 8.9 GeV/*c* (Be only) and 12 and 12.9 GeV/*c* (Al only)]. They are based on a complete correction of static and dynamic distortions of tracks in the HARP TPC, which allows the complete statistics of the collected data set to be used. The results include and supersede our previously

published results and are compatible with these. Results are compared with the GEANT4 and MARS Monte Carlo simulation.

I. INTRODUCTION

The HARP experiment [1] makes use of a large-acceptance spectrometer for a systematic study of hadron production on a large range of target nuclei for beam momenta from 1.5 to 15 GeV/c. This corresponds to a proton momentum region of great interest for neutrino beams and far from coverage by earlier dedicated hadroproduction experiments [2,3]. The main motivations for the experiment are to measure pion yields for a quantitative design of the proton driver of a future neutrino factory [4], to provide measurements to allow substantially improved calculations of the atmospheric neutrino flux [5–9] to be made, and to measure particle yields as input for the flux calculation of accelerator neutrino experiments [10], such as K2K [11,12], MiniBooNE [13], and SciBooNE [14].

This paper presents our final measurements of the double-differential cross section, $d^2\sigma^\pi/(dpd\theta)$, for $\pi^\pm$ production at large angles by protons of 3, 5, 8, and 8.9 GeV/c (Be only) and 12 and 12.9 GeV/c (Al only) momentum impinging on thin beryllium, carbon, aluminium, copper, tin, tantalum, or lead targets of 5% nuclear interaction length. A first set of results on the production of pions at large angles has been published by the HARP Collaboration in Refs. [15–17], based on the analysis of the data in the beginning of each accelerator spill. The reduction of the data set was necessary to avoid problems in the TPC detector responsible for dynamic distortions to the image of the particle trajectories as the ion charge was building up during each spill. Corrections that allow use of the full statistics, correcting for such distortions, have been developed in Ref. [18] and are fully applied in this analysis. The obtained results are fully compatible within the statistical errors and differential systematic uncertainties with those previously published. The increase of statistics is particularly useful in the 3 GeV/c data sets. Comparisons with Monte Carlo models are then shown for light and heavy targets.

This paper, covering an extended range of solid targets in the same experiment, makes it possible to perform systematic comparison of hadron production models with measurements at different incoming beam momenta over a large range of target atomic number A. Results for pion production in the forward direction are the subject of other HARP publications [19–21].

Pion production data at low momenta ($\simeq$200 MeV/c) are extremely scarce and HARP is the first experiment to provide a large data set, taken with many different targets, full particle identification, and large detector acceptance. In addition, the acceptance of the large-angle detector of the HARP experiment matches well the required phase-space region of pions relevant to the production of μs in a neutrino factory. It covers the large majority of the pions accepted in the focusing system of a typical design. For the optimization of the NF target, data were taken with high-Z nuclear targets such as tantalum and lead.

Data were taken in the T9 beam of the CERN PS. The collected statistics, for the different nuclear targets are reported in Table I.

The analysis proceeds by selecting tracks in the Time Projection Chamber (TPC), after corrections for static and dynamic distortions (see later for details), in events with incident proton beams. Momentum and polar angle measurements and particle identification are based on the measurements of track position and energy deposition in the TPC. An unfolding method is used to correct for experimental resolution, efficiency, and acceptance and to obtain the double-differential pion production cross sections. The method allows a full error evaluation to be made. A comparison with available data is presented. The analysis follows the same methods as used for the determination of $\pi^\pm$ production by protons on a tantalum target, which are described in Ref. [15] and will be only briefly outlined here.

---

*Now at FNAL, Batavia, Illinois, USA.

†Also supported by LPNHE, Paris, France.

‡Now at Imperial College, University of London, United Kingdom.

§ITEP, Moscow, Russian Federation.

‖Now at TRIUMF, Vancouver, Canada.

¶On leave from Novosibirsk University, Russia.

**On leave from Ecoanalitica, Moscow State University, Moscow, Russia.

††Now at Çukurova University, Adana, Turkey.

‡‡Now at III Phys. Inst. B, RWTH Aachen, Germany.

§§Now at SpinX Technologies, Geneva, Switzerland; on leave from INFN, Sezione di Ferrara, Italy.

‖‖Now at University of Rome "Tor Vergata," Italy.

¶¶Now at LBL, Berkeley, California, USA.

***MiniBooNE Collaboration.

†††Now at Section de Physique, Université de Genève, Switzerland.

‡‡‡maurizio.bonesini@mib.infn.it

II. EXPERIMENTAL APPARATUS AND DATA SELECTION

The HARP detector is shown in Fig. 1 and is fully described in Ref. [22]. The forward spectrometer, mainly used in the analysis for the conventional neutrino beams and atmospheric neutrino flux, comprises a dipole magnet, large planar drift chambers (NDCs) [23], a time-of-flight wall (TOFW) [24], a threshold Cerenkov counter (CHE), and an electromagnetic calorimeter (ECAL). In the large-angle region a cylindrical TPC with a radius of 408 mm is positioned inside a solenoidal magnet with a field of 0.7 T. The TPC detector was designed to measure and identify tracks in the angular region from 0.25 to 2.5 rad with respect to the beam axis. The target is placed inside the inner field cage (IFC) of the TPC such that, in addition to particles produced in the forward direction, backward-going tracks can be measured. The TPC is used for tracking, momentum determination, and measurement of the

TABLE I. Total number of events and tracks used in the various nuclear 5% λ_I target data sets and the number of protons on target as calculated from the prescaled incident proton triggers.

| Data set (GeV/c)		3	5	8	8.9	12	12.9
Total DAQ events	(Be)	1399714	1473815	1102415	7236396	1211220	–
	(C)	1345461	2628362	1878590	–	1855615	–
	(Al)	1586331	1787620	1706919	–	619021	5401701
	(Cu)	623965	2089292	2613229	–	748443	–
	(Sn)	1652751	2827934	2422110	–	1803035	–
	(Ta)	2202760	2094286	2045631	–	886307	–
	(Pb)	1299264	2110904	2314552	–	486875	–
Accepted protons with LAI	(Be)	76694	157625	200352	1267418	282272	–
	(C)	58421	228490	337150	–	504945	–
	(Al)	69794	195912	341687	–	169151	1391159
	(Cu)	38290	229316	544615	–	226245	–
	(Sn)	84330	304949	523432	–	558306	–
	(Ta)	97732	218293	442625	–	269927	–
	(Pb)	79188	194064	491672	–	145843	–
Fraction of triggers used	(Be)	79%	75%	83%	94%	79%	–
	(C)	95%	90%	83%	–	84%	–
	(Al)	78%	80%	63%	–	96%	72%
	(Cu)	91%	76%	66%	–	76%	–
	(Sn)	97%	73%	67%	–	76%	–
	(Ta)	86%	81%	69%	–	76%	–
	(Pb)	74%	56%	69%	–	50%	–
π^- selected with PID	(Be)	6553	20020	32078	231278	47608	–
	(C)	4831	33436	52105	–	72307	–
	(Al)	5496	26502	45442	–	37812	250037
	(Cu)	3065	28395	79497	–	46153	–
	(Sn)	7146	38337	89799	–	124925	–
	(Ta)	6758	27767	74977	–	63349	–
	(Pb)	4408	17766	81821	–	25050	–
π^+ selected with PID	(Be)	11245	27796	41683	294594	58882	–
	(C)	9944	52633	73157	–	95151	–
	(Al)	9519	38657	59345	–	47609	314552
	(Cu)	4976	39823	102797	–	56665	–
	(Sn)	10179	48820	104239	–	145923	–
	(Ta)	9270	33985	87226	–	72275	–
	(Pb)	6160	21074	92913	–	27085	–
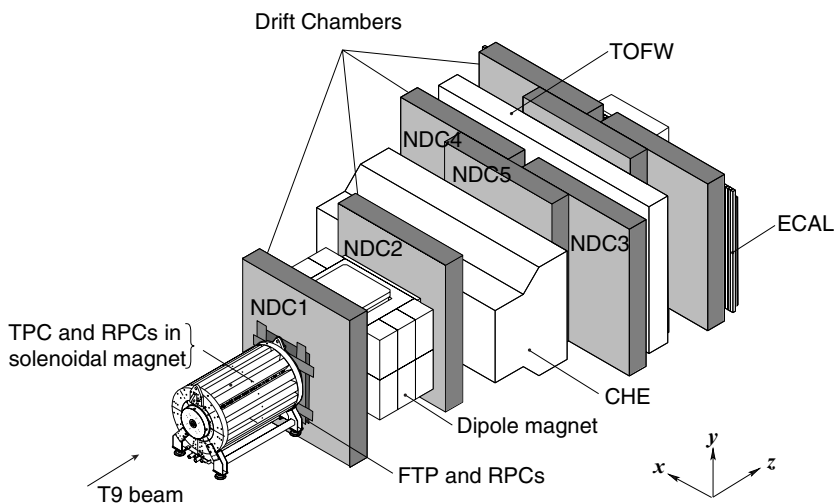
FIG. 1. Schematic layout of the HARP detector. The convention for the coordinate system is shown in the lower right corner. The three most downstream (unlabeled) drift chamber modules are only partly equipped with electronics and are not used for tracking. The detector covers a total length of 13.5 m along the beam axis and has a maximum width of 6.5 m perpendicular to the beam.

energy deposition dE/dx for particle identification [25]. A set of resistive plate chambers (RPCs) form a barrel inside the solenoid around the TPC to measure the arrival time of the secondary particles [26]. Charged particle identification (PID) can be achieved by measuring the ionization per unit length in the gas (dE/dx) as a function of the total momentum of the particle. Additional PID can be performed through a time-of-flight (TOF) measurement with the RPCs.

The momentum of the T9 beam is known with a precision of the order of 1% [27]. The absolute normalization of the number of incident protons was performed by using a total of 1,148,120 incident proton triggers. These are triggers where the same selection on the beam particle was applied but no selection on the interaction was performed. The rate of this trigger was down-scaled by a factor of 64. A cross-check of the absolute normalization was provided by counting tracks in the forward spectrometer.

Beam instrumentation provides identification of the incoming particle, the determination of the time when it hits the target, and the impact point and direction of the beam particle on the target. It is based on a set of four multiwire proportional chambers (MWPCs) to measure position and direction of the incoming beam particles and time-of-flight detectors and N_2-filled Cherenkov counters to identify incoming particles. Several trigger detectors are installed to select events with an interaction and to define the normalization.

Besides the usual need for calibration of the detector, a number of hardware shortfalls, discovered mainly after the end of data-taking, had to be overcome to use the TPC data reliably in the analysis. The TPC is affected by a relatively large number of dead or noisy pads and static and dynamic distortions of the reconstructed trajectories. The applied corrections are briefly described in the next section.

The beam of positive particles used for this measurement contains mainly positrons, pions, and protons, with small components of kaons and deuterons and heavier ions. Its composition depends on the selected beam momentum. The proton fraction in the incoming beam varies from 35% at 3 GeV/c to 92% at 12 GeV/c.

At momenta higher than 5 GeV/c, protons are selected by rejecting particles with a measured signal in either of the beam Cherenkov detectors. At 3 GeV/c the TOF measurement allows the selection of pions from protons to be made at more than 5σ. Deuterons (and heavier ions) are removed by TOF measurements. The selection of protons for the beam momenta with the Cherenkov detectors has been described in detail in Ref. [19]. More details on the beam particle selection can be found in Ref. [22]. The purity of the selection of protons is higher than 99% at all momenta. A set of MWPCs is used to select events with only one beam particle for which the trajectory extrapolates to the target. An identical beam particle selection was performed for events triggered with the incident-proton trigger to provide an absolute normalization of the incoming protons. This trigger selected every 64th beam particle coincidence outside the dead time of the data acquisition system.

The length of the accelerator spill is 400 ms with a typical intensity of 15,000 beam particles per spill. The average number of events recorded by the data acquisition ranges from 300 to 350 per spill for the different beam momenta. The analysis proceeds by first selecting a beam proton hitting the target, not accompanied by other tracks. Then an event is required to give a large angle interaction (LAI) trigger to be retained. After the event selection the sample of tracks to be used for analysis is defined. Table I shows the number of events and the number of $\pi^{\pm}$ selected in the analysis. The large difference between the first and second set of rows ("Total DAQ events" and "Accepted protons with LAI") is due to the relatively large fraction of pions in the beam and to the larger number of triggers taken for the measurements with the forward dipole spectrometer.

The TPC contains a relatively large number of dead or noisy pads. Noisy pads were considered equivalent to dead channels in this analysis. The large number of dead pads ($\simeq$15%) in the experimental data-taking required a day-by-day determination of the dead channel map. The same map was used in the simulation to provide a description of the TPC performances on a short-term scale. A method based on tracks accumulated during the data-taking was used to measure the gain variations of each pad; see Ref. [22] for details. It is used to reduce the fluctuations in response between different pads down to a 3% level.

Static distortions on reconstructed tracks are caused by the inhomogeneity of the electric field, resulting from an accidental mismatch between the inner and outer field cage (powered by two distinct high-voltage supplies). The day-by-day variations of this mismatch are consistent with the specifications of the stability and reproducibility of the power supplies. A specific calibration for each setting has been made.

Dynamic distortions are caused instead by the buildup of ion-charge density in the drift volume during the 400-ms-long beam spill. All these effects were fully studied and available corrections are described in detail in Refs. [15,18]. In our earlier published analyses a practical approach has been followed. Only the events corresponding to the early part of the spill, where the effects of the dynamic distortions are still small, have been used.[1] The time interval between spills is large enough to drain all charges in the TPC related to the effect of the beam. The combined effect of the distortions on the kinematic quantities used in the analysis has been studied in detail and only that part of the data for which the systematic errors can be assessed with physical benchmarks was used, as fully explained in Ref. [15]. More than 30%–40% of the recorded data were thus used in the published analyses. The influence of distortions was monitored by taking the average value of the extrapolated minimum distance of the secondary tracks from the incoming beam particle trajectory $\langle d_0' \rangle$. An example of the result of the corrections for one setting is shown in Fig. 2.

In the presented analysis, instead, the TPC track dynamic distortions are corrected on an event-by-event basis, as outlined in Ref. [18]. A direct measurement of the distortions as a function of the radius R and time in spill was performed by using the prediction of the trajectory of the recoil proton

_____

[1]This translates into a cut on the maximum number of events ($N_{\text{evt}} \simeq$ 100) to be retained.
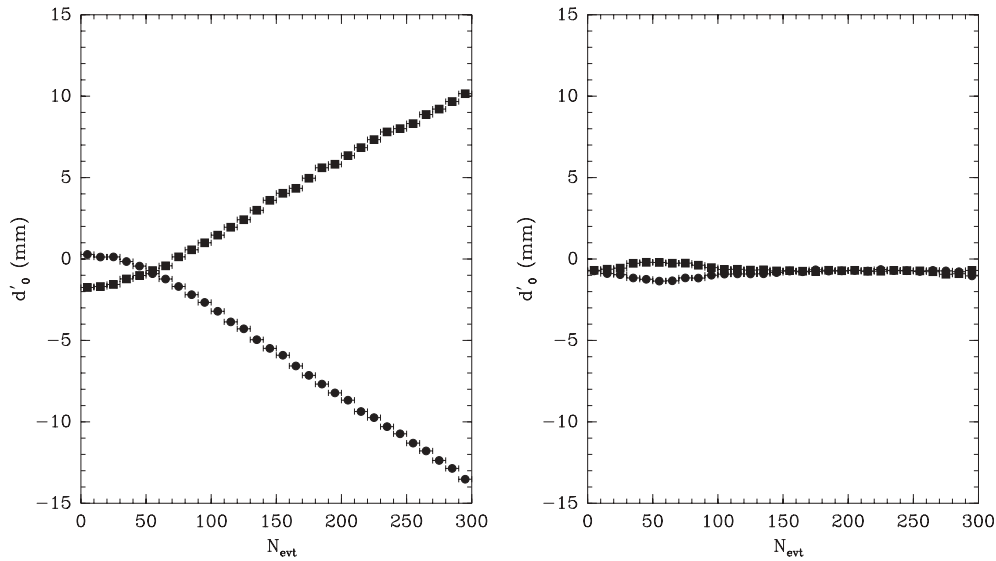
FIG. 2. Effect of dynamic distortions on a track in the HARP TPC for a p-Be interaction sample at 5 GeV/c, as a function of the event number in the spill before corrections (left) and after dynamic distortion corrections (right). The symbols show the average extrapolated distance from the incoming beam particle trajectory for π^- (filled squares) and π^+ (filled circles).

in elastic scattering events on a liquid hydrogen target. The measurement of the direction of the forward-scattered proton determined the kinematics and predicts the trajectory of the recoil proton. The actual measurements in the chamber are then compared with the prediction as a function of time. In addition to this direct measurement also a model of ion charges and their effect was developed.

The strength of the effect depends on many parameters, such as the beam intensity, the momentum, and the target. An iterative procedure is applied to find the value of the strength parameter until $\langle d'_0 \rangle$ is flattened down to ± 2 mm, by using the empirical model described in the following to shape the corrections. By taking into account the beam intensity, the data acquisition rate, and the target thickness, the HARP experiment was operated in conditions of $\approx 95\%$ dead time. The electrons are normally multiplied near the TPC plane with a multiplication factor of $\sim 10^5$, producing an equivalent number of Ar ions. Any inefficiency of the gating grid at the 10^{-4}–10^{-5} level would give an overwhelming number of ions drifting in the TPC gas volume. The phenomenological model is based on the fact that the field responsible for the force acting on each drift electron is equivalent to the following:

 (i) a field system where ions, in a given angular section at R values internal to the drift electron position, contribute to attract the drift electrons inward and

(ii) a field system where ions, in a given angular section at R values external to the drift electron position, contribute to attract the drift electrons outward.

This model makes it possible to understand all the peculiar features of the TPC dynamic distortions:

 (i) the dependence of the distortion on the event number in the spill;

(ii) the dependence of the distortion on tracks generated at different longitudinal coordinate Z in the TPC; in

particular, tracks produced at increasingly larger Z exhibit the distortion saturation at increasingly later times and the distortions tend to zero at Z values already passed by the ion packet;

(iii) the dependence of the distortion of cosmic-ray tracks collected out of the spill as a function of time and Z, with the nontrivial fact that cosmic rays just after the spill are more distorted than the cosmic rays taken later; and

(iv) the R-ϕ dependence as measured with elastic scattering; the distortions have a peculiar behavior as a function of the TPC pad rows: From the $E \times B$ calculation it follows that the inner rows are distorted by a radial electric field pointing inward; there exists a pad row around the middle of the chamber where the radial electric field vanishes.

The corrections, provided by the model, calibrated on a run-by-run basis allow full control of the TPC response along the spill. In Fig. 3 the Q/p_T spectrum for p-Be interactions at 8.9 GeV/c is shown separately for the first 50 events in the spill, the next 50, and so on up to the last 50, before and after the dynamic distortion correction. After the correction, the curves are compatible within the statistical errors, indicating that the correction is adequate.

The main point, by using beginning of the spill data or full spill data, is the presence of possible residual momentum bias in the TPC measurement owing to the dynamic distortions. A dedicated paper [18] addresses this point and shows that our estimation of momentum bias is below 3%, although the systematics can in principle be different in the uncorrected begin-of-spill data and the fully corrected data. From the studies made we conclude that the data of the full spill can be used for the analysis once the corrections for dynamic distortions have been applied. In a small number of data sets the distortions in the last part of the spill are too large to be reliably
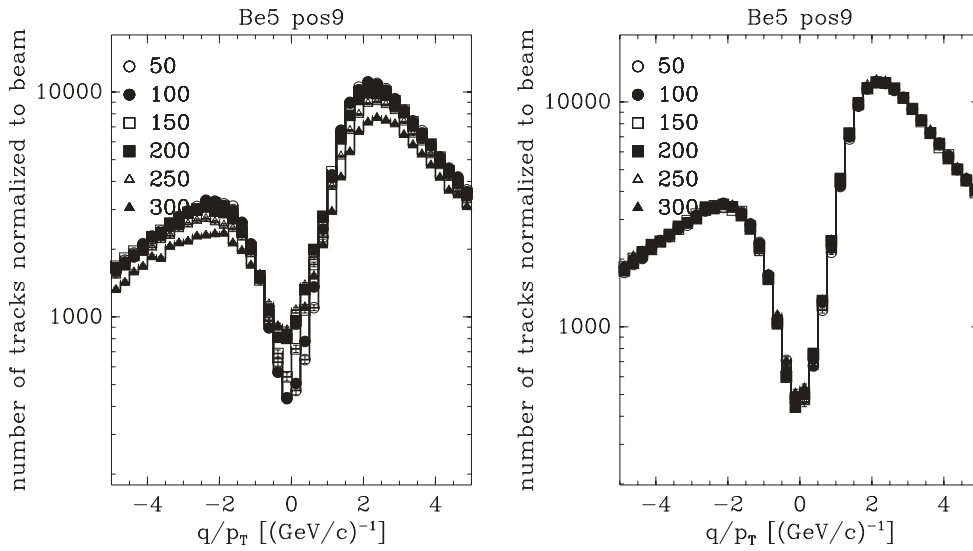
FIG. 3. Full spill analysis of Q/p_T for the highest statistics data sample: p-Be at 8.9 GeV/c before corrections (left) and after corrections (right). Six curves are drawn, each for the next 50 events in the spill. One notices that the distributions in the right panel are not distinguishable.

corrected. These are mainly high-A, high-beam-momentum settings, where sufficient statistics are available even without this part of the spill. The reliability of the correction has been checked by observing the stability as a function of the event number in the spill of the average momentum of protons in a small window of large dE/dx. An additional benchmark assesses the stability of the momentum measurement inside a spill after the dynamic distortion correction for the TPC tracks. The dependence of the average momentum for four different track samples as a function of $N_{\rm evt}$ is shown in Fig. 4. The range of p_T tested by this benchmark covers nearly the full range used in the analysis.

The stability of the TPC dE/dx and momentum calibration over the collected data sets is shown in Fig. 5. The X-axis runs over all settings starting at low A (Be) up to high A (Pb) and all used beam momenta from 3 to 12.9 GeV/c.

III. DATA ANALYSIS

Only a short outline of the data analysis procedure is presented here; for further details see Ref. [15]. The most relevant difference is the use of the full spill statistics by means of a correction of the dynamic distortions in the TPC tracks, as outlined before.

The double-differential cross section for the production of a particle of type α can be expressed in the laboratory system as

$$\frac{d^2\sigma_\alpha}{dp_i d\theta_j} = \frac{1}{N_{\rm pot}} \frac{A}{N_A \rho t} \frac{1}{\Delta p_j \Delta \theta_j} \sum_{i',j',\alpha'} M_{ij\alpha i'j'\alpha'}^{-1} \cdot N_{i'j'}^{\alpha'}, \quad (1)$$

where $\frac{d^2\sigma_\alpha}{dp_i d\theta_j}$ is expressed in bins of true momentum (p_i), angle (θ_j), and particle type (α), A is the atomic mass, N_A is Avogadro's number, ρ and t are the target density and thickness, respectively, and Δp_J and $\Delta \theta_j$ are the bin sizes in momentum and angle, respectively.

The "raw yield" $N_{i'j'}^{\alpha'}$ is the number of particles of observed type α' in bins of reconstructed momentum ($p_{i'}$) and angle ($\theta_{j'}$). These particles must satisfy the event, track, and PID

selection criteria. Although, owing to the stringent PID selection, the background from misidentified protons in the pion sample is small, the pion and proton raw yields ($N_{i'j'}^{\alpha'}$, for $\alpha' = \pi^-, \pi^+, p$) have been measured simultaneously. It is thus possible to correct for the small remaining proton background in the pion data without prior assumptions concerning the proton production cross section.
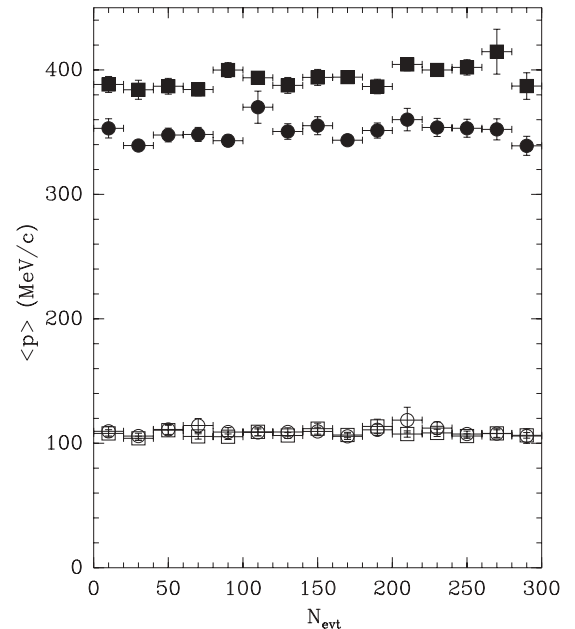
FIG. 4. As a momentum benchmark, after the dynamic distortion correction, the closed box shows the average momentum observed for protons selected using their range (reaching the second RPC) and dE/dx. Closed circles show protons selected within a high dE/dx region; open circles show π^- selected with dE/dx; open boxes show π^+ selected with dE/dx. The angle of the particles is restricted in a range with $\sin \theta \approx 0.9$. The variation in the uncorrected sample was $\approx$5% for the high-p_T samples. The corrected data stay stable well within 3%. The low-p_T data remain stable with or without correction.
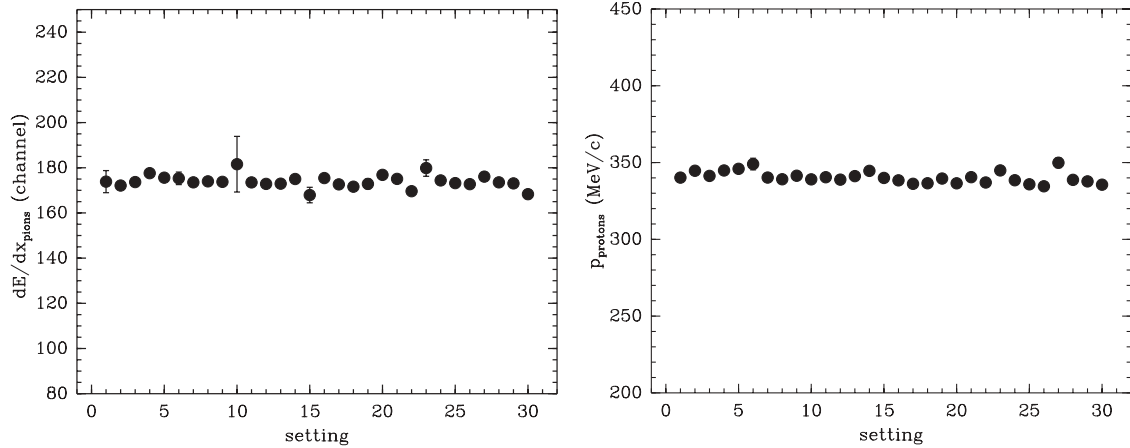
FIG. 5. Stability of the TPC calibration. (Left) dE/dx versus settings for pions with $300 \leqslant p \leqslant 500$ MeV/c. (Right) Mean momentum for protons with a dE/dx between 7 and 8 MIP versus setting. Settings go from low A to high A including beam momenta from 3 to 12.9 GeV/c.

The matrix $M^{-1}_{ij\alpha i'j'\alpha'}$ corrects for the efficiency and the resolution of the detector. It unfolds the true variables $ij\alpha$ from the reconstructed variables $i'j'\alpha'$ with a Bayesian technique [28] and corrects the observed number of particles to take into account effects such as trigger efficiency, reconstruction efficiency, acceptance, absorption, pion decay, tertiary production, PID efficiency, PID misidentification, and electron background. The method used to correct for the various effects is described in more detail in Ref. [15].

To predict the population of the migration matrix element $M_{ij\alpha i'j'\alpha'}$, the resolution, efficiency, and acceptance of the detector are obtained from a Monte Carlo simulation. This is accurate provided the Monte Carlo simulation describes these quantities correctly. Where some deviations from the control samples measured from the data are found, the data are used to introduce (small) *ad hoc* corrections to the Monte Carlo model. By using the unfolding approach, possible known biases in the measurements are taken into account automatically as long as they are described by the Monte Carlo model. In the experiment simulation, which is based on the GEANT4 toolkit [29], the materials in the beam line and the detector are accurately described as well as the relevant features of the detector response and the digitization process. In general, the Monte Carlo simulation compares well with the data, as shown in Ref. [15]. For all important issues physical benchmarkes have been used to validate the analysis. The absolute efficiency and the measurement of the angle and momentum were determined with elastic scattering. The momentum and angular resolution were determined by exploiting the two halves of cosmic-ray tracks crossing the TPC volume. The efficiency of the particle identification was checked by using two independent detector systems. Only the latter needs a small *ad hoc* correction compared to the simulation.

The factor $\frac{A}{N_A \rho t}$ in Eq. (1) is the inverse of the number of target nuclei per unit area.[2] The result is normalized to the number of incident protons on the target, N_{pot}. The absolute normalization of the result is calculated in the first instance relative to the number of incident beam particles accepted by the selection. After unfolding, the factor $\frac{A}{N_A \rho t}$ is applied. The beam normalization using down-scaled incident proton triggers has uncertainties smaller than 2% for all beam momentum settings.

The background from interactions of the primary protons outside the target (called the "Empty target background") is measured by using data taken without the target mounted in the target holder. Owing to the selection criteria, which only accept events from the target region, and the good definition of the interaction point this background is negligible ($<10^{-5}$).

The effects of the systematic uncertainties on the final results are estimated by repeating the analysis with the relevant input modified within the estimated uncertainty intervals. In many cases this procedure requires the construction of a set of different migration matrices. The correlations of the variations between the cross section bins are evaluated and expressed in the covariance matrix. Each systematic error source is represented by its own covariance matrix. The sum of these matrices describes the total systematic error. The magnitude of the systematic errors and their dependence on momentum and angle will be shown in Sec. IV.

IV. EXPERIMENTAL RESULTS

The measured double-differential cross sections for the production of π^+ and π^- in the laboratory system as a function of the momentum and the polar angle for each incident beam momentum are shown in Figures 6–12 for targets from Be to Pb. The error bars shown are the square roots of the diagonal elements in the covariance matrix, where statistical and systematic uncertainties are combined in quadrature. The correlation of the statistical errors (introduced by the unfolding procedure) are typically smaller than 20% for adjacent momentum bins and even smaller for adjacent angular bins. The correlations of the systematic errors are larger, typically 80% for adjacent bins. The overall scale error

_____

[2]We do not make a correction for the attenuation of the proton beam in the target, so that strictly speaking the cross sections are valid for a $\lambda_I = 5\%$ target.
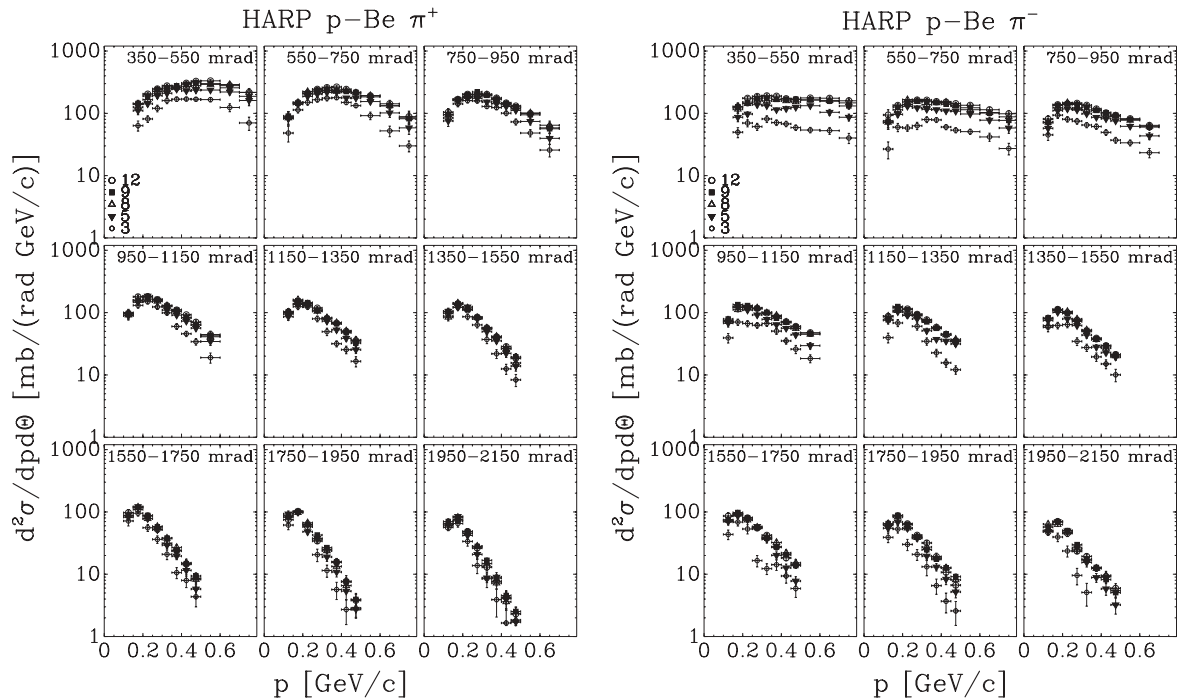
FIG. 6. Double-differential cross sections for π^+ production (left) and π^- production (right) in p-Be interactions as a function of momentum displayed in different angular bins (shown in mrad in the panels). In the figure, the symbol legend 9 refers to 8.9 GeV/c nominal beam momentum. The error bars represent the combination of statistical and systematic uncertainties.

($<2\%$) is not shown. The results of this analysis are also tabulated in the Appendix.

These results are in agreement with what was previously found by using only the first part of the spill and no dynamic distortion corrections. Figures 13 to 16 show the ratio of the cross sections without and with the correction factor for dynamic distortions in 8.9 GeV/c Be data (as an example of a light target), where the statistics are bigger, and in 8 GeV/c Ta
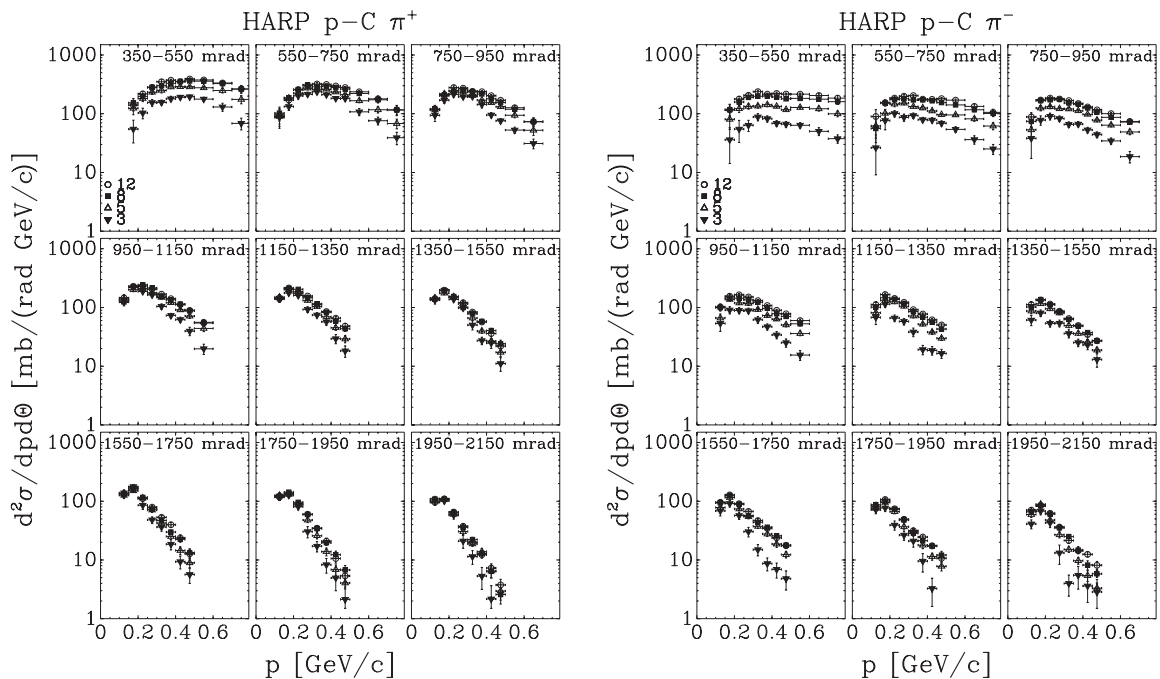
FIG. 7. Double-differential cross sections for π^+ production (left) and π^- production (right) in p-C interactions as a function of momentum displayed in different angular bins (shown in mrad in the panels). The error bars represent the combination of statistical and systematic uncertainties.
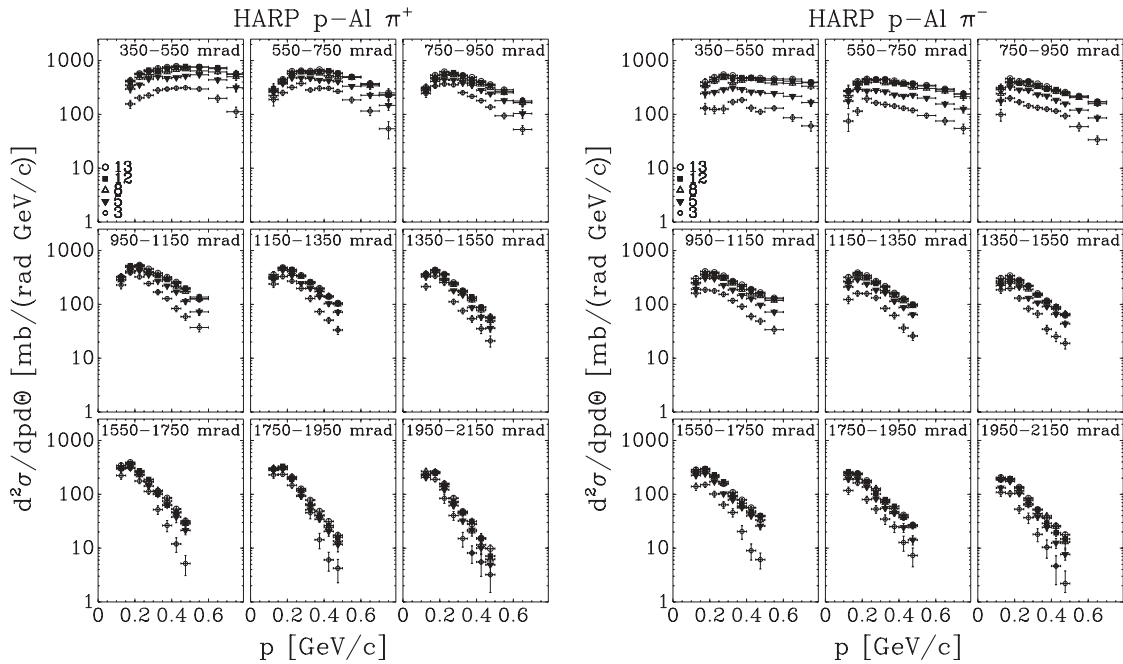
FIG. 8. Double-differential cross sections for π^+ production (left) and π^- production (right) in p-Al interactions as a function of momentum displayed in different angular bins (shown in mrad in the panels). In the figure, the symbol legend 13 refers to 12.9 GeV/c nominal beam momentum. The error bars represent the combination of statistical and systematic uncertainties.

data (as an example of a heavy target). The error band in the ratio takes into account the usual estimate of momentum error and the error on efficiency; the other errors are correlated. The agreement is within 1σ for most of the points.

The dependence of the averaged pion yields on the incident beam momentum is shown in Fig. 17. The π^+ and π^- yields are averaged over the region $0.35 \leqslant \theta < 1.55$ rad and $100 \leqslant p < 700$ MeV/c (i.e., pions produced in the forward
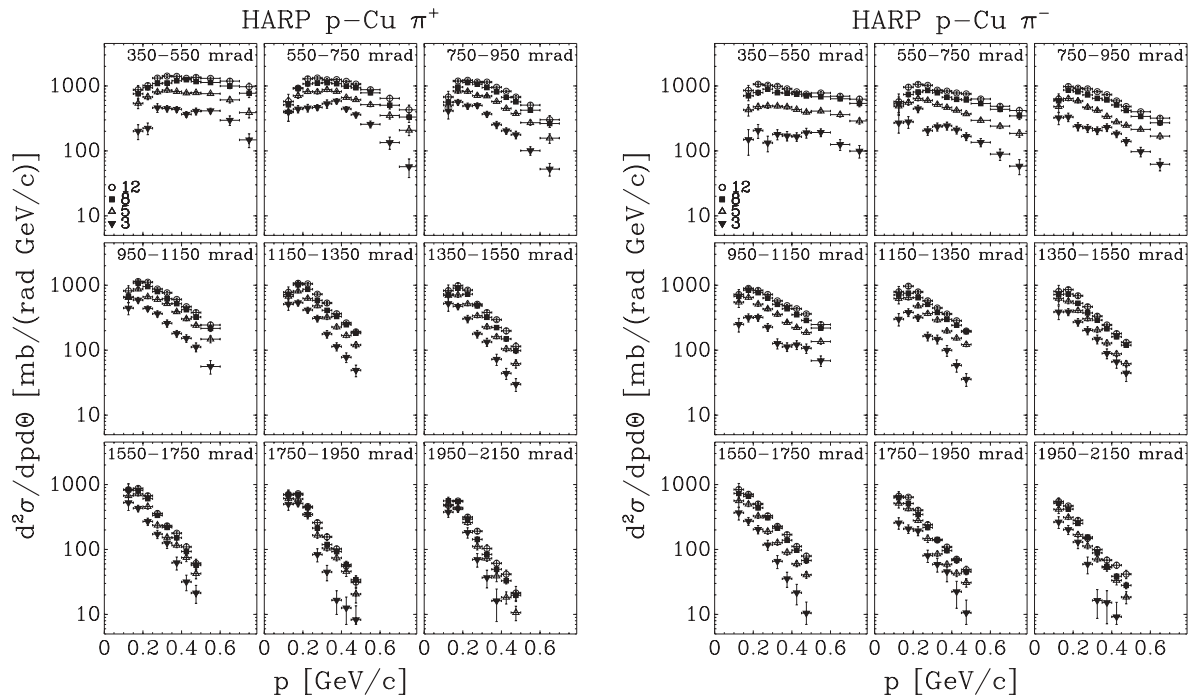
FIG. 9. Double-differential cross sections for π^+ production (left) and π^- production (right) in p-Cu interactions as a function of momentum displayed in different angular bins (shown in mrad in the panels). The error bars represent the combination of statistical and systematic uncertainties.
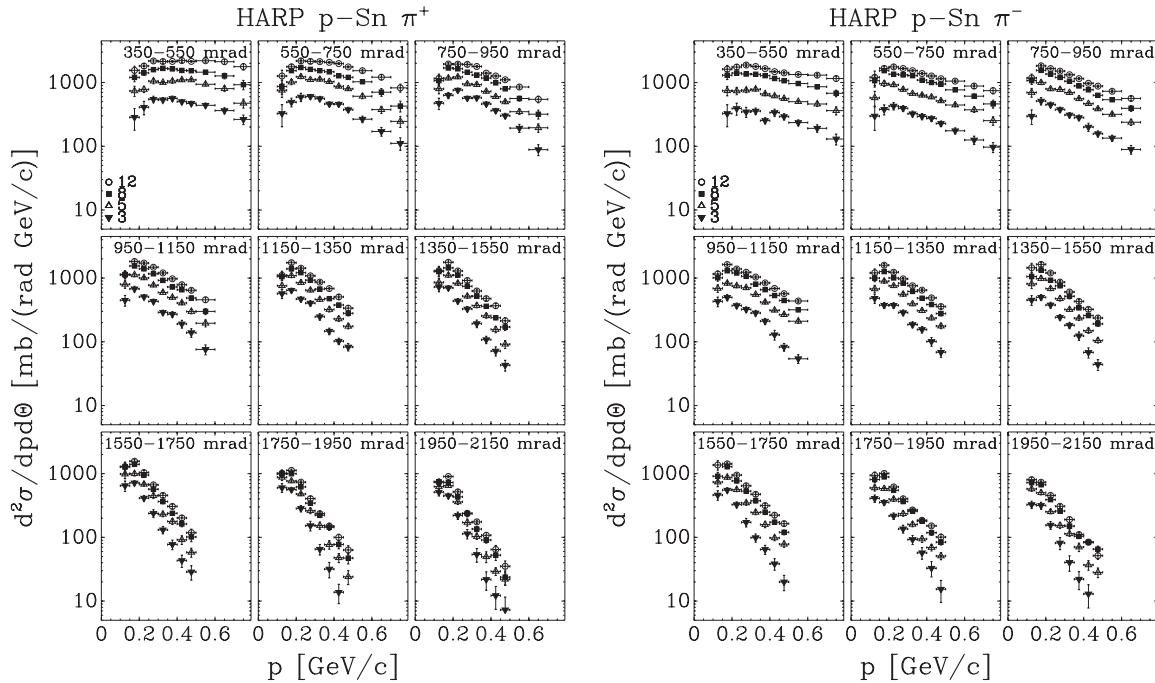
FIG. 10. Double-differential cross sections for π^+ production (left) and π^- production (right) in p-Sn interactions as a function of momentum displayed in different angular bins (shown in mrad in the panels). The error bars represent the combination of statistical and systematic uncertainties.

direction only). Whereas the beam energy dependence of the yields in the p-Be and p-C data differs clearly from the dependence in the p-Ta and p-Pb data one can observe that the p-Al, p-Cu, and p-Sn data display a smooth transition among

them. The dependence in the p-Be and p-C data is much flatter with a saturation of the yield between 8 and 12 GeV/c, with the p-Al, p-Cu, and p-Sn showing an intermediate behavior.
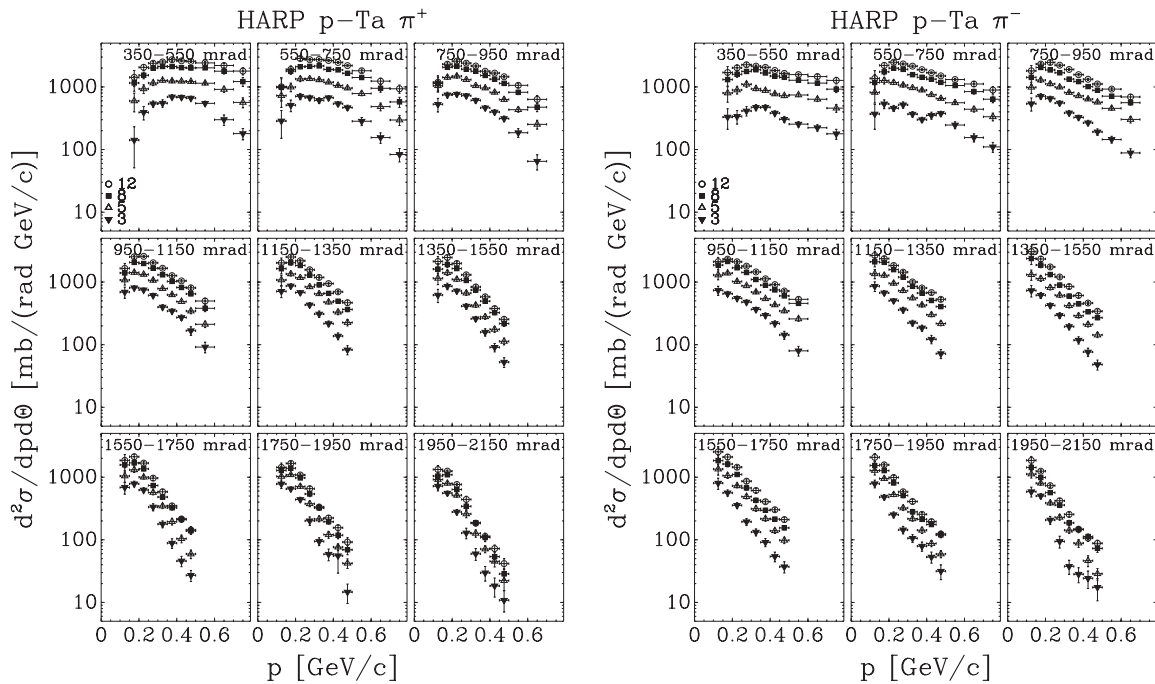
FIG. 11. Double-differential cross sections for π^+ production (left) and π^- production (right) in p-Ta interactions as a function of momentum displayed in different angular bins (shown in mrad in the panels). The error bars represent the combination of statistical and systematic uncertainties.
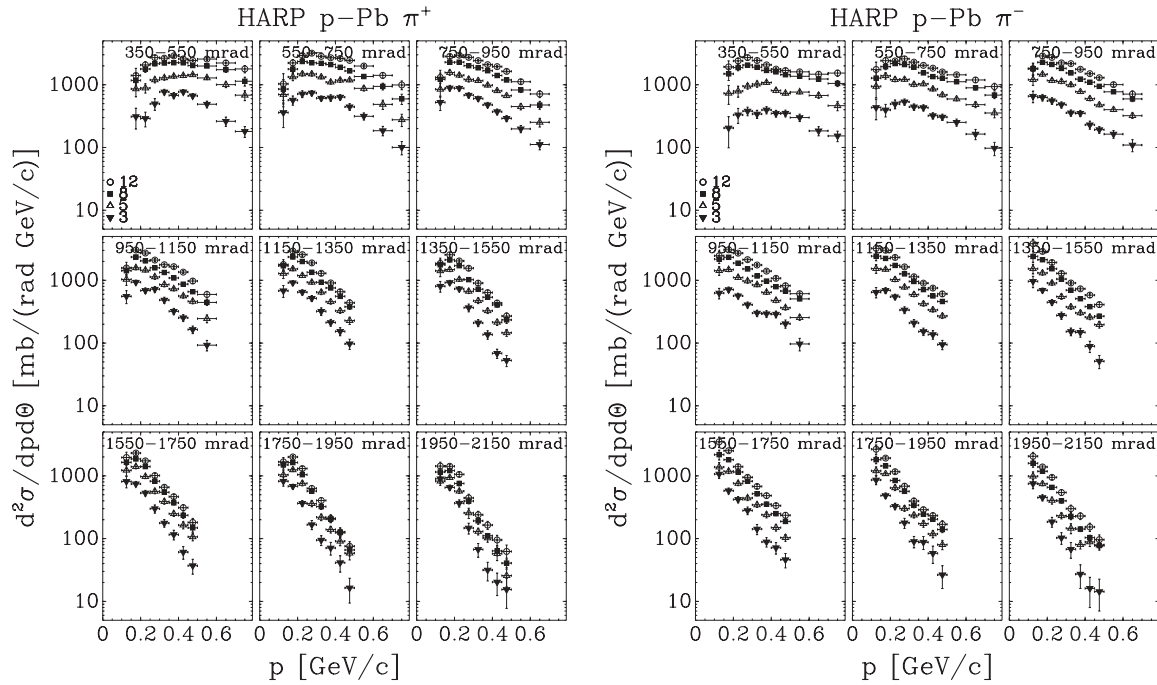
FIG. 12. Double-differential cross sections for π^+ production (left) and π^- production (right) in p-Pb interactions as a function of momentum displayed in different angular bins (shown in mrad in the panels). The error bars represent the combination of statistical and systematic uncertainties.

FIG. 13. Ratio of the π^- production cross sections measured without and with corrections for dynamic distortions in p-Be interactions at 8.9 GeV/c, as a function of momentum for different angular bins (shown in mrad in the panels). The error band in the ratio takes into account momentum error and the error on the efficiency; the other errors are correlated. The errors on the data points are statistical.

FIG. 14. Ratio of the π^+ production cross sections measured without and with corrections for dynamic distortions in p-Be interactions at 8.9 GeV/c, as a function of momentum for different angular bins (shown in mrad in the panels). The error band in the ratio takes into account momentum error and the error on the efficiency; the other errors are correlated. The errors on the data points are statistical.

FIG. 15. Ratio of the π^- production cross sections measured without and with corrections for dynamic distortions in p-Ta interactions at 8 GeV/c, as a function of momentum for different angular bins (shown in mrad in the panels). The error band in the ratio takes into account momentum error and the error on the efficiency; the other errors are correlated. The errors on the data points are statistical.

FIG. 16. Ratio of the π^+ production cross sections measured without and with corrections for dynamic distortions in p-Ta interactions at 8 GeV/c, as a function of momentum for different angular bins (shown in mrad in the panels). The error band in the ratio takes into account momentum error and the error on the efficiency; the other errors are correlated. The errors on the data points are statistical.

The integrated π^-/π^+ ratio in the forward direction is displayed in Fig. 18 as a function of the secondary momentum. In the covered part of the momentum range in most bins more π^+s are produced than π^-s. In the p-Ta and p-Pb data the ratio is closer to unity than for the p-Be, p-C, and p-Al data. The π^-/π^+ ratio is larger for higher incoming beam momenta than for lower momenta.

In the tantalum and lead data, the number of π^+s produced is smaller than the number of π^-s in the lowest momentum bin (100–150 MeV/c) for the 8 and 12 GeV/c incoming beam momenta. A similar effect was seen by E910 in their p-Au data [30]. Lighter targets do not show this behavior.

The dependence of the averaged pion yields on the atomic number A is shown in Fig. 19. The π^+ yields averaged over the region $0.350 \leqslant \theta < 1.550$ rad and $100 \leqslant p < 700$ MeV/c are shown in the left panel and the π^- data averaged over the same region in the right panel for four different beam momenta. One observes a smooth behavior of the averaged yields. The A dependence is slightly different for π^- and π^+ production, with the latter saturating earlier toward higher A, especially at lower beam momenta.

The analysis reported here (for p-Ta and p-Pb interactions) covers the major part of pions produced in the target and accepted by the focusing system of the input stage of a neutrino
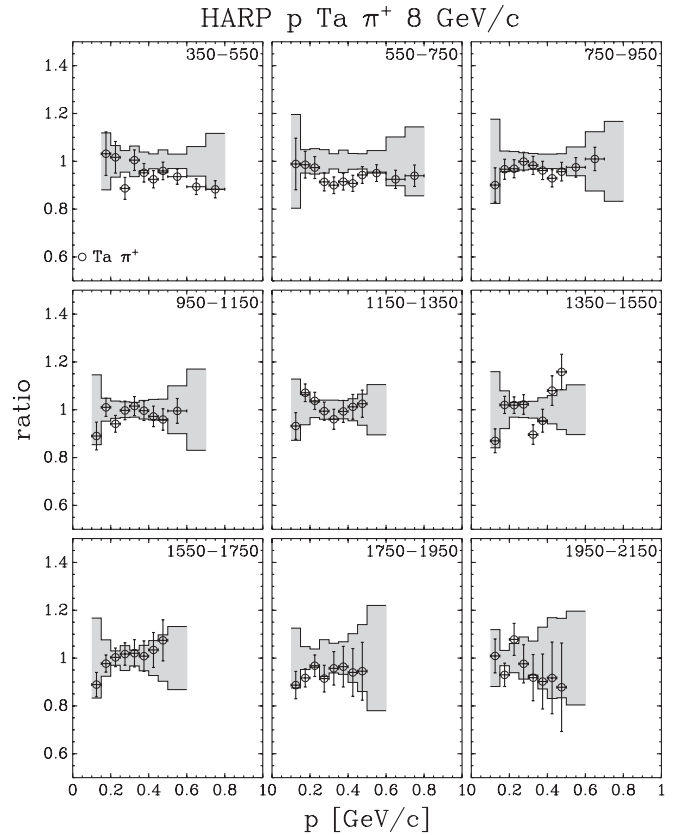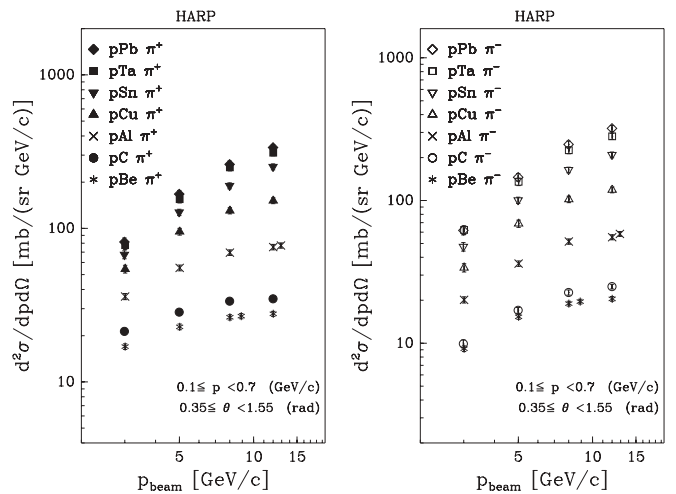
FIG. 17. The dependence on the beam momentum of the π^- (right) and π^+ (left) production yields in p-Be, p-C, p-Al, p-Cu, p-Sn, p-Ta, and p-Pb interactions averaged over the forward angular region ($0.350 \leqslant \theta < 1.550$ rad) and momentum region $100 \leqslant p < 700$ MeV/c. The results are given in arbitrary units, with a consistent scale between the left and right panels. Data points for different target nuclei and equal momenta are slightly shifted horizontally with respect to each other to increase their visibility.
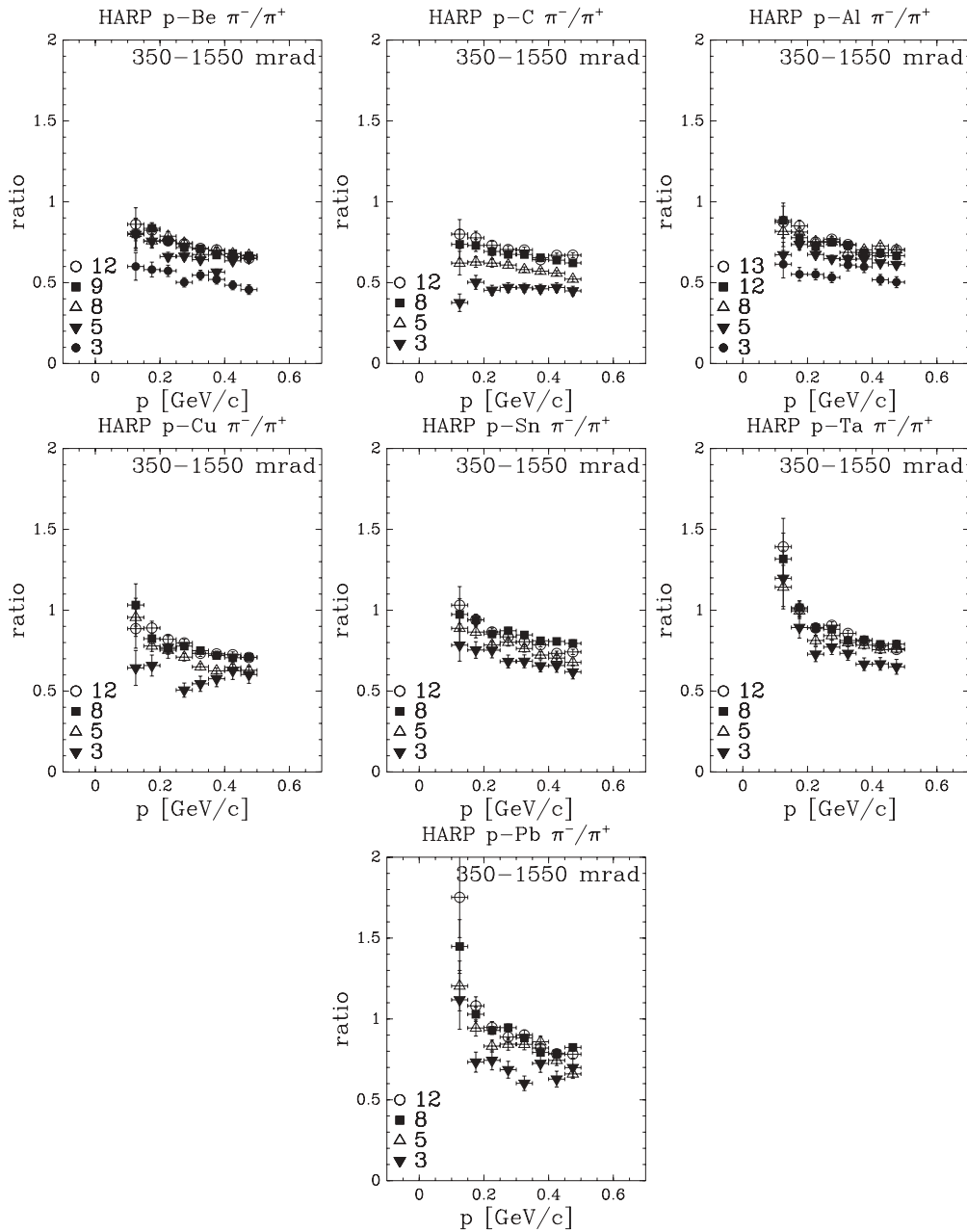
FIG. 18. From top-left panel to bottom-right, the ratio of the differential cross sections for π^- and π^+ production in p-Be, p-C, p-Al, p-Cu, p-Sn, p-Ta, and p-Pb interactions as a function of the secondary momentum integrated over the forward angular region (shown in mrad). In the figure, the symbol legends 13 and 9 refer to 12.9 and 8.9 GeV/c nominal beam momentum, respectively.

factory [31]. The effective coverage of the kinematic range can be defined as the fraction of the number of muons transported by the input stage of a neutrino factory design originating from decays for which the pion production cross section is within the kinematic range measured by the present experiment. As an example, this effective coverage was evaluated for the International Scoping Study (ISS) of a Neutrino Factory and Super-beam Facility input stage [31] to be 69% for π^+ and 72% for π^-, respectively [32], using a particular model for pion production at an incoming beam momentum of 10.9 GeV/c [33]. Since the data cover already a large fraction of the relevant phase space, one would expect that the

extrapolation to the full region with hadronic production models can be done reliably, once these models are adjusted to reproduce this data set in the region covered. Such tuning of models can also profit from the additional data provided with the HARP forward spectrometer.

As an indication of the overall pion yield as a function of incoming beam momentum, the π^+ and π^- production cross sections were averaged over the full HARP kinematic range in the forward hemisphere ($100 < p < 700$ MeV/c and $0.35 < \theta < 1.55$ rad). The results are shown in Fig. 20. The integrated yields are shown in the left panel and the integrated yields normalized to the kinetic energy of the incoming beam
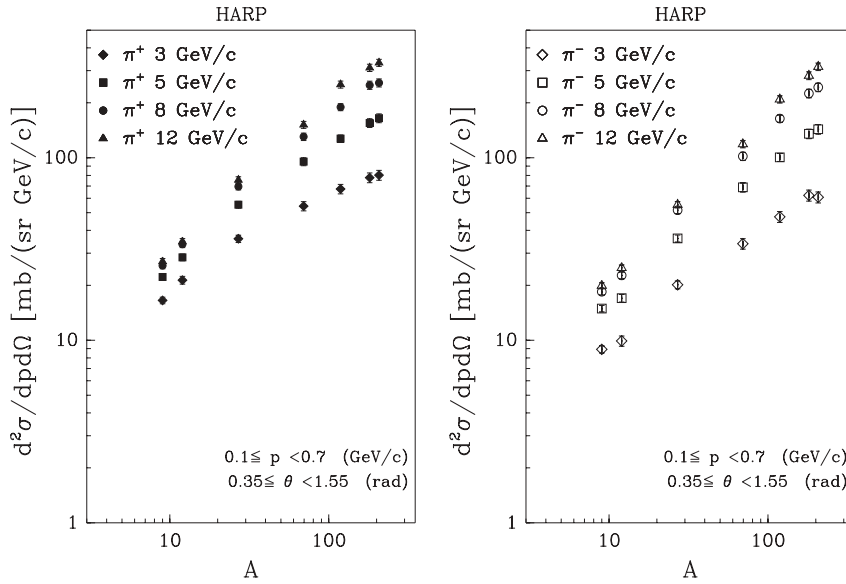
FIG. 19. The dependence on the atomic number A of the pion production yields in p-Be, p-Al, p-C, p-Cu, p-Sn, p-Ta, and p-Pb interactions averaged over the forward angular region ($0.35 \leqslant \theta < 1.55$ rad) and momentum region $100 \leqslant p < 700$ MeV/c. The results are given in arbitrary units, with a consistent scale between the left and right panels. The vertical scale used in this figure is consistent with the one in Fig. 17.

particles are shown in the right panel. The outer error bars indicate the total statistical and systematic errors. If one compares the π^+ and π^- rates for a given beam momentum or if one compares the rates at a different beam momentum the relative systematic error is reduced by about a factor of 2. The relative uncertainties are shown as inner error bars. It is shown that the pion yield increases with momentum and that in our kinematic coverage the optimum yield is between 5 and 8 GeV/c.

However, these calculations should be completed with more realistic kinematical cuts in the integration. To show the trend the rates within restricted ranges are also given: a restricted angular range ($0.35 < \theta < 0.95$ rad) and a range

further restricted in momentum ($250 < p < 500$ MeV/c). The latter range may be most representative for the neutrino factory.

Of course this analysis only gives a simplified picture of the results. One should note that the best result can be obtained by using the full information of the double-differential cross section and by developing designs optimized specifically for each single beam momentum. Then these optimized designs can be compared.

The experimental uncertainties are summarized for π^+ in Table II for all used targets and shown for two typical targets (one light and one heavy) in Figure 21. They are very similar for π^- and at the other beam energies (3, 5, 8, 12, and
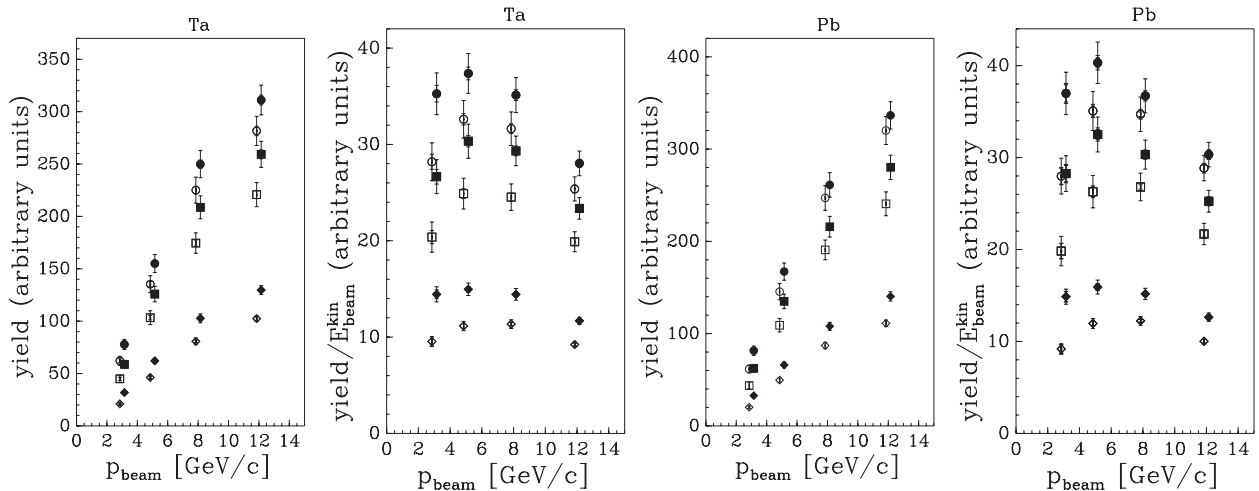
FIG. 20. Predictions of the π^+ (closed symbols) and π^- (open symbols) yields for different designs of the NF focusing stage. Integrated yields (left) and the integrated yields normalized to the kinetic energy of the proton (right) for p-Ta and p-Pb interactions. The circles indicate the integral over the full HARP acceptance ($100 < p < 700$ MeV/c and $0.35 < \theta < 1.55$ rad), the squares are integrated over $0.35 < \theta < 0.95$ rad, and the diamonds are calculated for the smaller angular range and $250 < p < 500$ MeV/c. Although the units are indicated as "arbitrary," for the largest region the yield is expressed as $d^2\sigma/dpd\Omega$ in mb/(GeV/c sr). For the other regions the same normalization is chosen, but now scaled with the relative bin size to show visually the correct ratio of number of pions produced in these kinematic regions. The full error bar shows the overall (systematic and statistical) error; the inner error bar shows the error relevant for the point-to-point comparison. For the latter error only the uncorrelated systematic uncertainties were added to the statistical error.

TABLE II. Experimental uncertainties for the analysis of the data taken with beryllium, carbon, aluminium, copper, tin, and lead targets at 3, 5, 8, 8.9, 12, and 12.9 GeV/c. The numbers represent the uncertainty in percent of the cross section integrated over the angle and momentum region indicated.

p (GeV/c) Angle (mrad)		0.1–0.3			0.3–0.5			0.5–0.7	
		350–950	950–1550	1550–2150	350–950	950–1550	1550–2150	350–950	950–1550
3 GeV/c									
Total syst.	(Be)	8.2	4.7	3.5	3.9	6.3	8.9	9.5	14.9
	(C)	13.2	5.2	3.2	3.8	6.9	10.1	9.5	16.5
	(Al)	9.3	4.8	3.5	3.8	7.2	13.1	10.0	13.6
	(Cu)	10.0	7.7	6.7	3.7	5.4	9.0	9.0	12.6
	(Sn)	14.2	6.7	5.1	3.4	6.5	9.8	8.1	14.2
	(Ta)	13.7	8.1	7.5	3.8	6.0	6.0	9.9	13.9
	(Pb)	13.2	7.5	6.7	3.7	5.7	7.8	9.5	14.1
Statistics	(Be)	2.8	2.6	3.6	2.2	3.7	9.0	2.9	6.8
	(C)	3.2	2.6	3.3	2.4	3.8	8.9	3.1	7.5
	(Al)	3.0	2.5	3.2	2.4	3.9	8.2	3.2	7.0
	(Cu)	4.4	3.8	4.6	3.6	5.4	11.2	4.7	9.7
	(Sn)	3.1	2.5	2.9	2.5	3.6	6.9	3.3	6.3
	(Ta)	3.3	2.6	3.1	2.5	3.5	6.5	3.4	6.2
	(Pb)	4.2	3.1	3.7	3.2	4.5	8.5	4.4	8.2
5 GeV/c									
Total syst.	(Be)	9.0	4.8	3.2	4.2	5.1	10.0	7.9	13.8
	(C)	11.1	5.0	3.2	3.9	5.3	8.0	6.9	11.7
	(Al)	9.5	5.0	3.3	3.9	4.8	8.9	7.8	12.7
	(Cu)	10.6	8.1	7.0	3.7	5.2	6.7	7.1	12.8
	(Sn)	10.1	6.2	5.1	3.5	5.2	8.0	7.3	11.6
	(Ta)	12.5	8.1	7.7	3.7	5.2	7.7	7.1	10.7
	(Pb)	12.6	7.6	6.6	3.7	5.6	6.5	7.3	11.5
Statistics	(Be)	1.7	1.6	2.1	1.3	2.1	4.3	1.5	3.3
	(C)	1.6	1.3	1.6	1.0	1.5	2.9	1.1	2.3
	(Al)	1.5	1.3	1.7	1.1	1.7	3.2	1.4	2.7
	(Cu)	1.6	1.4	1.7	1.2	1.7	3.1	1.4	2.6
	(Sn)	1.5	1.3	1.5	1.1	1.6	2.8	1.4	2.4
	(Ta)	1.7	1.4	1.7	1.3	1.7	3.0	1.5	2.5
	(Pb)	2.2	1.8	2.1	1.7	2.2	3.9	2.0	3.4
8 GeV/c									
Total syst.	(Be)	8.6	4.7	3.1	4.0	4.5	7.5	7.2	12.0
	(C)	10.4	4.8	3.1	3.7	3.8	7.0	6.6	11.8
	(Al)	9.4	5.0	3.5	3.8	4.3	7.5	7.2	11.2
	(Cu)	10.1	7.8	7.1	3.6	4.3	6.3	6.5	10.8
	(Sn)	9.1	6.2	5.3	3.3	5.0	6.9	7.1	11.2
	(Ta)	11.5	8.2	7.6	3.7	5.0	5.9	7.1	10.4
	(Pb)	11.2	7.5	6.5	3.5	4.9	6.9	6.4	9.9
Statistics	(Be)	1.4	1.3	1.7	1.0	1.6	3.1	1.2	2.4
	(C)	1.3	1.0	1.3	0.7	1.1	2.1	0.8	1.6
	(Al)	1.2	1.1	1.4	0.9	1.3	2.5	1.0	1.9
	(Cu)	1.0	0.9	1.1	0.7	1.0	1.8	0.8	1.4
	(Sn)	1.0	0.9	1.1	0.7	1.0	1.8	0.9	1.5
	(Ta)	1.1	0.9	1.2	0.8	1.1	1.9	0.9	1.6
	(Pb)	1.1	0.9	1.0	0.7	1.0	1.8	0.9	1.5
8.9 GeV/c									
Total syst.	(Be)	8.8	4.7	3.1	4.2	4.4	7.7	7.9	12.4
Statistics	(Be)	0.5	0.5	0.6	0.4	0.6	1.1	0.4	0.9
12 GeV/c									
Total syst.	(Be)	9.0	4.8	3.3	3.8	4.1	7.3	7.3	12.1
	(C)	9.8	5.8	4.1	3.9	4.5	6.8	7.5	10.8
	(Al)	9.6	5.4	3.9	3.5	4.0	7.6	7.6	11.7
	(Cu)	10.1	7.8	7.1	2.9	4.3	6.3	6.7	11.2

TABLE II. *(Continued.)*

p (GeV/c) Angle (mrad)		0.1–0.3			0.3–0.5			0.5–0.7	
		350–950	950–1550	1550–2150	350–950	950–1550	1550–2150	350–950	950–1550
	(Sn)	10.0	6.7	5.7	2.9	4.7	6.6	6.1	9.6
	(Ta)	11.4	7.2	6.8	2.3	4.4	5.9	6.6	9.4
	(Pb)	10.8	7.1	6.7	2.9	4.4	5.6	7.1	9.1
Statistics	(Be)	1.1	1.1	1.5	0.8	1.3	2.6	0.9	2.0
	(C)	1.9	1.9	2.4	1.5	2.2	4.4	1.6	3.2
	(Al)	1.3	1.2	1.5	0.9	1.5	2.8	1.1	2.1
	(Cu)	1.2	1.2	1.5	0.9	1.3	2.5	1.0	1.9
	(Sn)	0.8	0.8	0.9	0.6	0.9	1.5	0.7	1.2
	(Ta)	1.1	1.0	1.2	0.8	1.2	2.1	1.0	1.7
	(Pb)	1.8	1.6	2.0	1.4	1.9	3.5	1.6	2.7
12.9 GeV/c									
Total syst.	(Al)	9.6	5.2	3.7	3.5	4.1	6.8	7.4	11.7
Statistics	(Al)	0.5	0.5	0.6	0.4	0.6	1.1	0.4	0.8

12.9 GeV/c). Going from lighter (Be and C) to heavier targets (Ta and Pb) the corrections for π^0 (conversion) and absorption and tertiaries (particles produced in secondary interactions) are bigger.

One observes that only for the 3 GeV/c beam is the statistical error similar in magnitude to the systematic error, whereas the statistical error is negligible for the 8 and 12 GeV/c beam settings. The statistical error is calculated by error propagation as part of the unfolding procedure. It takes into account that the unfolding matrix is obtained from the data themselves[3] and hence contributes also to the statistical error. This procedure almost doubles the statistical error, but it avoids an important systematic error that would otherwise be introduced by assuming a cross-section model *a priori* to calculate the corrections.

The largest systematic error corresponds to the uncertainty in the absolute momentum scale, which was estimated to be around 3% by using elastic scattering [15]. Although the corrections for the dynamic distortions have been applied in this analysis, in contrast to the previously published ones, the systematic error has not been reduced. This is because now the full statistics have been used, introducing data with larger distortions. The benefit of the introduction of the larger statistics is evident mainly at low incident beam momenta (3 GeV/c), in the bins with higher secondary momenta and larger scattering angle. At low momentum in the relatively small angle forward direction the uncertainty in the subtraction of the electron and positron background from π^0 production is dominant ($\sim$6%–10%). This uncertainty is split between the variation in the shape of the π^0 spectrum and the normalization using the recognized electrons. The target region definition and the uncertainty in the PID efficiency and background from tertiaries are of similar size and are not negligible ($\sim$2%–3%). Relatively small errors are introduced by the uncertainties

in the absorption correction and absolute knowledge of the angular and the momentum resolution. The correction for tertiaries is relatively large at low momenta and large angles ($\sim$3%–5%). As expected, this region is most affected by this component. The errors are quoted for the positive pion data. Owing to the similarity of the spectra the errors are very similar for the negative pions.

As already mentioned, the overall normalization has an uncertainty of 2% and is not reported in the table. It is mainly due to the uncertainty in the efficiency that beam protons counted in the normalization actually hit the target, with smaller components from the target density and beam particle counting procedure.

As our final results, obtained with a full correction of the distortions of TPC tracks (static plus dynamic), are compatible with our preliminary ones published in Refs. [15–17], we refer to these papers for a comparison with published data. We only stress here that previous data sets are scarce, with big total errors, and cover only a limited region of the phase space covered by the HARP experiment.

In the following we will show only some comparisons with publicly available Monte Carlo simulations—GEANT4 [29] and MARS [34]—using different models. We stress that no tuning to our data has been done by the GEANT4 or MARS teams. The comparison will be shown for a limited set of plots and only for the C and Ta targets, as examples of light and heavy target nuclei, in Figs. 22–33. At intermediate energies (up to 5–10 GeV), GEANT4 uses two types of intranuclear cascade models: the Bertini model [35,36] (valid up to $\sim$10 GeV) and the binary model [37] (valid up to $\sim$3 GeV). Both models treat the target nucleus in detail, taking into account density variations and tracking in the nuclear field. The binary model is based on hadron collisions with nucleons, giving resonances that decay according to their quantum numbers. The Bertini model is based on the cascade code reported in Ref. [38] and hadron collisions are assumed to proceed according to free-space partial cross sections and final-state distributions measured for the incident particle types.

---

[3]The migration matrix is calculated without prior knowledge of the cross sections, whereas the unfolding procedure determined the unfolding matrix from the migration matrix and the distributions found in the data.
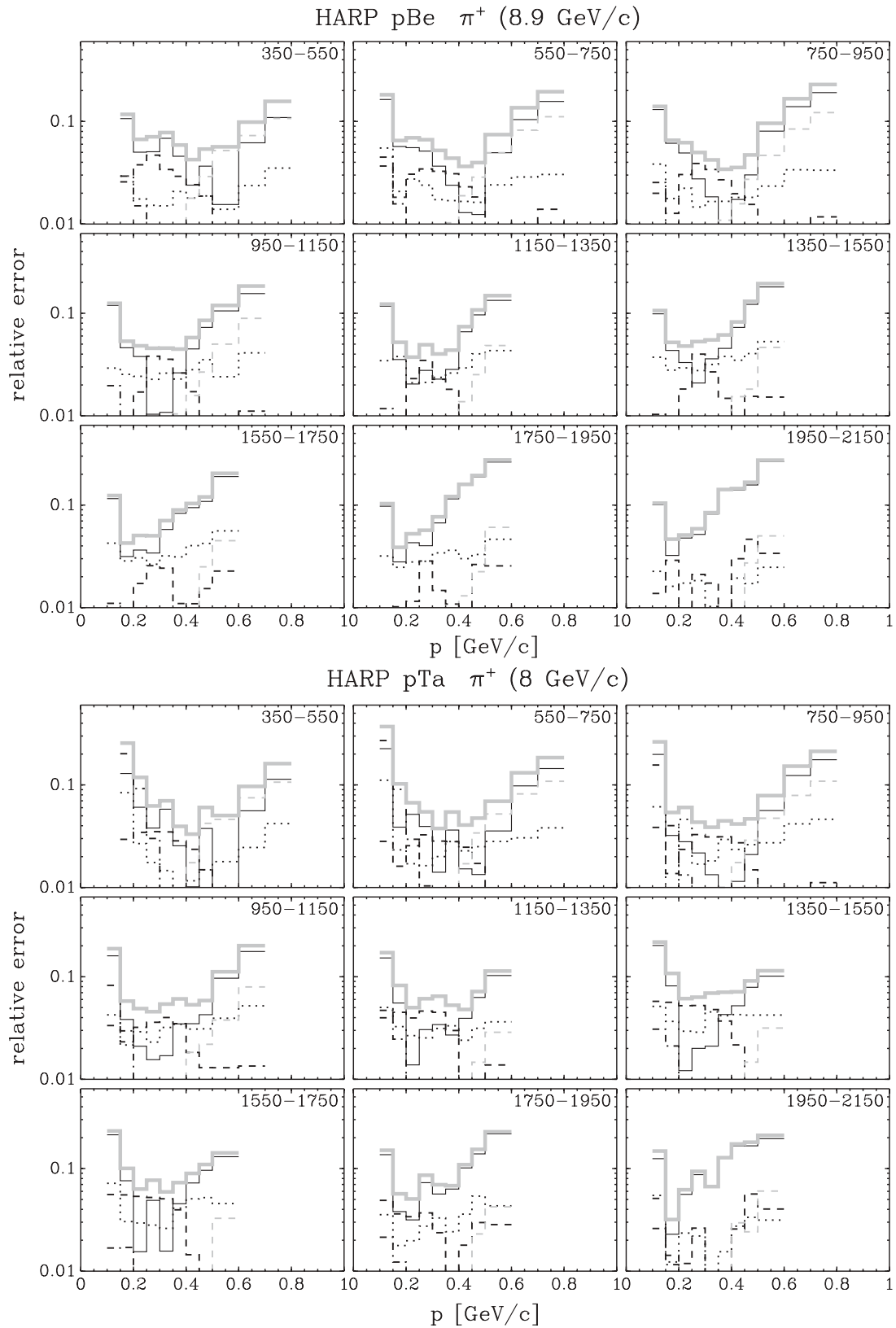
FIG. 21. Total systematic error (gray solid line) and main components: black short-dashed line for absorption and tertiary interactions, black dotted line for track efficiency and target pointing efficiency, black dot-dashed line for π^0 subtraction, black solid line for momentum scale plus resolution and angle scale, and gray short-dashed line for PID for two typical targets (Be and Ta).
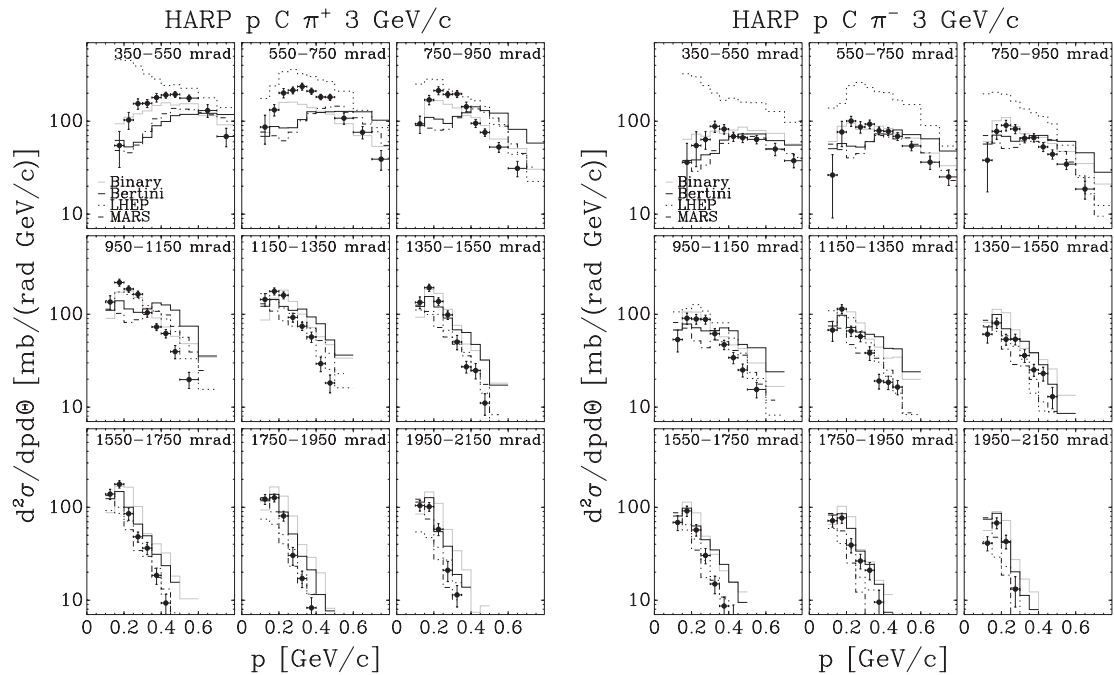
FIG. 22. Comparison of HARP double-differential π^+ (π^-) cross sections for p-C at 3 GeV/c with GEANT4 and MARS Monte Carlo predictions, using several generator models (see text for details).

At higher energies, instead, two parton string models, the quark-gluon string (QGS) model [35,39] and the Fritiof (FTP) model [39], are used, in addition to a high-energy parametrized (HEP) model derived from the high-energy part of the GHEISHA code used inside GEANT3 [40].

The parametrized models of GEANT4 (HEP and the low energy parametrized model, LEP) are intended to be fast, but
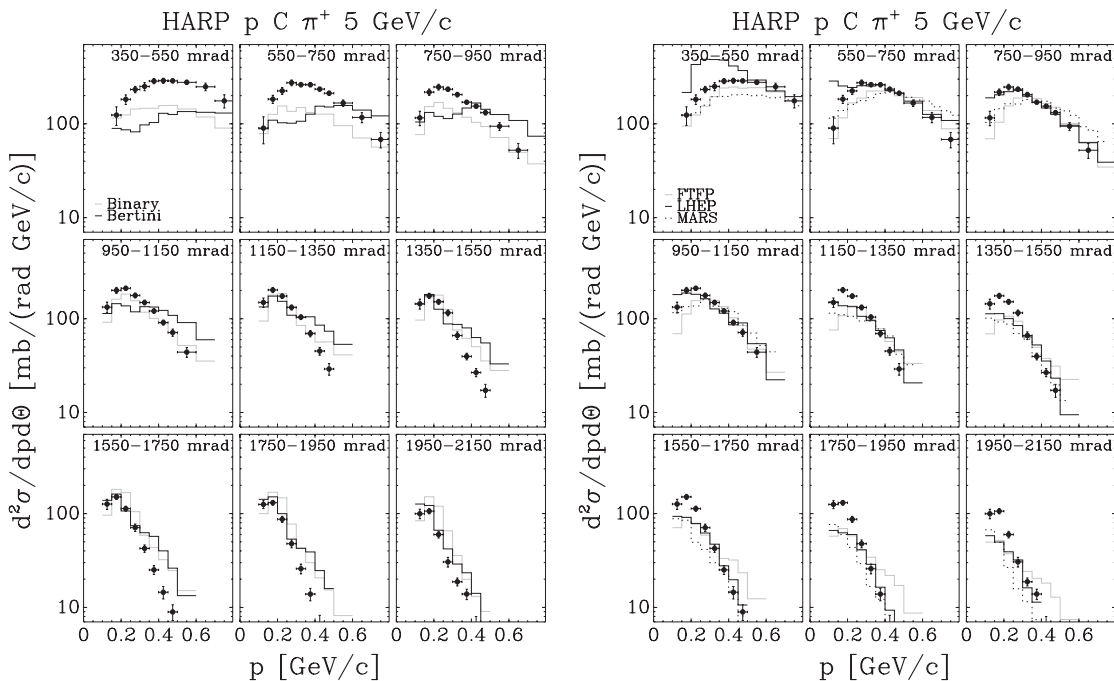
FIG. 23. Comparison of HARP double-differential π^+ cross sections for p-C at 5 GeV/c with GEANT4 and MARS Monte Carlo predictions, using several generator models (see text for details).
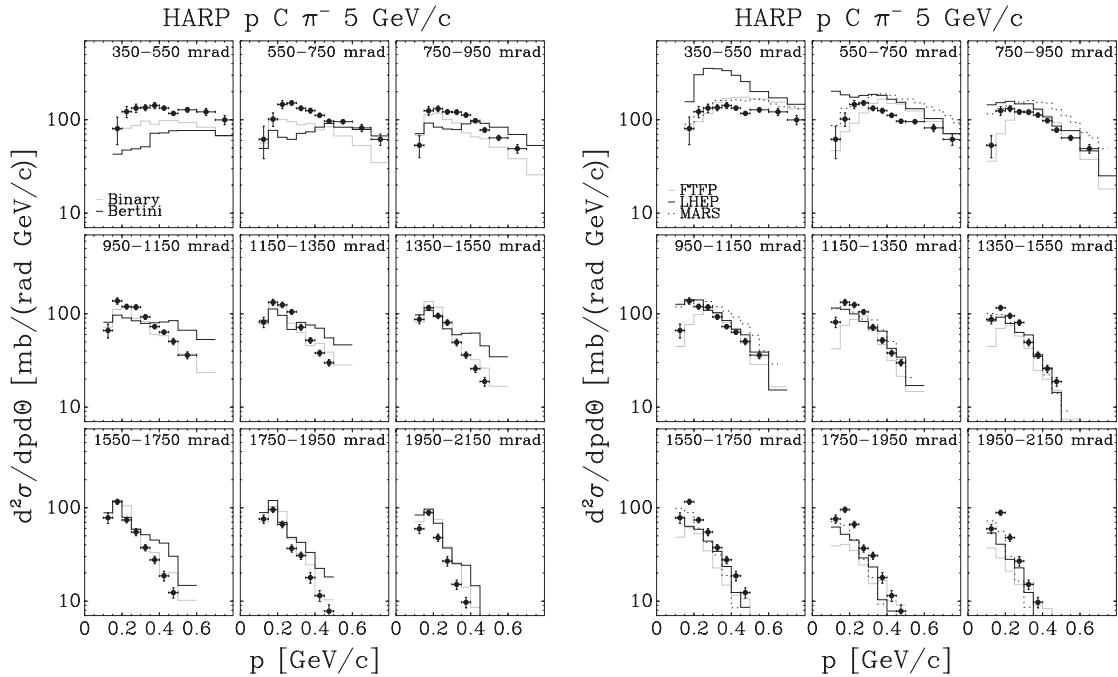
FIG. 24. Comparison of HARP double-differential π^- cross sections for p-C at 5 GeV/c with GEANT4 Monte Carlo predictions, using several generator models (see text for details).

they conserve energy and momentum on average and not event by event.

A realistic GEANT4 simulation is built by combining models and physics processes into what is called a "physics list." In high-energy calorimetry the two most commonly used are the QGSP physics list, based on the QGS model, the pre-

compound-nucleus model, and some of the LEP model,[4] and the LHEP physics list [41], based on the parametrized LEP model and HEP models.

———

[4]Also, at low energy, this model has its root in the GHEISHA code used inside GEANT3.
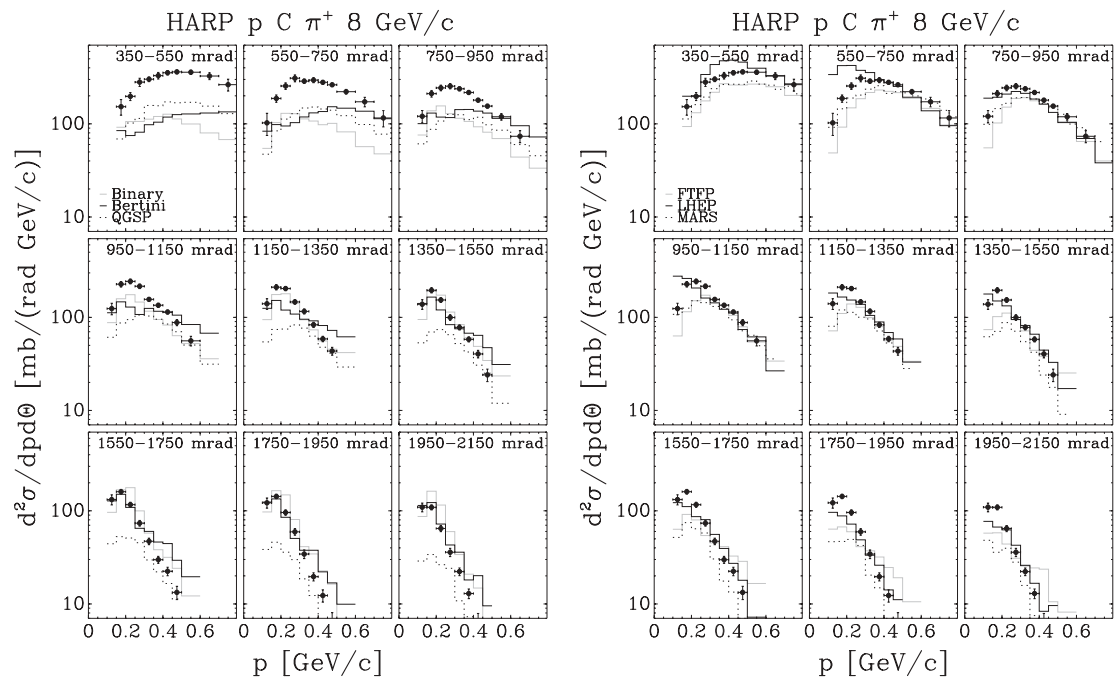
FIG. 25. Comparison of HARP double-differential π^+ cross sections for p-C at 8 GeV/c with GEANT4 and MARS Monte Carlo predictions, using several generator models (see text for details).
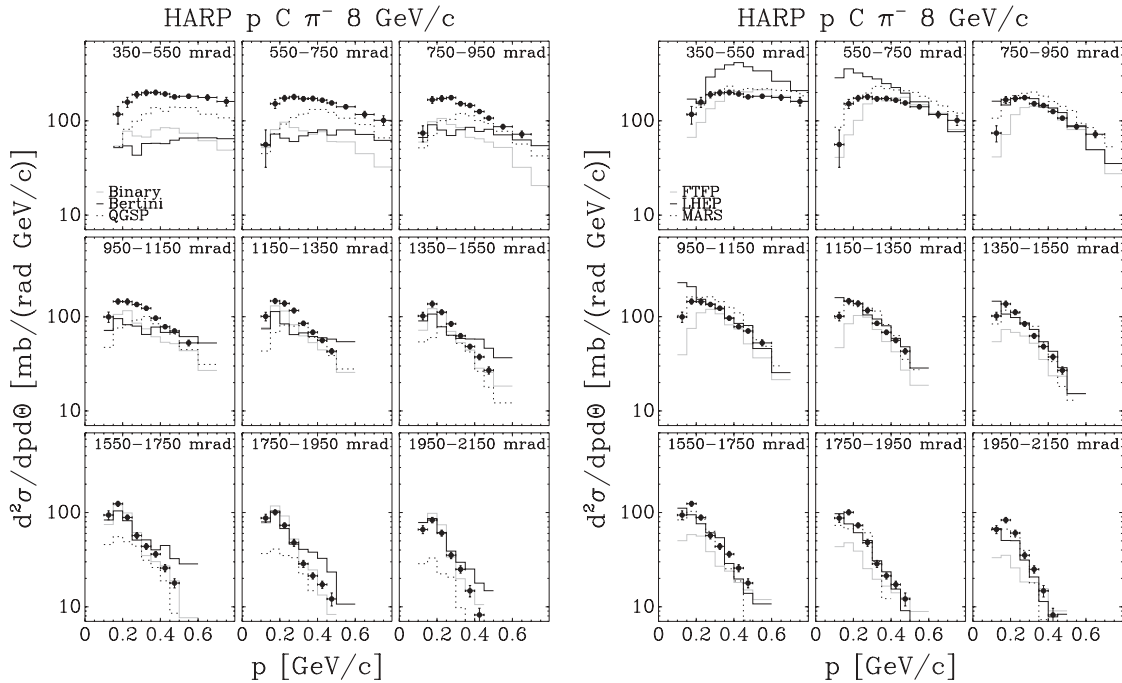
FIG. 26. Comparison of HARP double-differential π^- cross sections for p-C at 8 GeV/c with GEANT4 and MARS Monte Carlo predictions, using several generator models (see text for details).

The MARS code system [34] uses as basic model an inclusive multiparticle production approach originated by R. Feynman. Above 3 GeV/c phenomenological particle production models are used. Below 5 GeV/c a cascade-exciton model [42] combined with the Fermi breakup model, the coalescence model, an evaporation model, and a multifragmentation extension is used instead.

None of the considered models describe fully our data. However, backward or central region production seems to be described better than relatively more forward production,
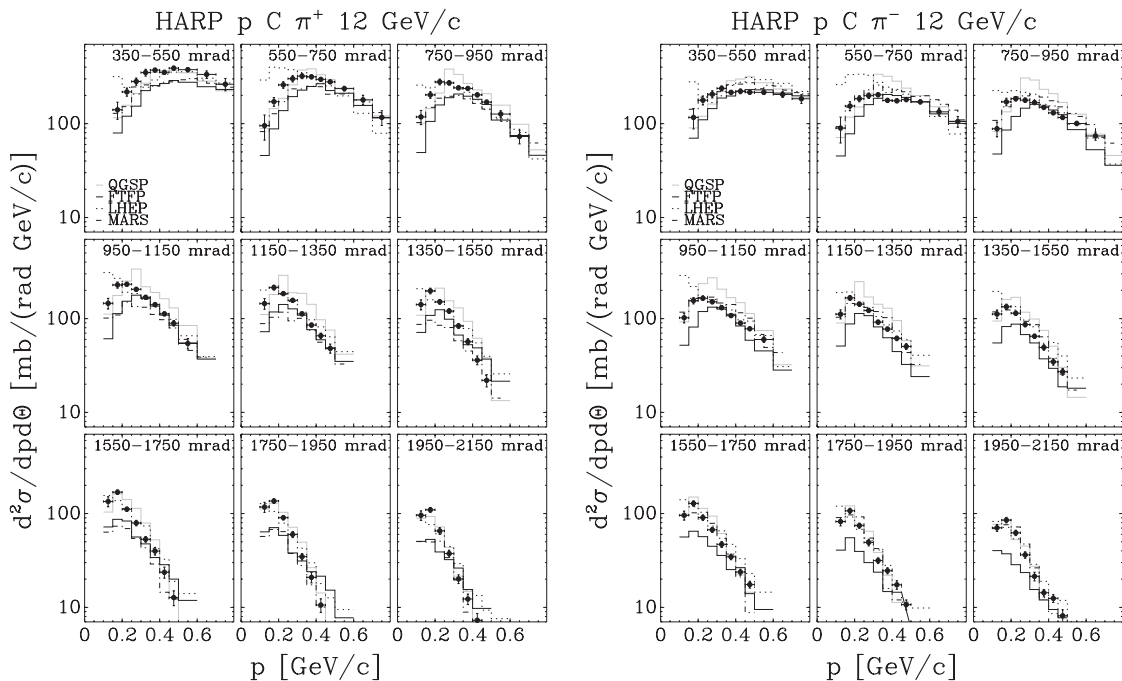
FIG. 27. Comparison of HARP double-differential $\pi^\pm$ cross sections for p-C at 12 GeV/c with GEANT4 and MARS Monte Carlo predictions, using several generator models (see text for details).
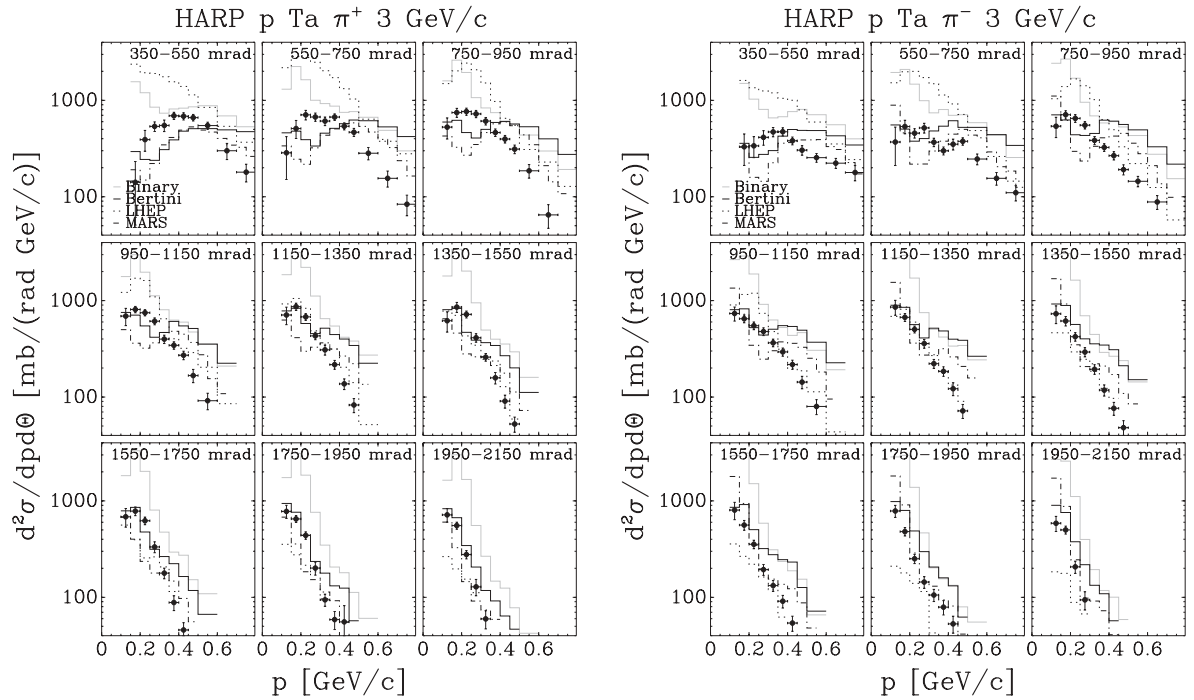
FIG. 28. Comparison of HARP double-differential $\pi^{\pm}$ cross sections for p-Ta at 3 GeV/c with GEANT4 and MARS Monte Carlo predictions, using several generator models (see text for details).

especially at higher incident momenta. In our data, the lowest angular bin corresponds to a transition region from forward to central production, which is more difficult to describe by Monte Carlo models.
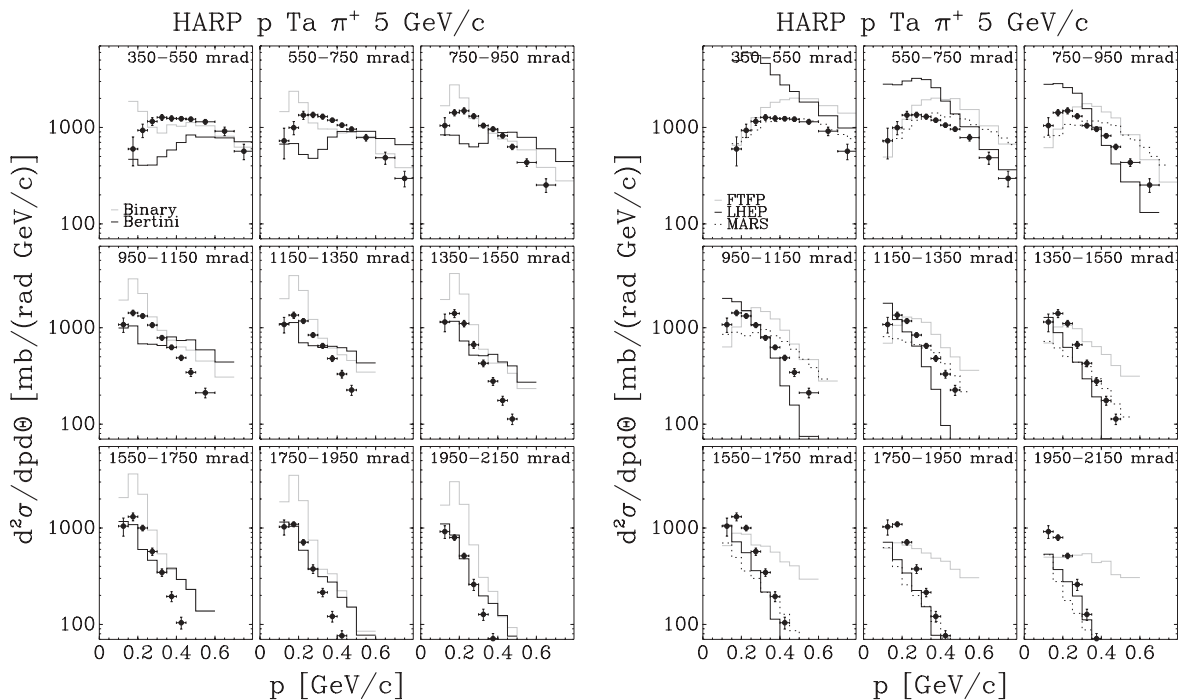
FIG. 29. Comparison of HARP double-differential π^{+} cross sections for p-Ta at 5 GeV/c with GEANT4 and MARS Monte Carlo predictions, using several generator models (see text for details).
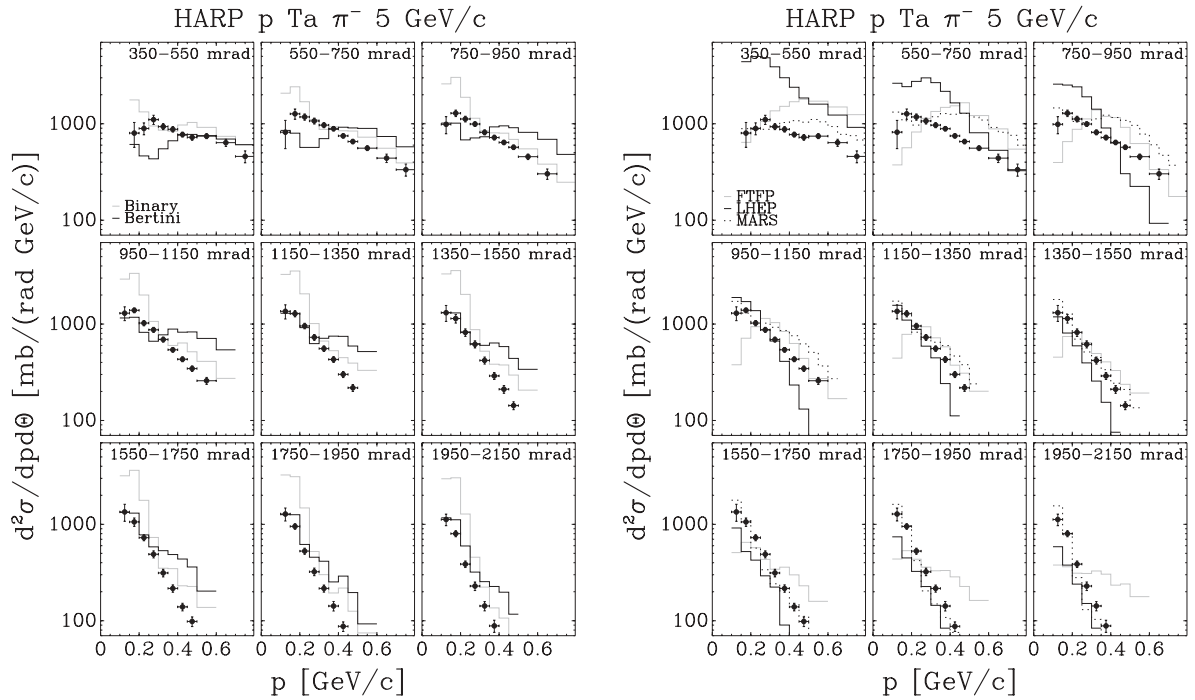
FIG. 30. Comparison of HARP double-differential π^- cross sections for p-Ta at 5 GeV/c with GEANT4 and MARS Monte Carlo predictions, using several generator models (see text for details).

In general, π^+ production is better described than π^- production. At higher energies the FTP model (from GEANT4)

and the MARS model describe the data better, but at the lowest energies the Bertini and binary cascade models (from GEANT4)
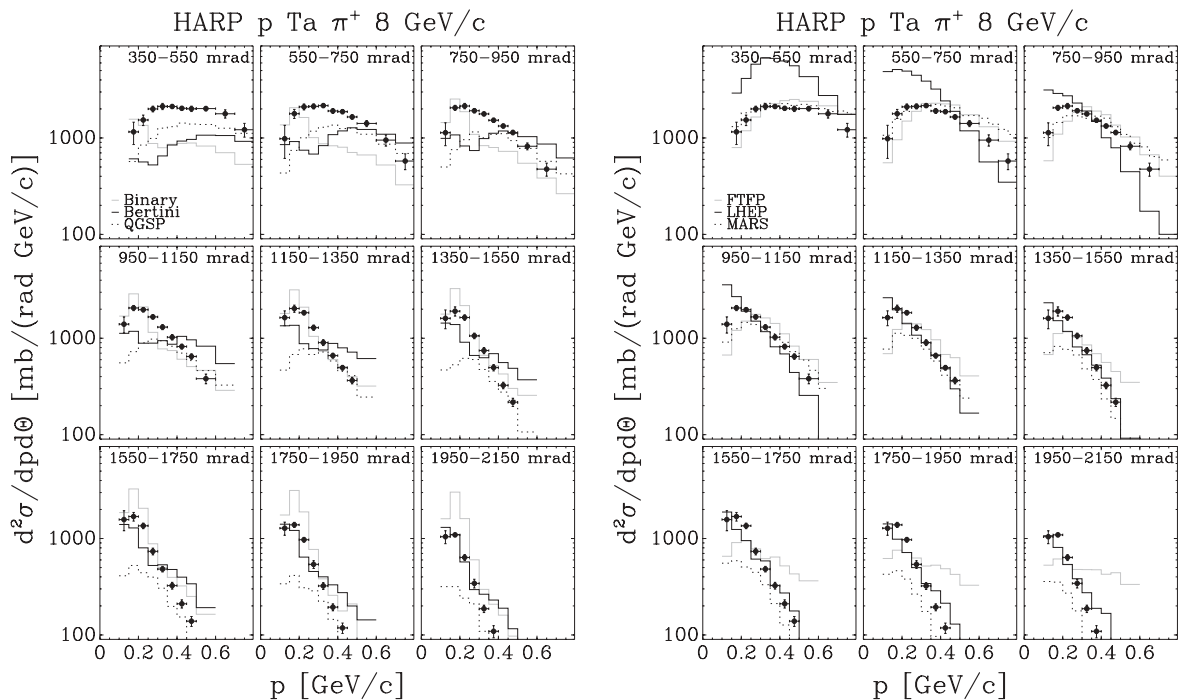
FIG. 31. Comparison of HARP double-differential π^+ cross sections for p-Ta at 8 GeV/c with GEANT4 and MARS Monte Carlo predictions, using several generator models (see text for details).
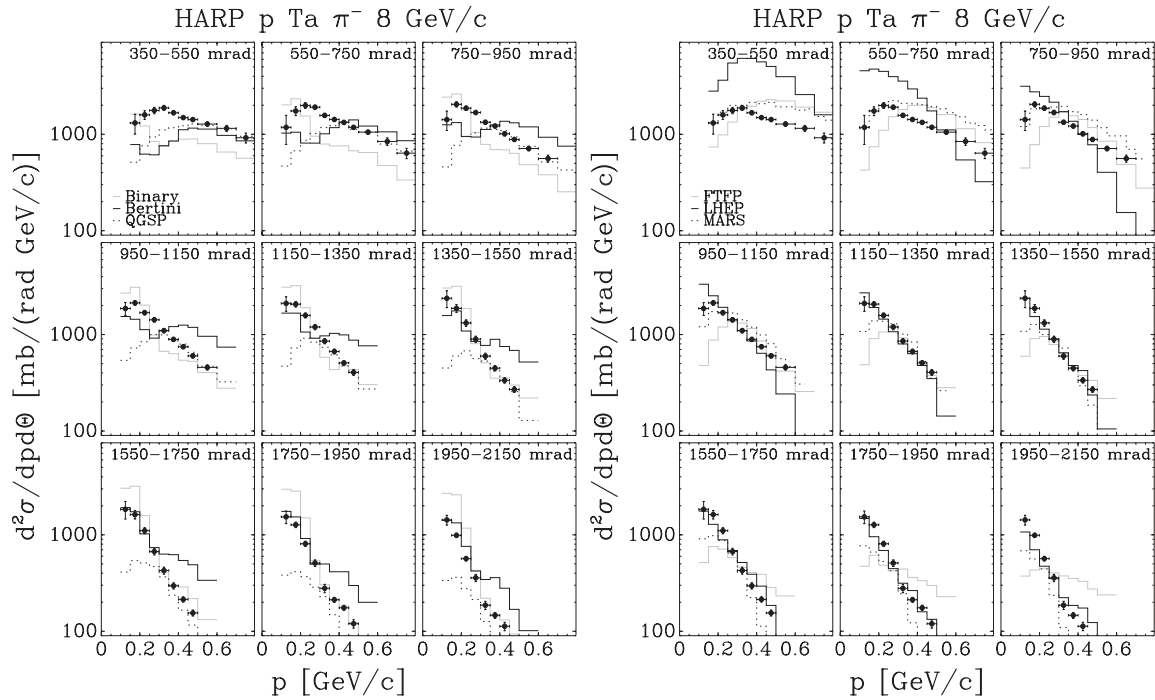
FIG. 32. Comparison of HARP double-differential π^- cross sections for p-Ta at 8 GeV/c with GEANT4 and MARS Monte Carlo predictions, using several generator models (see text for details).

seem more appropriate. Parametrized models, such as LHEP from GEANT4, show relevant discrepancies: up to a factor 3 in the forward region at low energies.

The comparison, just outlined in our paper, between data and models shows that the full set of HARP data, taken with targets spanning the full periodic table of elements, with
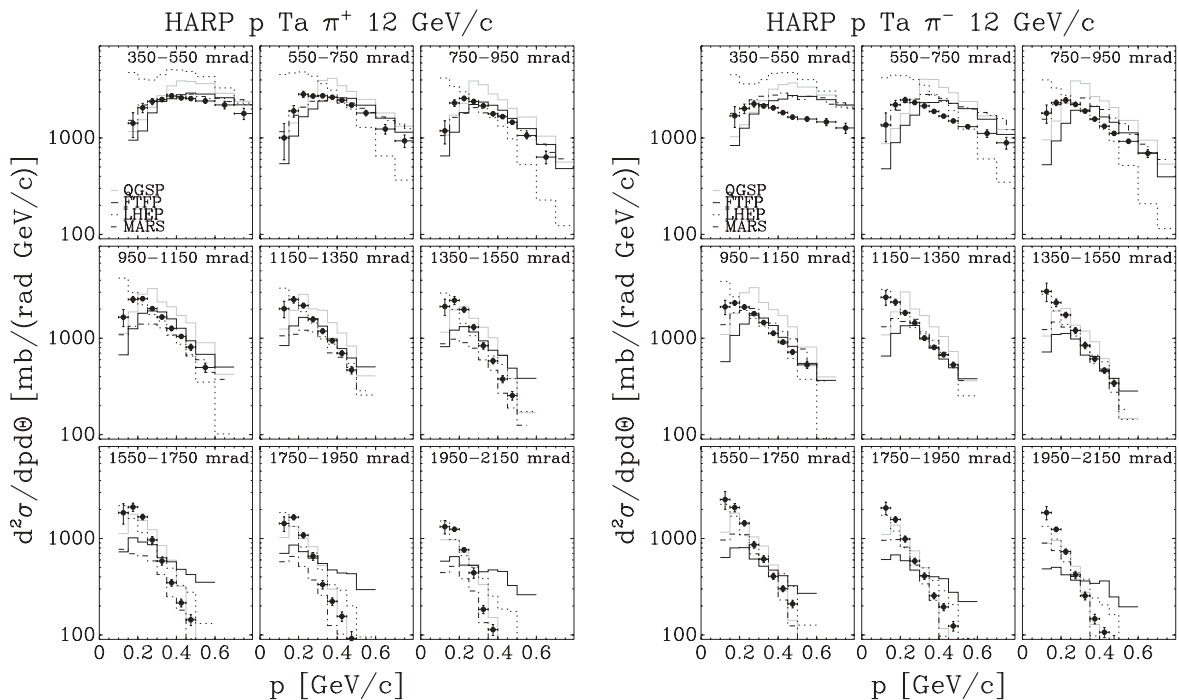
FIG. 33. Comparison of HARP double-differential $\pi^\pm$ cross sections for p-Ta at 12 GeV/c with GEANT4 and MARS Monte Carlo predictions, using several generator models (see text for details).

small total errors and large coverage of the solid angle with a single detector, may greatly help the tuning of models used in hadronic simulations in the difficult energy range between 3 and 15 GeV/*c* of incident momentum.

V. SUMMARY AND CONCLUSIONS

An analysis of the production of pions at large angles with respect to the beam direction for protons of 3, 5, 8, and 8.9 GeV/*c* (Be only) and 12 and 12.9 GeV/*c* (Al only) beam momentum impinging on thin (5% interaction length) beryllium, carbon, aluminium, copper, tin, tantalum, and lead targets has been described. The secondary pion yield is measured in a large angular and momentum range and double-differential cross sections are obtained. A detailed error estimation has been discussed. Results on the dependence from atomic number *A* of pion production were also presented.

The data taken with the lead and tantalum targets are relevant for the optimization of the targetry of a neutrino factory. The pion yield increases with momentum and in our kinematic range the optimum is between 5 and 8 GeV/*c*.

The use of a single detector for a range of beam momenta makes it possible to measure the dependence of the pion yield on the secondary particle momentum and emission angle θ with high precision. The *A* dependence of the cross section can be studied by using data from a single experiment. Very few pion production measurements in this energy range are reported in the literature. The only comparable results found in the literature agree with the analysis described in this paper. Hadronic production models describing this energy range have now been compared with our new results.

ACKNOWLEDGMENTS

APPENDIX: CROSS-SECTION DATA

Results on double-differential cross section for protons impinging on thin beryllium, carbon, aluminium, copper, tin, tantalum, and lead targets are reported in Tables III–XVI.

TABLE III. HARP results for the double-differential π^+ production cross section in the laboratory system, $d^2\sigma^{\pi^+}/(dp d\theta)$, for *p*-Be interactions. Each row refers to a different ($p_{\min} \leqslant p < p_{\max}$, $\theta_{\min} \leqslant \theta < \theta_{\max}$) bin, where *p* and θ are the pion momentum and polar angle, respectively. The central value as well as the square root of the diagonal elements of the covariance matrix are given.

$\theta_{\min}$ (rad)	$\theta_{\max}$ (rad)	$p_{\min}$ (GeV/*c*)	$p_{\max}$ (GeV/*c*)	$d^2\sigma^{\pi^+}/(dp d\theta)$ [b/(rad GeV/*c*)]				
				3 GeV/*c*	5 GeV/*c*	8 GeV/*c*	8.9 GeV/*c*	12 GeV/*c*
0.35	0.55	0.15	0.20	0.062 ± 0.011	0.107 ± 0.015	0.122 ± 0.017	0.140 ± 0.017	0.137 ± 0.020
		0.20	0.25	0.079 ± 0.010	0.138 ± 0.013	0.162 ± 0.013	0.184 ± 0.013	0.199 ± 0.013
		0.25	0.30	0.117 ± 0.014	0.187 ± 0.018	0.217 ± 0.020	0.231 ± 0.017	0.240 ± 0.020

TABLE III. *(Continued.)*

$\theta_{\min}$ (rad)	$\theta_{\max}$ (rad)	$p_{\min}$ (GeV/c)	$p_{\max}$ (GeV/c)	$d^2\sigma^{\pi^+}/(dpd\theta)$ [b/(rad GeV/c)]				
				3 GeV/c	5 GeV/c	8 GeV/c	8.9 GeV/c	12 GeV/c
		0.30	0.35	0.156 ± 0.017	0.204 ± 0.017	0.241 ± 0.017	0.249 ± 0.020	0.269 ± 0.018
		0.35	0.40	0.164 ± 0.014	0.238 ± 0.017	0.258 ± 0.021	0.269 ± 0.016	0.251 ± 0.014
		0.40	0.45	0.165 ± 0.011	0.223 ± 0.012	0.264 ± 0.012	0.284 ± 0.012	0.297 ± 0.022
		0.45	0.50	0.164 ± 0.011	0.230 ± 0.014	0.271 ± 0.014	0.300 ± 0.016	0.319 ± 0.016
		0.50	0.60	0.162 ± 0.013	0.230 ± 0.013	0.284 ± 0.016	0.292 ± 0.017	0.324 ± 0.016
		0.60	0.70	0.121 ± 0.018	0.214 ± 0.021	0.282 ± 0.027	0.250 ± 0.025	0.271 ± 0.029
		0.70	0.80	0.068 ± 0.016	0.157 ± 0.028	0.210 ± 0.032	0.182 ± 0.029	0.211 ± 0.033
0.55	0.75	0.10	0.15	0.047 ± 0.013	0.080 ± 0.017	0.082 ± 0.019	0.088 ± 0.016	0.085 ± 0.019
		0.15	0.20	0.111 ± 0.012	0.136 ± 0.013	0.145 ± 0.012	0.141 ± 0.010	0.145 ± 0.010
		0.20	0.25	0.146 ± 0.015	0.182 ± 0.014	0.218 ± 0.016	0.205 ± 0.015	0.201 ± 0.018
		0.25	0.30	0.161 ± 0.013	0.198 ± 0.016	0.220 ± 0.016	0.229 ± 0.015	0.237 ± 0.015
		0.30	0.35	0.171 ± 0.017	0.211 ± 0.017	0.226 ± 0.013	0.239 ± 0.013	0.252 ± 0.017
		0.35	0.40	0.173 ± 0.011	0.213 ± 0.011	0.219 ± 0.011	0.231 ± 0.010	0.258 ± 0.012
		0.40	0.45	0.145 ± 0.011	0.172 ± 0.009	0.224 ± 0.011	0.218 ± 0.008	0.237 ± 0.010
		0.45	0.50	0.130 ± 0.010	0.171 ± 0.009	0.206 ± 0.010	0.211 ± 0.009	0.210 ± 0.009
		0.50	0.60	0.089 ± 0.012	0.150 ± 0.012	0.187 ± 0.013	0.179 ± 0.013	0.186 ± 0.012
		0.60	0.70	0.051 ± 0.010	0.099 ± 0.015	0.129 ± 0.019	0.128 ± 0.018	0.138 ± 0.019
		0.70	0.80	0.029 ± 0.006	0.057 ± 0.012	0.083 ± 0.017	0.080 ± 0.016	0.086 ± 0.020
0.75	0.95	0.10	0.15	0.082 ± 0.013	0.073 ± 0.014	0.093 ± 0.014	0.092 ± 0.013	0.101 ± 0.015
		0.15	0.20	0.138 ± 0.015	0.161 ± 0.013	0.158 ± 0.011	0.163 ± 0.011	0.163 ± 0.013
		0.20	0.25	0.156 ± 0.014	0.175 ± 0.012	0.181 ± 0.014	0.195 ± 0.012	0.197 ± 0.012
		0.25	0.30	0.154 ± 0.012	0.169 ± 0.010	0.185 ± 0.011	0.214 ± 0.011	0.197 ± 0.012
		0.30	0.35	0.126 ± 0.010	0.148 ± 0.010	0.192 ± 0.012	0.189 ± 0.008	0.197 ± 0.010
		0.35	0.40	0.120 ± 0.009	0.139 ± 0.008	0.165 ± 0.008	0.165 ± 0.006	0.172 ± 0.007
		0.40	0.45	0.098 ± 0.009	0.125 ± 0.007	0.136 ± 0.007	0.140 ± 0.005	0.143 ± 0.006
		0.45	0.50	0.071 ± 0.008	0.109 ± 0.008	0.118 ± 0.006	0.123 ± 0.006	0.128 ± 0.007
		0.50	0.60	0.047 ± 0.006	0.072 ± 0.009	0.099 ± 0.008	0.092 ± 0.009	0.096 ± 0.009
		0.60	0.70	0.025 ± 0.006	0.039 ± 0.008	0.063 ± 0.010	0.055 ± 0.009	0.057 ± 0.010
0.95	1.15	0.10	0.15	0.097 ± 0.012	0.087 ± 0.013	0.089 ± 0.013	0.094 ± 0.012	0.094 ± 0.013
		0.15	0.20	0.127 ± 0.013	0.144 ± 0.011	0.153 ± 0.011	0.154 ± 0.009	0.175 ± 0.012
		0.20	0.25	0.145 ± 0.011	0.180 ± 0.014	0.160 ± 0.009	0.168 ± 0.008	0.177 ± 0.010
		0.25	0.30	0.120 ± 0.010	0.154 ± 0.011	0.148 ± 0.008	0.159 ± 0.008	0.157 ± 0.007
		0.30	0.35	0.097 ± 0.009	0.107 ± 0.006	0.125 ± 0.007	0.123 ± 0.006	0.126 ± 0.006
		0.35	0.40	0.058 ± 0.006	0.089 ± 0.006	0.102 ± 0.006	0.107 ± 0.005	0.108 ± 0.005
		0.40	0.45	0.045 ± 0.004	0.071 ± 0.005	0.080 ± 0.005	0.081 ± 0.005	0.090 ± 0.005
		0.45	0.50	0.033 ± 0.004	0.055 ± 0.005	0.062 ± 0.005	0.062 ± 0.005	0.069 ± 0.006
		0.50	0.60	0.018 ± 0.003	0.034 ± 0.005	0.040 ± 0.005	0.041 ± 0.005	0.043 ± 0.006
1.15	1.35	0.10	0.15	0.093 ± 0.012	0.084 ± 0.011	0.099 ± 0.012	0.101 ± 0.013	0.099 ± 0.013
		0.15	0.20	0.121 ± 0.013	0.131 ± 0.010	0.157 ± 0.010	0.151 ± 0.008	0.134 ± 0.009
		0.20	0.25	0.120 ± 0.010	0.126 ± 0.008	0.133 ± 0.007	0.141 ± 0.006	0.137 ± 0.006
		0.25	0.30	0.078 ± 0.008	0.106 ± 0.008	0.102 ± 0.006	0.106 ± 0.005	0.115 ± 0.006
		0.30	0.35	0.048 ± 0.007	0.071 ± 0.005	0.081 ± 0.006	0.078 ± 0.003	0.078 ± 0.005
		0.35	0.40	0.031 ± 0.003	0.051 ± 0.004	0.067 ± 0.004	0.065 ± 0.003	0.066 ± 0.003
		0.40	0.45	0.025 ± 0.003	0.038 ± 0.004	0.050 ± 0.004	0.046 ± 0.004	0.049 ± 0.004
		0.45	0.50	0.016 ± 0.003	0.025 ± 0.003	0.035 ± 0.004	0.032 ± 0.003	0.035 ± 0.004
1.35	1.55	0.10	0.15	0.086 ± 0.011	0.102 ± 0.012	0.082 ± 0.011	0.101 ± 0.011	0.096 ± 0.012
		0.15	0.20	0.118 ± 0.012	0.119 ± 0.009	0.139 ± 0.011	0.135 ± 0.007	0.136 ± 0.009
		0.20	0.25	0.084 ± 0.009	0.120 ± 0.008	0.116 ± 0.007	0.110 ± 0.006	0.108 ± 0.006
		0.25	0.30	0.062 ± 0.007	0.078 ± 0.007	0.081 ± 0.007	0.081 ± 0.005	0.082 ± 0.005
		0.30	0.35	0.036 ± 0.005	0.048 ± 0.005	0.055 ± 0.004	0.054 ± 0.003	0.056 ± 0.004
		0.35	0.40	0.021 ± 0.003	0.034 ± 0.003	0.040 ± 0.003	0.039 ± 0.003	0.040 ± 0.003
		0.40	0.45	0.012 ± 0.002	0.022 ± 0.003	0.026 ± 0.003	0.026 ± 0.002	0.028 ± 0.003
		0.45	0.50	0.008 ± 0.002	0.013 ± 0.002	0.015 ± 0.003	0.019 ± 0.003	0.018 ± 0.003

TABLE III. *(Continued.)*

θ_{min} (rad)	θ_{max} (rad)	p_{min} (GeV/*c*)	p_{max} (GeV/*c*)	$d^2\sigma^{\pi^+}/(dpd\theta)$ [b/(rad GeV/*c*)]				
				3 GeV/*c*	5 GeV/*c*	8 GeV/*c*	8.9 GeV/*c*	12 GeV/*c*
1.55	1.75	0.10	0.15	0.070 ± 0.012	0.080 ± 0.010	0.085 ± 0.012	0.085 ± 0.011	0.095 ± 0.011
		0.15	0.20	0.093 ± 0.009	0.118 ± 0.009	0.116 ± 0.007	0.115 ± 0.005	0.106 ± 0.006
		0.20	0.25	0.054 ± 0.007	0.076 ± 0.007	0.076 ± 0.005	0.086 ± 0.005	0.084 ± 0.005
		0.25	0.30	0.035 ± 0.005	0.050 ± 0.005	0.057 ± 0.004	0.056 ± 0.003	0.051 ± 0.005
		0.30	0.35	0.020 ± 0.004	0.029 ± 0.003	0.037 ± 0.003	0.037 ± 0.003	0.030 ± 0.002
		0.35	0.40	0.010 ± 0.002	0.019 ± 0.002	0.026 ± 0.003	0.023 ± 0.002	0.023 ± 0.002
		0.40	0.45	0.008 ± 0.002	0.011 ± 0.002	0.015 ± 0.002	0.014 ± 0.002	0.014 ± 0.002
		0.45	0.50	0.004 ± 0.001	0.006 ± 0.001	0.008 ± 0.002	0.009 ± 0.001	0.008 ± 0.002
1.75	1.95	0.10	0.15	0.060 ± 0.009	0.090 ± 0.011	0.086 ± 0.011	0.081 ± 0.009	0.073 ± 0.010
		0.15	0.20	0.096 ± 0.011	0.096 ± 0.007	0.096 ± 0.006	0.099 ± 0.004	0.099 ± 0.006
		0.20	0.25	0.060 ± 0.009	0.047 ± 0.005	0.065 ± 0.005	0.062 ± 0.004	0.056 ± 0.005
		0.25	0.30	0.020 ± 0.005	0.036 ± 0.004	0.036 ± 0.004	0.041 ± 0.003	0.033 ± 0.002
		0.30	0.35	0.011 ± 0.002	0.018 ± 0.003	0.023 ± 0.002	0.026 ± 0.002	0.024 ± 0.002
		0.35	0.40	0.006 ± 0.002	0.011 ± 0.002	0.013 ± 0.002	0.015 ± 0.002	0.015 ± 0.002
		0.40	0.45	0.003 ± 0.001	0.005 ± 0.001	0.006 ± 0.001	0.007 ± 0.001	0.007 ± 0.002
		0.45	0.50	0.001 ± 0.001	0.003 ± 0.001	0.003 ± 0.001	0.004 ± 0.001	0.004 ± 0.001
1.95	2.15	0.10	0.15	0.063 ± 0.011	0.060 ± 0.008	0.063 ± 0.008	0.068 ± 0.007	0.055 ± 0.007
		0.15	0.20	0.063 ± 0.008	0.082 ± 0.006	0.080 ± 0.006	0.070 ± 0.004	0.073 ± 0.005
		0.20	0.25	0.033 ± 0.005	0.041 ± 0.005	0.044 ± 0.004	0.047 ± 0.003	0.047 ± 0.005
		0.25	0.30	0.013 ± 0.003	0.020 ± 0.003	0.027 ± 0.003	0.027 ± 0.002	0.026 ± 0.003
		0.30	0.35	0.008 ± 0.002	0.009 ± 0.001	0.014 ± 0.002	0.016 ± 0.001	0.013 ± 0.002
		0.35	0.40	0.004 ± 0.002	0.009 ± 0.002	0.007 ± 0.001	0.008 ± 0.001	0.008 ± 0.001
		0.40	0.45	0.002 ± 0.001	0.004 ± 0.001	0.004 ± 0.001	0.004 ± 0.001	0.004 ± 0.001
		0.45	0.50		0.002 ± 0.001	0.002 ± 0.001	0.002 ± 0.001	0.002 ± 0.001

TABLE IV. HARP results for the double-differential π^- production cross section in the laboratory system, $d^2\sigma^{\pi^-}/(dpd\theta)$, for *p*-Be interactions. Each row refers to a different $(p_{min} \leqslant p < p_{max}, \theta_{min} \leqslant \theta < \theta_{max})$ bin, where *p* and θ are the pion momentum and polar angle, respectively. The central value as well as the square root of the diagonal elements of the covariance matrix are given.

θ_{min} (rad)	θ_{max} (rad)	p_{min} (GeV/*c*)	p_{max} (GeV/*c*)	$d^2\sigma^{\pi^-}/(dpd\theta)$ [b/(rad GeV/*c*)]				
				3 GeV/*c*	5 GeV/*c*	8 GeV/*c*	8.9 GeV/*c*	12 GeV/*c*
0.35	0.55	0.15	0.20	0.048 ± 0.009	0.084 ± 0.013	0.114 ± 0.015	0.124 ± 0.015	0.124 ± 0.020
		0.20	0.25	0.068 ± 0.009	0.095 ± 0.008	0.139 ± 0.011	0.147 ± 0.009	0.170 ± 0.011
		0.25	0.30	0.060 ± 0.008	0.134 ± 0.013	0.160 ± 0.012	0.170 ± 0.011	0.182 ± 0.012
		0.30	0.35	0.079 ± 0.010	0.129 ± 0.009	0.154 ± 0.011	0.171 ± 0.009	0.186 ± 0.013
		0.35	0.40	0.069 ± 0.007	0.111 ± 0.007	0.162 ± 0.010	0.163 ± 0.008	0.184 ± 0.010
		0.40	0.45	0.066 ± 0.007	0.116 ± 0.010	0.155 ± 0.008	0.165 ± 0.009	0.168 ± 0.008
		0.45	0.50	0.057 ± 0.006	0.121 ± 0.008	0.148 ± 0.008	0.164 ± 0.008	0.162 ± 0.008
		0.50	0.60	0.053 ± 0.005	0.129 ± 0.008	0.159 ± 0.010	0.160 ± 0.009	0.172 ± 0.010
		0.60	0.70	0.051 ± 0.006	0.101 ± 0.012	0.157 ± 0.013	0.152 ± 0.013	0.170 ± 0.013
		0.70	0.80	0.039 ± 0.007	0.084 ± 0.011	0.143 ± 0.018	0.128 ± 0.014	0.155 ± 0.018
0.55	0.75	0.10	0.15	0.026 ± 0.008	0.069 ± 0.015	0.070 ± 0.016	0.073 ± 0.015	0.092 ± 0.020
		0.15	0.20	0.058 ± 0.009	0.093 ± 0.009	0.111 ± 0.010	0.123 ± 0.006	0.131 ± 0.008
		0.20	0.25	0.057 ± 0.007	0.126 ± 0.009	0.161 ± 0.012	0.148 ± 0.010	0.135 ± 0.011
		0.25	0.30	0.062 ± 0.008	0.119 ± 0.009	0.152 ± 0.008	0.153 ± 0.009	0.160 ± 0.009
		0.30	0.35	0.077 ± 0.008	0.113 ± 0.009	0.134 ± 0.008	0.150 ± 0.008	0.159 ± 0.009
		0.35	0.40	0.076 ± 0.007	0.111 ± 0.007	0.144 ± 0.010	0.146 ± 0.007	0.151 ± 0.007
		0.40	0.45	0.059 ± 0.006	0.107 ± 0.006	0.146 ± 0.008	0.137 ± 0.006	0.148 ± 0.007
		0.45	0.50	0.052 ± 0.005	0.105 ± 0.007	0.127 ± 0.006	0.129 ± 0.005	0.140 ± 0.006

TABLE IV. *(Continued.)*

θ_{min} (rad)	θ_{max} (rad)	p_{min} (GeV/c)	p_{max} (GeV/c)	$d^2\sigma^{\pi^-}/(dpd\theta)$ [b/(rad GeV/c)]				
				3 GeV/c	5 GeV/c	8 GeV/c	8.9 GeV/c	12 GeV/c
		0.50	0.60	0.049 ± 0.005	0.095 ± 0.007	0.111 ± 0.006	0.120 ± 0.006	0.131 ± 0.007
		0.60	0.70	0.041 ± 0.006	0.076 ± 0.007	0.100 ± 0.008	0.098 ± 0.010	0.111 ± 0.011
		0.70	0.80	0.027 ± 0.006	0.057 ± 0.010	0.086 ± 0.013	0.075 ± 0.011	0.096 ± 0.012
0.75	0.95	0.10	0.15	0.044 ± 0.008	0.056 ± 0.009	0.070 ± 0.010	0.069 ± 0.009	0.079 ± 0.011
		0.15	0.20	0.091 ± 0.011	0.107 ± 0.010	0.120 ± 0.010	0.130 ± 0.008	0.134 ± 0.010
		0.20	0.25	0.078 ± 0.008	0.114 ± 0.008	0.144 ± 0.010	0.139 ± 0.007	0.136 ± 0.008
		0.25	0.30	0.073 ± 0.008	0.111 ± 0.007	0.119 ± 0.006	0.135 ± 0.007	0.141 ± 0.008
		0.30	0.35	0.063 ± 0.006	0.096 ± 0.006	0.110 ± 0.007	0.123 ± 0.005	0.132 ± 0.008
		0.35	0.40	0.060 ± 0.006	0.084 ± 0.005	0.109 ± 0.006	0.108 ± 0.004	0.115 ± 0.005
		0.40	0.45	0.048 ± 0.005	0.080 ± 0.005	0.091 ± 0.004	0.099 ± 0.003	0.099 ± 0.004
		0.45	0.50	0.036 ± 0.004	0.074 ± 0.004	0.087 ± 0.005	0.091 ± 0.003	0.091 ± 0.004
		0.50	0.60	0.033 ± 0.004	0.060 ± 0.005	0.075 ± 0.005	0.078 ± 0.004	0.080 ± 0.005
		0.60	0.70	0.023 ± 0.004	0.042 ± 0.006	0.060 ± 0.006	0.058 ± 0.006	0.062 ± 0.006
0.95	1.15	0.10	0.15	0.038 ± 0.007	0.066 ± 0.009	0.070 ± 0.009	0.077 ± 0.008	0.072 ± 0.009
		0.15	0.20	0.069 ± 0.008	0.120 ± 0.011	0.109 ± 0.009	0.131 ± 0.008	0.119 ± 0.008
		0.20	0.25	0.065 ± 0.008	0.107 ± 0.008	0.117 ± 0.008	0.126 ± 0.006	0.122 ± 0.007
		0.25	0.30	0.061 ± 0.006	0.090 ± 0.008	0.116 ± 0.007	0.114 ± 0.005	0.114 ± 0.006
		0.30	0.35	0.065 ± 0.007	0.076 ± 0.005	0.097 ± 0.005	0.098 ± 0.004	0.096 ± 0.004
		0.35	0.40	0.049 ± 0.006	0.062 ± 0.004	0.088 ± 0.004	0.079 ± 0.003	0.084 ± 0.004
		0.40	0.45	0.034 ± 0.004	0.055 ± 0.004	0.068 ± 0.005	0.068 ± 0.003	0.070 ± 0.004
		0.45	0.50	0.025 ± 0.004	0.043 ± 0.004	0.054 ± 0.003	0.058 ± 0.002	0.059 ± 0.003
		0.50	0.60	0.018 ± 0.003	0.029 ± 0.003	0.044 ± 0.003	0.044 ± 0.003	0.046 ± 0.003
1.15	1.35	0.10	0.15	0.039 ± 0.007	0.073 ± 0.010	0.085 ± 0.008	0.075 ± 0.007	0.085 ± 0.009
		0.15	0.20	0.067 ± 0.009	0.101 ± 0.007	0.105 ± 0.007	0.122 ± 0.008	0.117 ± 0.008
		0.20	0.25	0.088 ± 0.010	0.089 ± 0.006	0.100 ± 0.006	0.109 ± 0.004	0.112 ± 0.006
		0.25	0.30	0.059 ± 0.008	0.077 ± 0.005	0.087 ± 0.005	0.091 ± 0.004	0.092 ± 0.005
		0.30	0.35	0.034 ± 0.005	0.050 ± 0.005	0.072 ± 0.004	0.069 ± 0.003	0.075 ± 0.004
		0.35	0.40	0.022 ± 0.003	0.036 ± 0.003	0.055 ± 0.004	0.055 ± 0.002	0.057 ± 0.003
		0.40	0.45	0.015 ± 0.002	0.034 ± 0.003	0.043 ± 0.003	0.044 ± 0.002	0.043 ± 0.003
		0.45	0.50	0.012 ± 0.002	0.031 ± 0.003	0.036 ± 0.002	0.035 ± 0.002	0.034 ± 0.002
1.35	1.55	0.10	0.15	0.057 ± 0.009	0.073 ± 0.009	0.061 ± 0.007	0.080 ± 0.008	0.078 ± 0.009
		0.15	0.20	0.061 ± 0.007	0.098 ± 0.008	0.106 ± 0.009	0.109 ± 0.006	0.110 ± 0.009
		0.20	0.25	0.063 ± 0.007	0.077 ± 0.006	0.102 ± 0.006	0.095 ± 0.004	0.097 ± 0.006
		0.25	0.30	0.034 ± 0.005	0.060 ± 0.005	0.077 ± 0.005	0.070 ± 0.004	0.074 ± 0.005
		0.30	0.35	0.027 ± 0.004	0.043 ± 0.005	0.051 ± 0.004	0.050 ± 0.002	0.049 ± 0.003
		0.35	0.40	0.019 ± 0.003	0.027 ± 0.003	0.036 ± 0.003	0.037 ± 0.002	0.038 ± 0.002
		0.40	0.45	0.015 ± 0.002	0.022 ± 0.002	0.026 ± 0.002	0.029 ± 0.002	0.029 ± 0.003
		0.45	0.50	0.010 ± 0.002	0.019 ± 0.002	0.020 ± 0.002	0.021 ± 0.002	0.021 ± 0.002
1.55	1.75	0.10	0.15	0.042 ± 0.007	0.068 ± 0.008	0.072 ± 0.009	0.073 ± 0.008	0.084 ± 0.010
		0.15	0.20	0.067 ± 0.009	0.085 ± 0.007	0.090 ± 0.006	0.095 ± 0.005	0.090 ± 0.006
		0.20	0.25	0.052 ± 0.009	0.073 ± 0.006	0.072 ± 0.005	0.078 ± 0.004	0.078 ± 0.005
		0.25	0.30	0.016 ± 0.003	0.057 ± 0.005	0.055 ± 0.005	0.055 ± 0.003	0.054 ± 0.004
		0.30	0.35	0.012 ± 0.002	0.035 ± 0.005	0.038 ± 0.003	0.037 ± 0.002	0.041 ± 0.003
		0.35	0.40	0.014 ± 0.003	0.020 ± 0.003	0.032 ± 0.003	0.027 ± 0.002	0.027 ± 0.003
		0.40	0.45	0.009 ± 0.002	0.012 ± 0.002	0.021 ± 0.002	0.020 ± 0.001	0.018 ± 0.002
		0.45	0.50	0.006 ± 0.002	0.008 ± 0.001	0.015 ± 0.002	0.013 ± 0.001	0.014 ± 0.001
1.75	1.95	0.10	0.15	0.038 ± 0.007	0.053 ± 0.006	0.063 ± 0.008	0.063 ± 0.006	0.060 ± 0.008
		0.15	0.20	0.052 ± 0.007	0.067 ± 0.006	0.081 ± 0.006	0.086 ± 0.004	0.085 ± 0.006
		0.20	0.25	0.029 ± 0.006	0.053 ± 0.005	0.054 ± 0.004	0.061 ± 0.003	0.063 ± 0.004
		0.25	0.30	0.020 ± 0.004	0.037 ± 0.004	0.038 ± 0.003	0.039 ± 0.003	0.041 ± 0.003
		0.30	0.35	0.013 ± 0.004	0.019 ± 0.003	0.027 ± 0.002	0.024 ± 0.002	0.031 ± 0.002

TABLE IV. *(Continued.)*

θ_{min} (rad)	θ_{max} (rad)	p_{min} (GeV/c)	p_{max} (GeV/c)	$d^2\sigma^{\pi^-}/(dpd\theta)$ [b/(rad GeV/c)]				
				3 GeV/c	5 GeV/c	8 GeV/c	8.9 GeV/c	12 GeV/c
		0.35	0.40	0.006 ± 0.002	0.013 ± 0.002	0.018 ± 0.002	0.017 ± 0.001	0.019 ± 0.003
		0.40	0.45	0.004 ± 0.001	0.008 ± 0.001	0.012 ± 0.001	0.012 ± 0.001	0.010 ± 0.002
		0.45	0.50	0.003 ± 0.001	0.005 ± 0.001	0.008 ± 0.001	0.009 ± 0.001	0.007 ± 0.001
1.95	2.15	0.10	0.15	0.049 ± 0.008	0.047 ± 0.007	0.062 ± 0.007	0.055 ± 0.006	0.047 ± 0.005
		0.15	0.20	0.038 ± 0.006	0.068 ± 0.006	0.061 ± 0.005	0.067 ± 0.003	0.068 ± 0.006
		0.20	0.25	0.023 ± 0.005	0.048 ± 0.005	0.046 ± 0.004	0.049 ± 0.002	0.044 ± 0.005
		0.25	0.30	0.009 ± 0.003	0.026 ± 0.003	0.025 ± 0.003	0.029 ± 0.002	0.023 ± 0.002
		0.30	0.35	0.005 ± 0.002	0.015 ± 0.002	0.017 ± 0.002	0.017 ± 0.001	0.019 ± 0.002
		0.35	0.40	0.001 ± 0.001	0.009 ± 0.001	0.012 ± 0.001	0.013 ± 0.001	0.012 ± 0.001
		0.40	0.45		0.006 ± 0.001	0.009 ± 0.002	0.008 ± 0.001	0.009 ± 0.001
		0.45	0.50		0.003 ± 0.001	0.005 ± 0.001	0.005 ± 0.001	0.006 ± 0.001

TABLE V. HARP results for the double-differential π^+ production cross section in the laboratory system, $d^2\sigma^{\pi^+}/(dpd\theta)$, for p-C interactions. Each row refers to a different ($p_{min} \leqslant p < p_{max}$, $\theta_{min} \leqslant \theta < \theta_{max}$) bin, where p and θ are the pion momentum and polar angle, respectively. The central value as well as the square root of the diagonal elements of the covariance matrix are given.

θ_{min} (rad)	θ_{max} (rad)	p_{min} (GeV/c)	p_{max} (GeV/c)	$d^2\sigma^{\pi^+}/(dpd\theta)$ [b/(rad GeV/c)]			
				3 GeV/c	5 GeV/c	8 GeV/c	12 GeV/c
0.35	0.55	0.15	0.20	0.05 ± 0.02	0.12 ± 0.03	0.15 ± 0.03	0.14 ± 0.03
		0.20	0.25	0.10 ± 0.02	0.18 ± 0.02	0.20 ± 0.02	0.22 ± 0.02
		0.25	0.30	0.15 ± 0.02	0.23 ± 0.02	0.28 ± 0.03	0.28 ± 0.02
		0.30	0.35	0.16 ± 0.02	0.25 ± 0.03	0.30 ± 0.02	0.35 ± 0.03
		0.35	0.40	0.18 ± 0.02	0.29 ± 0.02	0.33 ± 0.03	0.37 ± 0.02
		0.40	0.45	0.19 ± 0.01	0.29 ± 0.02	0.35 ± 0.02	0.35 ± 0.02
		0.45	0.50	0.19 ± 0.01	0.29 ± 0.01	0.36 ± 0.02	0.39 ± 0.02
		0.50	0.60	0.18 ± 0.01	0.28 ± 0.01	0.36 ± 0.02	0.38 ± 0.02
		0.60	0.70	0.13 ± 0.02	0.25 ± 0.02	0.33 ± 0.03	0.33 ± 0.03
		0.70	0.80	0.07 ± 0.02	0.18 ± 0.03	0.26 ± 0.04	0.26 ± 0.04
0.55	0.75	0.10	0.15	0.09 ± 0.03	0.09 ± 0.03	0.10 ± 0.03	0.10 ± 0.03
		0.15	0.20	0.13 ± 0.02	0.18 ± 0.02	0.19 ± 0.02	0.17 ± 0.02
		0.20	0.25	0.20 ± 0.02	0.22 ± 0.02	0.26 ± 0.02	0.26 ± 0.02
		0.25	0.30	0.22 ± 0.02	0.27 ± 0.02	0.31 ± 0.03	0.30 ± 0.02
		0.30	0.35	0.24 ± 0.02	0.26 ± 0.01	0.29 ± 0.02	0.32 ± 0.02
		0.35	0.40	0.21 ± 0.02	0.26 ± 0.01	0.30 ± 0.02	0.32 ± 0.01
		0.40	0.45	0.18 ± 0.01	0.23 ± 0.01	0.28 ± 0.01	0.30 ± 0.01
		0.45	0.50	0.18 ± 0.01	0.21 ± 0.01	0.26 ± 0.01	0.28 ± 0.01
		0.50	0.60	0.11 ± 0.02	0.17 ± 0.01	0.22 ± 0.01	0.24 ± 0.01
		0.60	0.70	0.08 ± 0.01	0.12 ± 0.01	0.17 ± 0.02	0.18 ± 0.02
		0.70	0.80	0.04 ± 0.01	0.07 ± 0.01	0.12 ± 0.02	0.12 ± 0.02
0.75	0.95	0.10	0.15	0.09 ± 0.02	0.12 ± 0.02	0.12 ± 0.02	0.12 ± 0.02
		0.15	0.20	0.17 ± 0.02	0.22 ± 0.02	0.21 ± 0.02	0.20 ± 0.02
		0.20	0.25	0.21 ± 0.02	0.25 ± 0.02	0.24 ± 0.02	0.28 ± 0.02
		0.25	0.30	0.19 ± 0.02	0.23 ± 0.01	0.25 ± 0.02	0.27 ± 0.01
		0.30	0.35	0.20 ± 0.02	0.21 ± 0.01	0.24 ± 0.01	0.24 ± 0.01
		0.35	0.40	0.14 ± 0.02	0.17 ± 0.01	0.22 ± 0.01	0.24 ± 0.01
		0.40	0.45	0.10 ± 0.01	0.15 ± 0.01	0.18 ± 0.01	0.20 ± 0.01

TABLE V. *(Continued.)*

θ_{min} (rad)	θ_{max} (rad)	p_{min} (GeV/c)	p_{max} (GeV/c)	$d^2\sigma^{\pi^+}/(dpd\theta)$ [b/(rad GeV/c)]			
				3 GeV/c	5 GeV/c	8 GeV/c	12 GeV/c
		0.45	0.50	0.08 ± 0.01	0.13 ± 0.01	0.16 ± 0.01	0.17 ± 0.01
		0.50	0.60	0.05 ± 0.01	0.09 ± 0.01	0.12 ± 0.01	0.13 ± 0.01
		0.60	0.70	0.03 ± 0.01	0.05 ± 0.01	0.07 ± 0.01	0.07 ± 0.01
0.95	1.15	0.10	0.15	0.14 ± 0.02	0.13 ± 0.02	0.12 ± 0.02	0.15 ± 0.02
		0.15	0.20	0.22 ± 0.02	0.20 ± 0.02	0.23 ± 0.02	0.23 ± 0.02
		0.20	0.25	0.19 ± 0.01	0.21 ± 0.01	0.24 ± 0.01	0.23 ± 0.01
		0.25	0.30	0.16 ± 0.01	0.18 ± 0.01	0.22 ± 0.01	0.21 ± 0.01
		0.30	0.35	0.10 ± 0.01	0.15 ± 0.01	0.16 ± 0.01	0.17 ± 0.01
		0.35	0.40	0.07 ± 0.01	0.12 ± 0.01	0.13 ± 0.01	0.14 ± 0.01
		0.40	0.45	0.06 ± 0.01	0.09 ± 0.01	0.11 ± 0.01	0.11 ± 0.01
		0.45	0.50	0.04 ± 0.01	0.07 ± 0.01	0.09 ± 0.01	0.09 ± 0.01
		0.50	0.60	0.02 ± 0.01	0.04 ± 0.01	0.06 ± 0.01	0.05 ± 0.01
1.15	1.35	0.10	0.15	0.14 ± 0.02	0.15 ± 0.02	0.14 ± 0.02	0.14 ± 0.02
		0.15	0.20	0.18 ± 0.02	0.20 ± 0.01	0.21 ± 0.01	0.21 ± 0.01
		0.20	0.25	0.16 ± 0.01	0.17 ± 0.01	0.20 ± 0.01	0.18 ± 0.01
		0.25	0.30	0.09 ± 0.01	0.13 ± 0.01	0.15 ± 0.01	0.16 ± 0.01
		0.30	0.35	0.07 ± 0.01	0.10 ± 0.01	0.12 ± 0.01	0.11 ± 0.01
		0.35	0.40	0.06 ± 0.01	0.07 ± 0.01	0.08 ± 0.01	0.09 ± 0.01
		0.40	0.45	0.03 ± 0.01	0.05 ± 0.01	0.06 ± 0.01	0.07 ± 0.01
		0.45	0.50	0.02 ± 0.01	0.03 ± 0.01	0.04 ± 0.01	0.05 ± 0.01
1.35	1.55	0.10	0.15	0.13 ± 0.02	0.14 ± 0.02	0.14 ± 0.02	0.14 ± 0.02
		0.15	0.20	0.19 ± 0.02	0.18 ± 0.01	0.20 ± 0.01	0.20 ± 0.01
		0.20	0.25	0.14 ± 0.01	0.15 ± 0.01	0.15 ± 0.01	0.15 ± 0.01
		0.25	0.30	0.10 ± 0.01	0.12 ± 0.01	0.10 ± 0.01	0.12 ± 0.01
		0.30	0.35	0.05 ± 0.01	0.07 ± 0.01	0.08 ± 0.01	0.08 ± 0.01
		0.35	0.40	0.03 ± 0.01	0.04 ± 0.01	0.06 ± 0.01	0.06 ± 0.01
		0.40	0.45	0.02 ± 0.01	0.03 ± 0.01	0.04 ± 0.01	0.04 ± 0.01
		0.45	0.50	0.01 ± 0.01	0.02 ± 0.01	0.02 ± 0.01	0.02 ± 0.01
1.55	1.75	0.10	0.15	0.14 ± 0.02	0.13 ± 0.02	0.13 ± 0.02	0.13 ± 0.02
		0.15	0.20	0.18 ± 0.02	0.15 ± 0.01	0.16 ± 0.01	0.17 ± 0.01
		0.20	0.25	0.09 ± 0.01	0.11 ± 0.01	0.12 ± 0.01	0.11 ± 0.01
		0.25	0.30	0.05 ± 0.01	0.07 ± 0.01	0.07 ± 0.01	0.08 ± 0.01
		0.30	0.35	0.04 ± 0.01	0.04 ± 0.01	0.05 ± 0.01	0.05 ± 0.01
		0.35	0.40	0.02 ± 0.01	0.03 ± 0.01	0.03 ± 0.01	0.04 ± 0.01
		0.40	0.45	0.01 ± 0.01	0.01 ± 0.01	0.02 ± 0.01	0.02 ± 0.01
		0.45	0.50			0.01 ± 0.01	0.01 ± 0.01
1.75	1.95	0.10	0.15	0.12 ± 0.02	0.13 ± 0.01	0.12 ± 0.02	0.12 ± 0.01
		0.15	0.20	0.13 ± 0.01	0.13 ± 0.01	0.14 ± 0.01	0.14 ± 0.01
		0.20	0.25	0.08 ± 0.01	0.09 ± 0.01	0.10 ± 0.01	0.09 ± 0.01
		0.25	0.30	0.03 ± 0.01	0.05 ± 0.01	0.06 ± 0.01	0.06 ± 0.01
		0.30	0.35	0.02 ± 0.01	0.03 ± 0.01	0.03 ± 0.01	0.03 ± 0.01
		0.35	0.40		0.01 ± 0.01	0.02 ± 0.01	0.02 ± 0.01
		0.40	0.45			0.01 ± 0.01	0.01 ± 0.01
		0.45	0.50				
1.95	2.15	0.10	0.15	0.10 ± 0.01	0.10 ± 0.01	0.11 ± 0.01	0.10 ± 0.01
		0.15	0.20	0.10 ± 0.01	0.11 ± 0.01	0.11 ± 0.01	0.11 ± 0.01
		0.20	0.25	0.06 ± 0.01	0.06 ± 0.01	0.06 ± 0.01	0.07 ± 0.01
		0.25	0.30	0.02 ± 0.01	0.03 ± 0.01	0.04 ± 0.01	0.04 ± 0.01
		0.30	0.35	0.01 ± 0.01	0.02 ± 0.01	0.02 ± 0.01	0.02 ± 0.01
		0.35	0.40		0.01 ± 0.01	0.01 ± 0.01	0.01 ± 0.01
		0.40	0.45				
		0.45	0.50				

TABLE VI. HARP results for the double-differential π^- production cross section in the laboratory system, $d^2\sigma^{\pi^-}/(dpd\theta)$, for p-C interactions. Each row refers to a different ($p_{\min} \leqslant p < p_{\max}, \theta_{\min} \leqslant \theta < \theta_{\max}$) bin, where p and θ are the pion momentum and polar angle, respectively. The central value as well as the square root of the diagonal elements of the covariance matrix are given.

$\theta_{\min}$ (rad)	$\theta_{\max}$ (rad)	$p_{\min}$ (GeV/c)	$p_{\max}$ (GeV/c)	$d^2\sigma^{\pi^-}/(dpd\theta)$ [b/(rad GeV/c)]			
				3 GeV/c	5 GeV/c	8 GeV/c	12 GeV/c
0.35	0.55	0.15	0.20	0.04 ± 0.02	0.08 ± 0.03	0.12 ± 0.03	0.12 ± 0.03
		0.20	0.25	0.05 ± 0.02	0.12 ± 0.02	0.16 ± 0.02	0.18 ± 0.02
		0.25	0.30	0.06 ± 0.01	0.13 ± 0.01	0.19 ± 0.01	0.21 ± 0.02
		0.30	0.35	0.09 ± 0.01	0.13 ± 0.01	0.20 ± 0.01	0.24 ± 0.01
		0.35	0.40	0.08 ± 0.01	0.14 ± 0.01	0.20 ± 0.01	0.22 ± 0.01
		0.40	0.45	0.07 ± 0.01	0.13 ± 0.01	0.19 ± 0.01	0.22 ± 0.01
		0.45	0.50	0.07 ± 0.01	0.12 ± 0.01	0.18 ± 0.01	0.22 ± 0.01
		0.50	0.60	0.06 ± 0.01	0.13 ± 0.01	0.18 ± 0.01	0.22 ± 0.01
		0.60	0.70	0.05 ± 0.01	0.12 ± 0.01	0.18 ± 0.01	0.20 ± 0.01
		0.70	0.80	0.04 ± 0.01	0.10 ± 0.01	0.16 ± 0.02	0.18 ± 0.02
0.55	0.75	0.10	0.15	0.03 ± 0.02	0.06 ± 0.02	0.06 ± 0.02	0.09 ± 0.03
		0.15	0.20	0.08 ± 0.02	0.10 ± 0.02	0.15 ± 0.02	0.15 ± 0.02
		0.20	0.25	0.10 ± 0.01	0.15 ± 0.01	0.17 ± 0.01	0.18 ± 0.01
		0.25	0.30	0.09 ± 0.01	0.15 ± 0.01	0.18 ± 0.01	0.20 ± 0.01
		0.30	0.35	0.09 ± 0.01	0.13 ± 0.01	0.17 ± 0.01	0.20 ± 0.01
		0.35	0.40	0.08 ± 0.01	0.13 ± 0.01	0.17 ± 0.01	0.18 ± 0.01
		0.40	0.45	0.08 ± 0.01	0.11 ± 0.01	0.17 ± 0.01	0.18 ± 0.01
		0.45	0.50	0.07 ± 0.01	0.10 ± 0.01	0.15 ± 0.01	0.18 ± 0.01
		0.50	0.60	0.05 ± 0.01	0.10 ± 0.01	0.14 ± 0.01	0.17 ± 0.01
		0.60	0.70	0.04 ± 0.01	0.08 ± 0.01	0.12 ± 0.01	0.13 ± 0.01
		0.70	0.80	0.03 ± 0.01	0.06 ± 0.01	0.10 ± 0.01	0.11 ± 0.01
0.75	0.95	0.10	0.15	0.04 ± 0.02	0.05 ± 0.01	0.07 ± 0.01	0.09 ± 0.02
		0.15	0.20	0.08 ± 0.01	0.12 ± 0.01	0.17 ± 0.01	0.17 ± 0.02
		0.20	0.25	0.09 ± 0.01	0.13 ± 0.01	0.17 ± 0.01	0.18 ± 0.01
		0.25	0.30	0.08 ± 0.01	0.12 ± 0.01	0.18 ± 0.01	0.18 ± 0.01
		0.30	0.35	0.07 ± 0.01	0.12 ± 0.01	0.15 ± 0.01	0.17 ± 0.01
		0.35	0.40	0.07 ± 0.01	0.11 ± 0.01	0.15 ± 0.01	0.15 ± 0.01
		0.40	0.45	0.05 ± 0.01	0.10 ± 0.01	0.13 ± 0.01	0.13 ± 0.01
		0.45	0.50	0.04 ± 0.01	0.08 ± 0.01	0.11 ± 0.01	0.12 ± 0.01
		0.50	0.60	0.03 ± 0.01	0.06 ± 0.01	0.09 ± 0.01	0.10 ± 0.01
		0.60	0.70	0.02 ± 0.01	0.05 ± 0.01	0.07 ± 0.01	0.07 ± 0.01
0.95	1.15	0.10	0.15	0.05 ± 0.01	0.07 ± 0.01	0.10 ± 0.01	0.10 ± 0.01
		0.15	0.20	0.09 ± 0.01	0.14 ± 0.01	0.15 ± 0.01	0.16 ± 0.01
		0.20	0.25	0.09 ± 0.01	0.12 ± 0.01	0.14 ± 0.01	0.16 ± 0.01
		0.25	0.30	0.09 ± 0.01	0.12 ± 0.01	0.13 ± 0.01	0.15 ± 0.01
		0.30	0.35	0.06 ± 0.01	0.09 ± 0.01	0.12 ± 0.01	0.13 ± 0.01
		0.35	0.40	0.05 ± 0.01	0.07 ± 0.01	0.10 ± 0.01	0.11 ± 0.01
		0.40	0.45	0.03 ± 0.01	0.06 ± 0.01	0.08 ± 0.01	0.09 ± 0.01
		0.45	0.50	0.03 ± 0.01	0.05 ± 0.01	0.07 ± 0.01	0.08 ± 0.01
		0.50	0.60	0.02 ± 0.01	0.04 ± 0.01	0.05 ± 0.01	0.06 ± 0.01
1.15	1.35	0.10	0.15	0.07 ± 0.02	0.08 ± 0.01	0.10 ± 0.01	0.11 ± 0.01
		0.15	0.20	0.11 ± 0.01	0.13 ± 0.01	0.15 ± 0.01	0.17 ± 0.01
		0.20	0.25	0.07 ± 0.01	0.12 ± 0.01	0.14 ± 0.01	0.14 ± 0.01
		0.25	0.30	0.06 ± 0.01	0.10 ± 0.01	0.12 ± 0.01	0.12 ± 0.01
		0.30	0.35	0.04 ± 0.01	0.07 ± 0.01	0.09 ± 0.01	0.09 ± 0.01
		0.35	0.40	0.02 ± 0.01	0.05 ± 0.01	0.07 ± 0.01	0.08 ± 0.01
		0.40	0.45	0.02 ± 0.01	0.04 ± 0.01	0.06 ± 0.01	0.06 ± 0.01
		0.45	0.50	0.02 ± 0.01	0.03 ± 0.01	0.04 ± 0.01	0.05 ± 0.01
1.35	1.55	0.10	0.15	0.06 ± 0.01	0.09 ± 0.01	0.10 ± 0.01	0.11 ± 0.01
		0.15	0.20	0.08 ± 0.01	0.12 ± 0.01	0.14 ± 0.01	0.13 ± 0.01
		0.20	0.25	0.05 ± 0.01	0.10 ± 0.01	0.11 ± 0.01	0.11 ± 0.01

TABLE VI. *(Continued.)*

$\theta_{\min}$ (rad)	$\theta_{\max}$ (rad)	$p_{\min}$ (GeV/c)	$p_{\max}$ (GeV/c)	$d^2\sigma^{\pi^-}/(dpd\theta)$ [b/(rad GeV/c)]			
				3 GeV/c	5 GeV/c	8 GeV/c	12 GeV/c
		0.25	0.30	0.05 ± 0.01	0.08 ± 0.01	0.08 ± 0.01	0.09 ± 0.01
		0.30	0.35	0.04 ± 0.01	0.05 ± 0.01	0.06 ± 0.01	0.06 ± 0.01
		0.35	0.40	0.03 ± 0.01	0.04 ± 0.01	0.05 ± 0.01	0.05 ± 0.01
		0.40	0.45	0.02 ± 0.01	0.03 ± 0.01	0.04 ± 0.01	0.03 ± 0.01
		0.45	0.50	0.01 ± 0.01	0.02 ± 0.01	0.03 ± 0.01	0.03 ± 0.01
1.55	1.75	0.10	0.15	0.07 ± 0.01	0.08 ± 0.01	0.09 ± 0.01	0.10 ± 0.01
		0.15	0.20	0.09 ± 0.01	0.12 ± 0.01	0.12 ± 0.01	0.13 ± 0.01
		0.20	0.25	0.06 ± 0.01	0.07 ± 0.01	0.09 ± 0.01	0.09 ± 0.01
		0.25	0.30	0.03 ± 0.01	0.05 ± 0.01	0.06 ± 0.01	0.07 ± 0.01
		0.30	0.35	0.01 ± 0.01	0.04 ± 0.01	0.04 ± 0.01	0.05 ± 0.01
		0.35	0.40		0.03 ± 0.01	0.04 ± 0.01	0.03 ± 0.01
		0.40	0.45		0.02 ± 0.01	0.03 ± 0.01	0.02 ± 0.01
		0.45	0.50		0.01 ± 0.01	0.02 ± 0.01	0.02 ± 0.01
1.75	1.95	0.10	0.15	0.07 ± 0.01	0.08 ± 0.01	0.09 ± 0.01	0.08 ± 0.01
		0.15	0.20	0.08 ± 0.01	0.10 ± 0.01	0.10 ± 0.01	0.11 ± 0.01
		0.20	0.25	0.04 ± 0.01	0.07 ± 0.01	0.07 ± 0.01	0.07 ± 0.01
		0.25	0.30	0.03 ± 0.01	0.04 ± 0.01	0.05 ± 0.01	0.05 ± 0.01
		0.30	0.35	0.02 ± 0.01	0.03 ± 0.01	0.03 ± 0.01	0.03 ± 0.01
		0.35	0.40	0.01 ± 0.01	0.02 ± 0.01	0.02 ± 0.01	0.02 ± 0.01
		0.40	0.45		0.01 ± 0.01	0.02 ± 0.01	0.02 ± 0.01
		0.45	0.50			0.01 ± 0.01	0.01 ± 0.01
1.95	2.15	0.10	0.15	0.04 ± 0.01	0.06 ± 0.01	0.07 ± 0.01	0.07 ± 0.01
		0.15	0.20	0.07 ± 0.01	0.09 ± 0.01	0.08 ± 0.01	0.09 ± 0.01
		0.20	0.25	0.04 ± 0.01	0.05 ± 0.01	0.06 ± 0.01	0.06 ± 0.01
		0.25	0.30	0.01 ± 0.01	0.03 ± 0.01	0.04 ± 0.01	0.04 ± 0.01
		0.30	0.35		0.02 ± 0.01	0.02 ± 0.01	0.02 ± 0.01
		0.35	0.40		0.01 ± 0.01	0.01 ± 0.01	0.01 ± 0.01
		0.40	0.45				0.01 ± 0.01
		0.45	0.50				

TABLE VII. HARP results for the double-differential π^+ production cross section in the laboratory system, $d^2\sigma^{\pi^+}/(dpd\theta)$, for p-Al interactions. Each row refers to a different ($p_{\min} \leqslant p < p_{\max}$, $\theta_{\min} \leqslant \theta < \theta_{\max}$) bin, where p and θ are the pion momentum and polar angle, respectively. The central value as well as the square root of the diagonal elements of the covariance matrix are given.

$\theta_{\min}$ (rad)	$\theta_{\max}$ (rad)	$p_{\min}$ (GeV/c)	$p_{\max}$ (GeV/c)	$d^2\sigma^{\pi^+}/(dpd\theta)$ [b/(rad GeV/c)]				
				3 GeV/c	5 GeV/c	8 GeV/c	12 GeV/c	12.9 GeV/c
0.35	0.55	0.15	0.20	0.156 ± 0.027	0.296 ± 0.045	0.351 ± 0.048	0.407 ± 0.066	0.424 ± 0.064
		0.20	0.25	0.203 ± 0.025	0.354 ± 0.030	0.488 ± 0.044	0.559 ± 0.038	0.573 ± 0.038
		0.25	0.30	0.226 ± 0.025	0.454 ± 0.038	0.549 ± 0.037	0.667 ± 0.053	0.635 ± 0.042
		0.30	0.35	0.282 ± 0.034	0.503 ± 0.036	0.621 ± 0.043	0.662 ± 0.038	0.716 ± 0.051
		0.35	0.40	0.297 ± 0.024	0.469 ± 0.027	0.615 ± 0.033	0.723 ± 0.047	0.753 ± 0.043
		0.40	0.45	0.308 ± 0.025	0.484 ± 0.027	0.678 ± 0.045	0.758 ± 0.046	0.784 ± 0.034
		0.45	0.50	0.314 ± 0.024	0.515 ± 0.030	0.696 ± 0.033	0.779 ± 0.038	0.747 ± 0.029
		0.50	0.60	0.297 ± 0.027	0.546 ± 0.032	0.644 ± 0.035	0.761 ± 0.044	0.760 ± 0.036
		0.60	0.70	0.199 ± 0.030	0.439 ± 0.048	0.616 ± 0.058	0.739 ± 0.076	0.708 ± 0.072
		0.70	0.80	0.112 ± 0.025	0.315 ± 0.054	0.503 ± 0.074	0.569 ± 0.091	0.555 ± 0.095
0.55	0.75	0.10	0.15	0.189 ± 0.046	0.261 ± 0.061	0.225 ± 0.054	0.298 ± 0.074	0.277 ± 0.070
		0.15	0.20	0.253 ± 0.029	0.372 ± 0.026	0.395 ± 0.036	0.419 ± 0.035	0.447 ± 0.037
		0.20	0.25	0.318 ± 0.031	0.477 ± 0.046	0.570 ± 0.045	0.579 ± 0.041	0.634 ± 0.037

TABLE VII. *(Continued.)*

θ_{min} (rad)	θ_{max} (rad)	p_{min} (GeV/c)	p_{max} (GeV/c)	$d^2\sigma^{\pi^+}/(dpd\theta)$ [b/(rad GeV/c)]				
				3 GeV/c	5 GeV/c	8 GeV/c	12 GeV/c	12.9 GeV/c
		0.25	0.30	0.377 ± 0.037	0.476 ± 0.027	0.615 ± 0.041	0.621 ± 0.039	0.647 ± 0.040
		0.30	0.35	0.285 ± 0.025	0.465 ± 0.026	0.583 ± 0.027	0.607 ± 0.028	0.639 ± 0.031
		0.35	0.40	0.307 ± 0.032	0.432 ± 0.027	0.580 ± 0.028	0.622 ± 0.038	0.679 ± 0.032
		0.40	0.45	0.305 ± 0.022	0.424 ± 0.021	0.523 ± 0.025	0.646 ± 0.029	0.625 ± 0.021
		0.45	0.50	0.268 ± 0.021	0.407 ± 0.020	0.504 ± 0.024	0.587 ± 0.028	0.577 ± 0.019
		0.50	0.60	0.186 ± 0.024	0.333 ± 0.025	0.485 ± 0.029	0.501 ± 0.035	0.496 ± 0.030
		0.60	0.70	0.116 ± 0.021	0.227 ± 0.030	0.340 ± 0.049	0.361 ± 0.053	0.374 ± 0.049
		0.70	0.80	0.054 ± 0.019	0.147 ± 0.028	0.233 ± 0.044	0.227 ± 0.043	0.252 ± 0.047
0.75	0.95	0.10	0.15	0.245 ± 0.038	0.302 ± 0.048	0.276 ± 0.048	0.292 ± 0.047	0.317 ± 0.051
		0.15	0.20	0.337 ± 0.032	0.410 ± 0.028	0.479 ± 0.032	0.469 ± 0.041	0.534 ± 0.035
		0.20	0.25	0.367 ± 0.032	0.443 ± 0.024	0.554 ± 0.035	0.548 ± 0.034	0.620 ± 0.039
		0.25	0.30	0.355 ± 0.027	0.437 ± 0.029	0.542 ± 0.028	0.598 ± 0.038	0.573 ± 0.024
		0.30	0.35	0.253 ± 0.021	0.381 ± 0.021	0.460 ± 0.022	0.519 ± 0.022	0.532 ± 0.019
		0.35	0.40	0.216 ± 0.017	0.347 ± 0.017	0.424 ± 0.020	0.439 ± 0.018	0.489 ± 0.017
		0.40	0.45	0.180 ± 0.017	0.280 ± 0.017	0.362 ± 0.017	0.392 ± 0.018	0.413 ± 0.015
		0.45	0.50	0.137 ± 0.014	0.242 ± 0.014	0.313 ± 0.017	0.346 ± 0.016	0.358 ± 0.017
		0.50	0.60	0.094 ± 0.012	0.180 ± 0.018	0.253 ± 0.021	0.269 ± 0.022	0.287 ± 0.025
		0.60	0.70	0.052 ± 0.010	0.104 ± 0.019	0.165 ± 0.028	0.178 ± 0.029	0.167 ± 0.027
0.95	1.15	0.10	0.15	0.229 ± 0.036	0.319 ± 0.041	0.283 ± 0.037	0.291 ± 0.046	0.323 ± 0.045
		0.15	0.20	0.385 ± 0.033	0.412 ± 0.021	0.494 ± 0.037	0.521 ± 0.043	0.506 ± 0.028
		0.20	0.25	0.324 ± 0.027	0.420 ± 0.031	0.504 ± 0.023	0.519 ± 0.024	0.538 ± 0.028
		0.25	0.30	0.244 ± 0.022	0.354 ± 0.022	0.390 ± 0.020	0.404 ± 0.019	0.456 ± 0.021
		0.30	0.35	0.169 ± 0.019	0.271 ± 0.015	0.346 ± 0.020	0.341 ± 0.017	0.380 ± 0.013
		0.35	0.40	0.128 ± 0.012	0.221 ± 0.012	0.298 ± 0.016	0.288 ± 0.014	0.320 ± 0.010
		0.40	0.45	0.084 ± 0.011	0.171 ± 0.012	0.217 ± 0.015	0.245 ± 0.012	0.259 ± 0.014
		0.45	0.50	0.059 ± 0.009	0.114 ± 0.013	0.173 ± 0.011	0.201 ± 0.014	0.194 ± 0.017
		0.50	0.60	0.037 ± 0.006	0.073 ± 0.010	0.128 ± 0.013	0.137 ± 0.017	0.125 ± 0.014
1.15	1.35	0.10	0.15	0.239 ± 0.034	0.320 ± 0.042	0.320 ± 0.044	0.298 ± 0.041	0.355 ± 0.050
		0.15	0.20	0.328 ± 0.030	0.428 ± 0.024	0.460 ± 0.027	0.474 ± 0.031	0.483 ± 0.022
		0.20	0.25	0.269 ± 0.023	0.344 ± 0.021	0.406 ± 0.019	0.438 ± 0.022	0.438 ± 0.018
		0.25	0.30	0.197 ± 0.020	0.245 ± 0.016	0.332 ± 0.018	0.332 ± 0.017	0.347 ± 0.015
		0.30	0.35	0.128 ± 0.017	0.198 ± 0.011	0.247 ± 0.013	0.260 ± 0.015	0.258 ± 0.012
		0.35	0.40	0.073 ± 0.009	0.140 ± 0.010	0.195 ± 0.012	0.173 ± 0.015	0.199 ± 0.010
		0.40	0.45	0.051 ± 0.006	0.103 ± 0.011	0.142 ± 0.011	0.139 ± 0.009	0.140 ± 0.009
		0.45	0.50	0.033 ± 0.006	0.072 ± 0.008	0.101 ± 0.010	0.104 ± 0.009	0.105 ± 0.010
1.35	1.55	0.10	0.15	0.214 ± 0.030	0.324 ± 0.041	0.357 ± 0.040	0.354 ± 0.049	0.365 ± 0.051
		0.15	0.20	0.334 ± 0.034	0.385 ± 0.024	0.422 ± 0.024	0.433 ± 0.025	0.436 ± 0.020
		0.20	0.25	0.255 ± 0.032	0.283 ± 0.018	0.299 ± 0.016	0.356 ± 0.019	0.364 ± 0.015
		0.25	0.30	0.112 ± 0.013	0.179 ± 0.011	0.232 ± 0.014	0.241 ± 0.014	0.254 ± 0.014
		0.30	0.35	0.076 ± 0.009	0.150 ± 0.010	0.171 ± 0.012	0.178 ± 0.011	0.179 ± 0.009
		0.35	0.40	0.054 ± 0.008	0.087 ± 0.009	0.119 ± 0.009	0.137 ± 0.011	0.129 ± 0.008
		0.40	0.45	0.035 ± 0.007	0.058 ± 0.008	0.078 ± 0.008	0.089 ± 0.010	0.087 ± 0.009
		0.45	0.50	0.021 ± 0.005	0.036 ± 0.006	0.049 ± 0.006	0.058 ± 0.009	0.056 ± 0.008
1.55	1.75	0.10	0.15	0.224 ± 0.033	0.311 ± 0.038	0.310 ± 0.037	0.301 ± 0.039	0.341 ± 0.041
		0.15	0.20	0.304 ± 0.026	0.312 ± 0.019	0.360 ± 0.018	0.370 ± 0.023	0.391 ± 0.017
		0.20	0.25	0.176 ± 0.019	0.234 ± 0.016	0.228 ± 0.013	0.274 ± 0.020	0.260 ± 0.012
		0.25	0.30	0.113 ± 0.013	0.142 ± 0.012	0.171 ± 0.011	0.190 ± 0.013	0.173 ± 0.010
		0.30	0.35	0.052 ± 0.009	0.101 ± 0.008	0.118 ± 0.009	0.101 ± 0.011	0.115 ± 0.006
		0.35	0.40	0.026 ± 0.006	0.063 ± 0.006	0.075 ± 0.007	0.062 ± 0.005	0.086 ± 0.007
		0.40	0.45	0.012 ± 0.004	0.038 ± 0.008	0.047 ± 0.006	0.046 ± 0.005	0.053 ± 0.006
		0.45	0.50	0.005 ± 0.002	0.021 ± 0.004	0.028 ± 0.005	0.029 ± 0.005	0.032 ± 0.005
1.75	1.95	0.10	0.15	0.230 ± 0.032	0.281 ± 0.032	0.306 ± 0.034	0.292 ± 0.036	0.296 ± 0.033
		0.15	0.20	0.235 ± 0.021	0.292 ± 0.017	0.309 ± 0.022	0.332 ± 0.019	0.315 ± 0.014

TABLE VII. *(Continued.)*

θ_{min} (rad)	θ_{max} (rad)	p_{min} (GeV/c)	p_{max} (GeV/c)	$d^2\sigma^{\pi^+}/(dpd\theta)$ [b/(rad GeV/c)]				
				3 GeV/c	5 GeV/c	8 GeV/c	12 GeV/c	12.9 GeV/c
		0.20	0.25	0.147 ± 0.017	0.193 ± 0.013	0.211 ± 0.014	0.192 ± 0.016	0.207 ± 0.009
		0.25	0.30	0.094 ± 0.012	0.093 ± 0.011	0.117 ± 0.011	0.116 ± 0.010	0.126 ± 0.009
		0.30	0.35	0.046 ± 0.011	0.051 ± 0.006	0.065 ± 0.006	0.063 ± 0.008	0.078 ± 0.006
		0.35	0.40	0.014 ± 0.005	0.034 ± 0.004	0.041 ± 0.005	0.041 ± 0.004	0.049 ± 0.005
		0.40	0.45	0.006 ± 0.002	0.020 ± 0.004	0.024 ± 0.004	0.026 ± 0.004	0.031 ± 0.004
		0.45	0.50	0.004 ± 0.002	0.012 ± 0.003	0.013 ± 0.003	0.016 ± 0.003	0.017 ± 0.002
1.95	2.15	0.10	0.15	0.228 ± 0.027	0.205 ± 0.025	0.268 ± 0.031	0.223 ± 0.028	0.234 ± 0.029
		0.15	0.20	0.189 ± 0.020	0.253 ± 0.016	0.260 ± 0.014	0.246 ± 0.016	0.258 ± 0.011
		0.20	0.25	0.084 ± 0.016	0.121 ± 0.012	0.158 ± 0.018	0.140 ± 0.015	0.156 ± 0.009
		0.25	0.30	0.040 ± 0.008	0.061 ± 0.008	0.072 ± 0.007	0.073 ± 0.006	0.085 ± 0.007
		0.30	0.35	0.015 ± 0.005	0.032 ± 0.004	0.045 ± 0.005	0.046 ± 0.006	0.048 ± 0.004
		0.35	0.40	0.008 ± 0.003	0.022 ± 0.003	0.021 ± 0.004	0.031 ± 0.004	0.028 ± 0.003
		0.40	0.45	0.006 ± 0.003	0.010 ± 0.002	0.012 ± 0.002	0.015 ± 0.004	0.015 ± 0.002
		0.45	0.50	0.003 ± 0.002	0.005 ± 0.002	0.006 ± 0.001	0.007 ± 0.002	0.010 ± 0.002

TABLE VIII. HARP results for the double-differential π^- production cross section in the laboratory system, $d^2\sigma^{\pi^-}/(dpd\theta)$, for p-Al interactions. Each row refers to a different ($p_{min} \leqslant p < p_{max}$, $\theta_{min} \leqslant \theta < \theta_{max}$) bin, where p and θ are the pion momentum and polar angle, respectively. The central value as well as the square root of the diagonal elements of the covariance matrix are given.

θ_{min} (rad)	θ_{max} (rad)	p_{min} (GeV/c)	p_{max} (GeV/c)	$d^2\sigma^{\pi^-}/(dpd\theta)$ [b/(rad GeV/c)]				
				3 GeV/c	5 GeV/c	8 GeV/c	12 GeV/c	12.9 GeV/c
0.35	0.55	0.15	0.20	0.131 ± 0.030	0.243 ± 0.042	0.338 ± 0.051	0.342 ± 0.053	0.397 ± 0.065
		0.20	0.25	0.124 ± 0.021	0.258 ± 0.022	0.411 ± 0.037	0.442 ± 0.037	0.492 ± 0.035
		0.25	0.30	0.126 ± 0.022	0.289 ± 0.024	0.479 ± 0.027	0.516 ± 0.032	0.548 ± 0.030
		0.30	0.35	0.170 ± 0.020	0.312 ± 0.024	0.387 ± 0.023	0.470 ± 0.031	0.529 ± 0.020
		0.35	0.40	0.186 ± 0.021	0.293 ± 0.018	0.428 ± 0.034	0.485 ± 0.027	0.468 ± 0.018
		0.40	0.45	0.132 ± 0.017	0.262 ± 0.015	0.463 ± 0.026	0.485 ± 0.025	0.475 ± 0.024
		0.45	0.50	0.112 ± 0.012	0.257 ± 0.015	0.428 ± 0.022	0.440 ± 0.022	0.473 ± 0.020
		0.50	0.60	0.131 ± 0.014	0.246 ± 0.017	0.383 ± 0.022	0.431 ± 0.025	0.458 ± 0.024
		0.60	0.70	0.087 ± 0.013	0.217 ± 0.019	0.377 ± 0.029	0.415 ± 0.034	0.454 ± 0.035
		0.70	0.80	0.061 ± 0.013	0.166 ± 0.025	0.334 ± 0.040	0.398 ± 0.041	0.388 ± 0.049
0.55	0.75	0.10	0.15	0.075 ± 0.027	0.176 ± 0.047	0.223 ± 0.060	0.275 ± 0.075	0.270 ± 0.066
		0.15	0.20	0.115 ± 0.019	0.290 ± 0.024	0.383 ± 0.031	0.353 ± 0.028	0.411 ± 0.030
		0.20	0.25	0.196 ± 0.027	0.273 ± 0.020	0.438 ± 0.028	0.389 ± 0.029	0.456 ± 0.024
		0.25	0.30	0.164 ± 0.018	0.279 ± 0.018	0.429 ± 0.025	0.443 ± 0.030	0.448 ± 0.021
		0.30	0.35	0.153 ± 0.018	0.265 ± 0.016	0.382 ± 0.021	0.447 ± 0.028	0.447 ± 0.020
		0.35	0.40	0.143 ± 0.014	0.231 ± 0.012	0.397 ± 0.024	0.371 ± 0.015	0.422 ± 0.015
		0.40	0.45	0.130 ± 0.013	0.219 ± 0.015	0.361 ± 0.017	0.374 ± 0.020	0.388 ± 0.012
		0.45	0.50	0.119 ± 0.012	0.228 ± 0.014	0.317 ± 0.016	0.374 ± 0.017	0.373 ± 0.013
		0.50	0.60	0.095 ± 0.010	0.201 ± 0.013	0.304 ± 0.017	0.337 ± 0.020	0.348 ± 0.016
		0.60	0.70	0.076 ± 0.011	0.156 ± 0.017	0.269 ± 0.026	0.287 ± 0.027	0.297 ± 0.026
		0.70	0.80	0.055 ± 0.011	0.126 ± 0.020	0.214 ± 0.031	0.240 ± 0.034	0.239 ± 0.034
0.75	0.95	0.10	0.15	0.099 ± 0.025	0.177 ± 0.030	0.243 ± 0.043	0.313 ± 0.054	0.292 ± 0.050
		0.15	0.20	0.200 ± 0.023	0.322 ± 0.022	0.394 ± 0.023	0.404 ± 0.023	0.463 ± 0.023
		0.20	0.25	0.170 ± 0.019	0.286 ± 0.020	0.384 ± 0.025	0.378 ± 0.031	0.412 ± 0.019
		0.25	0.30	0.145 ± 0.015	0.280 ± 0.016	0.350 ± 0.021	0.402 ± 0.021	0.411 ± 0.020
		0.30	0.35	0.134 ± 0.015	0.233 ± 0.013	0.327 ± 0.016	0.339 ± 0.015	0.371 ± 0.014
		0.35	0.40	0.125 ± 0.012	0.220 ± 0.012	0.304 ± 0.015	0.296 ± 0.014	0.330 ± 0.011
		0.40	0.45	0.115 ± 0.012	0.185 ± 0.011	0.267 ± 0.012	0.291 ± 0.013	0.274 ± 0.008

TABLE VIII. *(Continued.)*

θ_{min} (rad)	θ_{max} (rad)	p_{min} (GeV/c)	p_{max} (GeV/c)	$d^2\sigma^{\pi^-}/(dpd\theta)$ [b/(rad GeV/c)]				
				3 GeV/c	5 GeV/c	8 GeV/c	12 GeV/c	12.9 GeV/c
		0.45	0.50	0.094 ± 0.011	0.158 ± 0.009	0.241 ± 0.011	0.249 ± 0.014	0.259 ± 0.009
		0.50	0.60	0.059 ± 0.010	0.120 ± 0.009	0.205 ± 0.013	0.217 ± 0.014	0.219 ± 0.012
		0.60	0.70	0.034 ± 0.006	0.086 ± 0.011	0.158 ± 0.017	0.171 ± 0.018	0.172 ± 0.019
0.95	1.15	0.10	0.15	0.161 ± 0.025	0.190 ± 0.024	0.249 ± 0.032	0.253 ± 0.037	0.301 ± 0.036
		0.15	0.20	0.187 ± 0.021	0.305 ± 0.027	0.364 ± 0.024	0.356 ± 0.026	0.408 ± 0.024
		0.20	0.25	0.178 ± 0.019	0.300 ± 0.017	0.339 ± 0.018	0.373 ± 0.021	0.392 ± 0.017
		0.25	0.30	0.154 ± 0.015	0.227 ± 0.013	0.301 ± 0.016	0.321 ± 0.018	0.340 ± 0.013
		0.30	0.35	0.118 ± 0.012	0.186 ± 0.011	0.246 ± 0.013	0.265 ± 0.013	0.269 ± 0.009
		0.35	0.40	0.091 ± 0.011	0.147 ± 0.009	0.188 ± 0.009	0.214 ± 0.010	0.232 ± 0.007
		0.40	0.45	0.060 ± 0.008	0.128 ± 0.008	0.160 ± 0.007	0.187 ± 0.010	0.191 ± 0.006
		0.45	0.50	0.049 ± 0.006	0.097 ± 0.007	0.144 ± 0.009	0.157 ± 0.009	0.166 ± 0.005
		0.50	0.60	0.034 ± 0.006	0.072 ± 0.007	0.118 ± 0.008	0.126 ± 0.009	0.132 ± 0.009
1.15	1.35	0.10	0.15	0.123 ± 0.020	0.211 ± 0.025	0.266 ± 0.032	0.266 ± 0.037	0.319 ± 0.033
		0.15	0.20	0.160 ± 0.018	0.288 ± 0.019	0.346 ± 0.020	0.366 ± 0.023	0.386 ± 0.023
		0.20	0.25	0.159 ± 0.017	0.239 ± 0.015	0.305 ± 0.017	0.321 ± 0.018	0.344 ± 0.012
		0.25	0.30	0.132 ± 0.015	0.185 ± 0.013	0.257 ± 0.014	0.243 ± 0.014	0.270 ± 0.009
		0.30	0.35	0.084 ± 0.011	0.164 ± 0.010	0.181 ± 0.012	0.208 ± 0.012	0.216 ± 0.008
		0.35	0.40	0.062 ± 0.009	0.114 ± 0.008	0.142 ± 0.008	0.156 ± 0.010	0.162 ± 0.006
		0.40	0.45	0.036 ± 0.006	0.087 ± 0.007	0.115 ± 0.006	0.126 ± 0.008	0.127 ± 0.006
		0.45	0.50	0.026 ± 0.004	0.064 ± 0.006	0.094 ± 0.006	0.100 ± 0.007	0.099 ± 0.006
1.35	1.55	0.10	0.15	0.187 ± 0.027	0.224 ± 0.027	0.251 ± 0.027	0.270 ± 0.033	0.305 ± 0.035
		0.15	0.20	0.198 ± 0.020	0.247 ± 0.017	0.289 ± 0.017	0.298 ± 0.021	0.341 ± 0.017
		0.20	0.25	0.130 ± 0.016	0.209 ± 0.014	0.251 ± 0.013	0.273 ± 0.018	0.284 ± 0.012
		0.25	0.30	0.083 ± 0.011	0.130 ± 0.011	0.190 ± 0.012	0.221 ± 0.014	0.221 ± 0.010
		0.30	0.35	0.067 ± 0.010	0.107 ± 0.008	0.147 ± 0.009	0.151 ± 0.011	0.160 ± 0.008
		0.35	0.40	0.035 ± 0.006	0.091 ± 0.007	0.110 ± 0.007	0.115 ± 0.007	0.117 ± 0.007
		0.40	0.45	0.025 ± 0.005	0.066 ± 0.006	0.089 ± 0.006	0.090 ± 0.007	0.083 ± 0.005
		0.45	0.50	0.019 ± 0.004	0.044 ± 0.006	0.067 ± 0.006	0.065 ± 0.007	0.062 ± 0.005
1.55	1.75	0.10	0.15	0.140 ± 0.022	0.224 ± 0.025	0.257 ± 0.033	0.267 ± 0.036	0.285 ± 0.030
		0.15	0.20	0.151 ± 0.017	0.241 ± 0.015	0.270 ± 0.016	0.300 ± 0.019	0.295 ± 0.014
		0.20	0.25	0.101 ± 0.013	0.171 ± 0.013	0.208 ± 0.013	0.229 ± 0.014	0.217 ± 0.010
		0.25	0.30	0.064 ± 0.009	0.102 ± 0.009	0.158 ± 0.011	0.171 ± 0.013	0.157 ± 0.008
		0.30	0.35	0.046 ± 0.008	0.079 ± 0.006	0.091 ± 0.009	0.095 ± 0.011	0.109 ± 0.007
		0.35	0.40	0.020 ± 0.006	0.057 ± 0.005	0.060 ± 0.005	0.068 ± 0.005	0.079 ± 0.005
		0.40	0.45	0.009 ± 0.003	0.040 ± 0.005	0.046 ± 0.004	0.049 ± 0.004	0.056 ± 0.004
		0.45	0.50	0.006 ± 0.002	0.026 ± 0.004	0.033 ± 0.003	0.040 ± 0.005	0.039 ± 0.003
1.75	1.95	0.10	0.15	0.118 ± 0.019	0.190 ± 0.019	0.227 ± 0.023	0.261 ± 0.029	0.247 ± 0.026
		0.15	0.20	0.163 ± 0.018	0.191 ± 0.013	0.235 ± 0.013	0.240 ± 0.015	0.244 ± 0.010
		0.20	0.25	0.080 ± 0.012	0.136 ± 0.010	0.168 ± 0.010	0.170 ± 0.012	0.181 ± 0.006
		0.25	0.30	0.053 ± 0.009	0.082 ± 0.008	0.129 ± 0.009	0.102 ± 0.008	0.119 ± 0.007
		0.30	0.35	0.035 ± 0.007	0.055 ± 0.005	0.070 ± 0.008	0.080 ± 0.006	0.075 ± 0.005
		0.35	0.40	0.025 ± 0.006	0.044 ± 0.005	0.047 ± 0.004	0.060 ± 0.005	0.054 ± 0.002
		0.40	0.45	0.013 ± 0.004	0.024 ± 0.005	0.037 ± 0.003	0.038 ± 0.005	0.041 ± 0.003
		0.45	0.50	0.007 ± 0.003	0.014 ± 0.003	0.026 ± 0.003	0.027 ± 0.004	0.027 ± 0.003
1.95	2.15	0.10	0.15	0.109 ± 0.017	0.132 ± 0.015	0.197 ± 0.019	0.187 ± 0.020	0.206 ± 0.020
		0.15	0.20	0.104 ± 0.014	0.173 ± 0.012	0.190 ± 0.012	0.196 ± 0.015	0.187 ± 0.010
		0.20	0.25	0.053 ± 0.009	0.103 ± 0.009	0.117 ± 0.009	0.130 ± 0.012	0.136 ± 0.006
		0.25	0.30	0.037 ± 0.008	0.066 ± 0.007	0.064 ± 0.008	0.078 ± 0.007	0.085 ± 0.005
		0.30	0.35	0.018 ± 0.005	0.038 ± 0.005	0.044 ± 0.004	0.052 ± 0.006	0.052 ± 0.004
		0.35	0.40	0.010 ± 0.004	0.024 ± 0.004	0.040 ± 0.004	0.029 ± 0.004	0.036 ± 0.003
		0.40	0.45	0.005 ± 0.003	0.012 ± 0.003	0.025 ± 0.004	0.019 ± 0.003	0.026 ± 0.002
		0.45	0.50	0.002 ± 0.002	0.008 ± 0.002	0.013 ± 0.003	0.015 ± 0.003	0.018 ± 0.002

TABLE IX. HARP results for the double-differential π^+ production cross section in the laboratory system, $d^2\sigma^{\pi^+}/(dpd\theta)$, for p-Cu interactions. Each row refers to a different ($p_{min} \leqslant p < p_{max}$, $\theta_{min} \leqslant \theta < \theta_{max}$) bin, where p and θ are the pion momentum and polar angle, respectively. The central value as well as the square root of the diagonal elements of the covariance matrix are given.

θ_{min} (rad)	θ_{max} (rad)	p_{min} (GeV/c)	p_{max} (GeV/c)	$d^2\sigma^{\pi^+}/(dpd\theta)$ [b/(rad GeV/c)]			
				3 GeV/c	5 GeV/c	8 GeV/c	12 GeV/c
0.35	0.55	0.15	0.20	0.20 ± 0.05	0.54 ± 0.09	0.76 ± 0.13	0.87 ± 0.15
		0.20	0.25	0.22 ± 0.05	0.68 ± 0.07	0.94 ± 0.08	1.01 ± 0.08
		0.25	0.30	0.46 ± 0.07	0.81 ± 0.06	1.09 ± 0.06	1.32 ± 0.10
		0.30	0.35	0.45 ± 0.05	0.86 ± 0.06	1.11 ± 0.08	1.42 ± 0.08
		0.35	0.40	0.44 ± 0.05	0.82 ± 0.04	1.20 ± 0.07	1.40 ± 0.07
		0.40	0.45	0.37 ± 0.04	0.78 ± 0.04	1.25 ± 0.06	1.31 ± 0.05
		0.45	0.50	0.41 ± 0.05	0.78 ± 0.04	1.17 ± 0.05	1.35 ± 0.08
		0.50	0.60	0.41 ± 0.04	0.76 ± 0.04	1.13 ± 0.05	1.31 ± 0.07
		0.60	0.70	0.30 ± 0.05	0.61 ± 0.07	1.00 ± 0.09	1.19 ± 0.11
		0.70	0.80	0.15 ± 0.04	0.39 ± 0.07	0.77 ± 0.11	0.97 ± 0.13
0.55	0.75	0.10	0.15	0.40 ± 0.11	0.40 ± 0.12	0.51 ± 0.15	0.58 ± 0.17
		0.15	0.20	0.44 ± 0.06	0.71 ± 0.07	0.91 ± 0.07	0.92 ± 0.08
		0.20	0.25	0.46 ± 0.06	0.82 ± 0.05	1.08 ± 0.08	1.28 ± 0.10
		0.25	0.30	0.47 ± 0.05	0.81 ± 0.06	1.11 ± 0.06	1.33 ± 0.06
		0.30	0.35	0.53 ± 0.08	0.88 ± 0.06	1.12 ± 0.06	1.24 ± 0.06
		0.35	0.40	0.58 ± 0.05	0.82 ± 0.04	1.08 ± 0.04	1.25 ± 0.05
		0.40	0.45	0.44 ± 0.04	0.66 ± 0.04	0.99 ± 0.04	1.18 ± 0.05
		0.45	0.50	0.36 ± 0.04	0.61 ± 0.03	0.94 ± 0.04	1.07 ± 0.04
		0.50	0.60	0.26 ± 0.03	0.52 ± 0.04	0.78 ± 0.05	0.88 ± 0.06
		0.60	0.70	0.13 ± 0.03	0.35 ± 0.04	0.50 ± 0.06	0.64 ± 0.08
		0.70	0.80	0.06 ± 0.02	0.21 ± 0.04	0.33 ± 0.06	0.43 ± 0.08
0.75	0.95	0.10	0.15	0.41 ± 0.10	0.51 ± 0.11	0.56 ± 0.13	0.68 ± 0.15
		0.15	0.20	0.56 ± 0.06	0.83 ± 0.06	0.96 ± 0.06	1.19 ± 0.08
		0.20	0.25	0.49 ± 0.05	0.82 ± 0.05	1.13 ± 0.08	1.22 ± 0.06
		0.25	0.30	0.50 ± 0.05	0.71 ± 0.04	1.06 ± 0.06	1.15 ± 0.07
		0.30	0.35	0.37 ± 0.04	0.70 ± 0.04	0.94 ± 0.04	1.15 ± 0.05
		0.35	0.40	0.25 ± 0.03	0.58 ± 0.03	0.81 ± 0.03	0.95 ± 0.04
		0.40	0.45	0.20 ± 0.02	0.45 ± 0.03	0.67 ± 0.03	0.83 ± 0.03
		0.45	0.50	0.18 ± 0.02	0.38 ± 0.02	0.57 ± 0.03	0.67 ± 0.04
		0.50	0.60	0.10 ± 0.02	0.27 ± 0.02	0.42 ± 0.03	0.51 ± 0.04
		0.60	0.70	0.05 ± 0.01	0.16 ± 0.03	0.26 ± 0.03	0.30 ± 0.05
0.95	1.15	0.10	0.15	0.44 ± 0.09	0.65 ± 0.11	0.66 ± 0.12	0.82 ± 0.16
		0.15	0.20	0.59 ± 0.06	0.87 ± 0.05	1.08 ± 0.07	1.14 ± 0.07
		0.20	0.25	0.44 ± 0.04	0.66 ± 0.04	0.95 ± 0.04	1.11 ± 0.06
		0.25	0.30	0.36 ± 0.04	0.60 ± 0.04	0.80 ± 0.04	0.87 ± 0.05
		0.30	0.35	0.26 ± 0.03	0.52 ± 0.03	0.62 ± 0.03	0.76 ± 0.04
		0.35	0.40	0.18 ± 0.02	0.39 ± 0.02	0.52 ± 0.03	0.60 ± 0.03
		0.40	0.45	0.15 ± 0.02	0.30 ± 0.02	0.42 ± 0.02	0.47 ± 0.03
		0.45	0.50	0.11 ± 0.02	0.24 ± 0.02	0.32 ± 0.02	0.38 ± 0.03
		0.50	0.60	0.06 ± 0.01	0.15 ± 0.02	0.22 ± 0.02	0.24 ± 0.03
1.15	1.35	0.10	0.15	0.51 ± 0.10	0.68 ± 0.14	0.72 ± 0.15	0.78 ± 0.16
		0.15	0.20	0.54 ± 0.06	0.81 ± 0.05	1.01 ± 0.07	1.07 ± 0.08
		0.20	0.25	0.41 ± 0.04	0.63 ± 0.04	0.87 ± 0.04	1.05 ± 0.05
		0.25	0.30	0.31 ± 0.04	0.48 ± 0.03	0.58 ± 0.04	0.73 ± 0.04
		0.30	0.35	0.18 ± 0.02	0.32 ± 0.03	0.41 ± 0.02	0.53 ± 0.03
		0.35	0.40	0.11 ± 0.02	0.23 ± 0.02	0.33 ± 0.02	0.36 ± 0.02
		0.40	0.45	0.08 ± 0.01	0.17 ± 0.01	0.25 ± 0.01	0.26 ± 0.02
		0.45	0.50	0.05 ± 0.01	0.12 ± 0.01	0.18 ± 0.01	0.19 ± 0.02
1.35	1.55	0.10	0.15	0.52 ± 0.12	0.70 ± 0.15	0.73 ± 0.18	0.83 ± 0.18
		0.15	0.20	0.47 ± 0.05	0.71 ± 0.06	0.90 ± 0.07	0.99 ± 0.09

TABLE IX. *(Continued.)*

θ_{min} (rad)	θ_{max} (rad)	p_{min} (GeV/c)	p_{max} (GeV/c)	$d^2\sigma^{\pi^+}/(dpd\theta)$ [b/(rad GeV/c)]			
				3 GeV/c	5 GeV/c	8 GeV/c	12 GeV/c
		0.20	0.25	0.30 ± 0.04	0.52 ± 0.04	0.73 ± 0.04	0.84 ± 0.05
		0.25	0.30	0.18 ± 0.02	0.34 ± 0.03	0.48 ± 0.04	0.51 ± 0.03
		0.30	0.35	0.13 ± 0.02	0.23 ± 0.02	0.32 ± 0.02	0.38 ± 0.02
		0.35	0.40	0.07 ± 0.01	0.16 ± 0.01	0.22 ± 0.02	0.29 ± 0.02
		0.40	0.45	0.04 ± 0.01	0.11 ± 0.01	0.15 ± 0.01	0.20 ± 0.02
		0.45	0.50	0.03 ± 0.01	0.06 ± 0.01	0.10 ± 0.01	0.11 ± 0.02
1.55	1.75	0.10	0.15	0.53 ± 0.13	0.67 ± 0.15	0.83 ± 0.19	0.83 ± 0.20
		0.15	0.20	0.43 ± 0.05	0.72 ± 0.05	0.81 ± 0.06	0.87 ± 0.07
		0.20	0.25	0.27 ± 0.03	0.46 ± 0.04	0.61 ± 0.04	0.67 ± 0.05
		0.25	0.30	0.17 ± 0.03	0.24 ± 0.02	0.34 ± 0.02	0.36 ± 0.03
		0.30	0.35	0.13 ± 0.02	0.15 ± 0.01	0.22 ± 0.02	0.23 ± 0.02
		0.35	0.40	0.06 ± 0.01	0.12 ± 0.01	0.15 ± 0.01	0.18 ± 0.01
		0.40	0.45	0.03 ± 0.01	0.08 ± 0.01	0.09 ± 0.01	0.11 ± 0.01
		0.45	0.50	0.02 ± 0.01	0.04 ± 0.01	0.06 ± 0.01	0.06 ± 0.01
1.75	1.95	0.10	0.15	0.50 ± 0.10	0.61 ± 0.10	0.70 ± 0.12	0.70 ± 0.12
		0.15	0.20	0.51 ± 0.05	0.60 ± 0.04	0.69 ± 0.04	0.72 ± 0.04
		0.20	0.25	0.35 ± 0.05	0.34 ± 0.03	0.44 ± 0.03	0.46 ± 0.03
		0.25	0.30	0.08 ± 0.02	0.17 ± 0.02	0.21 ± 0.02	0.26 ± 0.02
		0.30	0.35	0.04 ± 0.01	0.10 ± 0.01	0.12 ± 0.01	0.16 ± 0.02
		0.35	0.40	0.02 ± 0.01	0.07 ± 0.01	0.09 ± 0.01	0.10 ± 0.01
		0.40	0.45	0.01 ± 0.01	0.05 ± 0.01	0.06 ± 0.01	0.06 ± 0.01
		0.45	0.50		0.02 ± 0.01	0.03 ± 0.01	0.03 ± 0.01
1.95	2.15	0.10	0.15	0.38 ± 0.06	0.49 ± 0.07	0.56 ± 0.08	0.48 ± 0.08
		0.15	0.20	0.42 ± 0.05	0.44 ± 0.03	0.55 ± 0.02	0.56 ± 0.03
		0.20	0.25	0.18 ± 0.03	0.26 ± 0.02	0.29 ± 0.02	0.31 ± 0.02
		0.25	0.30	0.07 ± 0.02	0.11 ± 0.01	0.14 ± 0.01	0.19 ± 0.02
		0.30	0.35	0.04 ± 0.01	0.07 ± 0.01	0.08 ± 0.01	0.10 ± 0.01
		0.35	0.40	0.02 ± 0.01	0.04 ± 0.01	0.05 ± 0.01	0.06 ± 0.01
		0.40	0.45		0.02 ± 0.01	0.03 ± 0.01	0.04 ± 0.01
		0.45	0.50		0.01 ± 0.01	0.02 ± 0.01	0.02 ± 0.01

TABLE X. HARP results for the double-differential π^- production cross section in the laboratory system, $d^2\sigma^{\pi^-}/(dpd\theta)$, for p-Cu interactions. Each row refers to a different ($p_{min} \leqslant p < p_{max}, \theta_{min} \leqslant \theta < \theta_{max}$) bin, where p and θ are the pion momentum and polar angle, respectively. The central value as well as the square root of the diagonal elements of the covariance matrix are given.

θ_{min} (rad)	θ_{max} (rad)	p_{min} (GeV/c)	p_{max} (GeV/c)	$d^2\sigma^{\pi^-}/(dpd\theta)$ [b/(rad GeV/c)]			
				3 GeV/c	5 GeV/c	8 GeV/c	12 GeV/c
0.35	0.55	0.15	0.20	0.15 ± 0.06	0.43 ± 0.08	0.70 ± 0.11	0.85 ± 0.17
		0.20	0.25	0.21 ± 0.05	0.48 ± 0.05	0.79 ± 0.07	1.06 ± 0.07
		0.25	0.30	0.13 ± 0.04	0.49 ± 0.04	0.89 ± 0.06	1.03 ± 0.06
		0.30	0.35	0.18 ± 0.03	0.49 ± 0.03	0.79 ± 0.04	0.99 ± 0.06
		0.35	0.40	0.17 ± 0.03	0.47 ± 0.03	0.78 ± 0.04	0.90 ± 0.04
		0.40	0.45	0.17 ± 0.02	0.43 ± 0.03	0.74 ± 0.03	0.81 ± 0.03
		0.45	0.50	0.19 ± 0.03	0.39 ± 0.02	0.70 ± 0.03	0.75 ± 0.03
		0.50	0.60	0.19 ± 0.03	0.41 ± 0.02	0.68 ± 0.03	0.78 ± 0.04
		0.60	0.70	0.13 ± 0.02	0.36 ± 0.03	0.63 ± 0.04	0.69 ± 0.06
		0.70	0.80	0.10 ± 0.02	0.29 ± 0.03	0.54 ± 0.06	0.63 ± 0.07
0.55	0.75	0.10	0.15	0.27 ± 0.08	0.49 ± 0.13	0.53 ± 0.15	0.57 ± 0.18
		0.15	0.20	0.28 ± 0.06	0.56 ± 0.05	0.74 ± 0.07	0.96 ± 0.09

TABLE X. *(Continued.)*

θ_{min} (rad)	θ_{max} (rad)	p_{min} (GeV/c)	p_{max} (GeV/c)	$d^2\sigma^{\pi^-}/(dpd\theta)$ [b/(rad GeV/c)]			
				3 GeV/c	5 GeV/c	8 GeV/c	12 GeV/c
		0.20	0.25	0.44 ± 0.06	0.64 ± 0.05	0.81 ± 0.05	1.06 ± 0.06
		0.25	0.30	0.20 ± 0.03	0.60 ± 0.04	0.85 ± 0.06	1.02 ± 0.05
		0.30	0.35	0.24 ± 0.03	0.52 ± 0.03	0.78 ± 0.04	0.86 ± 0.04
		0.35	0.40	0.24 ± 0.03	0.47 ± 0.03	0.67 ± 0.03	0.83 ± 0.04
		0.40	0.45	0.21 ± 0.03	0.42 ± 0.02	0.62 ± 0.03	0.78 ± 0.03
		0.45	0.50	0.17 ± 0.02	0.37 ± 0.02	0.61 ± 0.02	0.75 ± 0.03
		0.50	0.60	0.14 ± 0.02	0.29 ± 0.02	0.54 ± 0.02	0.63 ± 0.04
		0.60	0.70	0.09 ± 0.02	0.24 ± 0.02	0.44 ± 0.04	0.49 ± 0.04
		0.70	0.80	0.06 ± 0.02	0.19 ± 0.02	0.35 ± 0.04	0.42 ± 0.05
0.75	0.95	0.10	0.15	0.32 ± 0.07	0.48 ± 0.09	0.59 ± 0.12	0.63 ± 0.13
		0.15	0.20	0.33 ± 0.05	0.64 ± 0.05	0.86 ± 0.05	0.98 ± 0.06
		0.20	0.25	0.24 ± 0.03	0.59 ± 0.04	0.81 ± 0.05	0.92 ± 0.05
		0.25	0.30	0.22 ± 0.03	0.47 ± 0.03	0.73 ± 0.04	0.90 ± 0.06
		0.30	0.35	0.21 ± 0.03	0.42 ± 0.02	0.64 ± 0.03	0.82 ± 0.04
		0.35	0.40	0.23 ± 0.03	0.34 ± 0.02	0.61 ± 0.03	0.73 ± 0.03
		0.40	0.45	0.18 ± 0.02	0.28 ± 0.02	0.51 ± 0.02	0.59 ± 0.03
		0.45	0.50	0.14 ± 0.02	0.25 ± 0.01	0.42 ± 0.02	0.48 ± 0.02
		0.50	0.60	0.10 ± 0.02	0.21 ± 0.01	0.34 ± 0.02	0.40 ± 0.02
		0.60	0.70	0.06 ± 0.01	0.17 ± 0.02	0.27 ± 0.02	0.32 ± 0.03
0.95	1.15	0.10	0.15	0.25 ± 0.06	0.55 ± 0.09	0.68 ± 0.11	0.72 ± 0.14
		0.15	0.20	0.32 ± 0.05	0.65 ± 0.04	0.84 ± 0.05	0.89 ± 0.06
		0.20	0.25	0.32 ± 0.04	0.51 ± 0.04	0.77 ± 0.04	0.83 ± 0.05
		0.25	0.30	0.23 ± 0.03	0.43 ± 0.03	0.63 ± 0.03	0.72 ± 0.04
		0.30	0.35	0.13 ± 0.02	0.36 ± 0.02	0.51 ± 0.03	0.57 ± 0.03
		0.35	0.40	0.11 ± 0.02	0.27 ± 0.02	0.43 ± 0.02	0.49 ± 0.02
		0.40	0.45	0.12 ± 0.02	0.22 ± 0.01	0.35 ± 0.02	0.43 ± 0.02
		0.45	0.50	0.11 ± 0.02	0.19 ± 0.01	0.29 ± 0.01	0.36 ± 0.02
		0.50	0.60	0.07 ± 0.01	0.14 ± 0.01	0.22 ± 0.02	0.25 ± 0.02
1.15	1.35	0.10	0.15	0.30 ± 0.07	0.63 ± 0.11	0.71 ± 0.13	0.79 ± 0.17
		0.15	0.20	0.38 ± 0.05	0.64 ± 0.05	0.75 ± 0.06	0.97 ± 0.07
		0.20	0.25	0.32 ± 0.04	0.48 ± 0.03	0.64 ± 0.04	0.79 ± 0.05
		0.25	0.30	0.16 ± 0.03	0.37 ± 0.02	0.51 ± 0.03	0.58 ± 0.03
		0.30	0.35	0.15 ± 0.02	0.29 ± 0.02	0.38 ± 0.02	0.45 ± 0.02
		0.35	0.40	0.10 ± 0.02	0.20 ± 0.01	0.30 ± 0.01	0.36 ± 0.02
		0.40	0.45	0.06 ± 0.01	0.15 ± 0.01	0.24 ± 0.01	0.28 ± 0.02
		0.45	0.50	0.04 ± 0.01	0.12 ± 0.01	0.19 ± 0.01	0.20 ± 0.02
1.35	1.55	0.10	0.15	0.39 ± 0.09	0.63 ± 0.13	0.72 ± 0.16	0.80 ± 0.19
		0.15	0.20	0.39 ± 0.05	0.57 ± 0.05	0.73 ± 0.06	0.85 ± 0.07
		0.20	0.25	0.27 ± 0.04	0.41 ± 0.03	0.53 ± 0.03	0.69 ± 0.04
		0.25	0.30	0.20 ± 0.03	0.30 ± 0.02	0.37 ± 0.02	0.47 ± 0.03
		0.30	0.35	0.15 ± 0.02	0.20 ± 0.02	0.29 ± 0.02	0.33 ± 0.02
		0.35	0.40	0.09 ± 0.02	0.13 ± 0.01	0.21 ± 0.01	0.24 ± 0.02
		0.40	0.45	0.07 ± 0.01	0.09 ± 0.01	0.16 ± 0.01	0.18 ± 0.01
		0.45	0.50	0.04 ± 0.01	0.06 ± 0.01	0.12 ± 0.01	0.13 ± 0.01
1.55	1.75	0.10	0.15	0.37 ± 0.08	0.56 ± 0.12	0.73 ± 0.17	0.84 ± 0.20
		0.15	0.20	0.27 ± 0.04	0.50 ± 0.04	0.66 ± 0.05	0.71 ± 0.06
		0.20	0.25	0.20 ± 0.03	0.33 ± 0.03	0.44 ± 0.03	0.50 ± 0.04
		0.25	0.30	0.12 ± 0.02	0.19 ± 0.02	0.31 ± 0.02	0.33 ± 0.03
		0.30	0.35	0.07 ± 0.01	0.13 ± 0.01	0.21 ± 0.02	0.23 ± 0.02
		0.35	0.40	0.04 ± 0.01	0.09 ± 0.01	0.14 ± 0.01	0.17 ± 0.01
		0.40	0.45	0.02 ± 0.01	0.06 ± 0.01	0.10 ± 0.01	0.11 ± 0.01
		0.45	0.50	0.01 ± 0.01	0.04 ± 0.01	0.07 ± 0.01	0.08 ± 0.01
1.75	1.95	0.10	0.15	0.26 ± 0.05	0.51 ± 0.08	0.63 ± 0.10	0.66 ± 0.11
		0.15	0.20	0.21 ± 0.03	0.42 ± 0.03	0.51 ± 0.03	0.64 ± 0.04

TABLE X. *(Continued.)*

θ_{min} (rad)	θ_{max} (rad)	p_{min} (GeV/c)	p_{max} (GeV/c)	$d^2\sigma^{\pi^-}/(dpd\theta)$ [b/(rad GeV/c)]			
				3 GeV/c	5 GeV/c	8 GeV/c	12 GeV/c
		0.20	0.25	0.19 ± 0.03	0.28 ± 0.02	0.35 ± 0.02	0.40 ± 0.03
		0.25	0.30	0.08 ± 0.02	0.15 ± 0.02	0.22 ± 0.02	0.24 ± 0.02
		0.30	0.35	0.06 ± 0.01	0.09 ± 0.01	0.14 ± 0.01	0.14 ± 0.01
		0.35	0.40	0.05 ± 0.01	0.06 ± 0.01	0.10 ± 0.01	0.11 ± 0.01
		0.40	0.45	0.02 ± 0.01	0.04 ± 0.01	0.07 ± 0.01	0.07 ± 0.01
		0.45	0.50	0.01 ± 0.01	0.03 ± 0.01	0.05 ± 0.01	0.05 ± 0.01
1.95	2.15	0.10	0.15	0.26 ± 0.05	0.42 ± 0.06	0.52 ± 0.07	0.55 ± 0.08
		0.15	0.20	0.20 ± 0.03	0.31 ± 0.02	0.42 ± 0.02	0.47 ± 0.03
		0.20	0.25	0.13 ± 0.03	0.17 ± 0.01	0.25 ± 0.01	0.28 ± 0.02
		0.25	0.30	0.06 ± 0.02	0.11 ± 0.01	0.16 ± 0.01	0.15 ± 0.02
		0.30	0.35	0.02 ± 0.01	0.07 ± 0.01	0.09 ± 0.01	0.10 ± 0.01
		0.35	0.40	0.02 ± 0.01	0.05 ± 0.01	0.05 ± 0.01	0.07 ± 0.01
		0.40	0.45	0.01 ± 0.01	0.03 ± 0.01	0.04 ± 0.01	0.06 ± 0.01
		0.45	0.50		0.02 ± 0.01	0.03 ± 0.01	0.04 ± 0.01

TABLE XI. HARP results for the double-differential π^+ production cross section in the laboratory system, $d^2\sigma^{\pi^+}/(dpd\theta)$, for p-Sn interactions. Each row refers to a different ($p_{min} \leqslant p < p_{max}$, $\theta_{min} \leqslant \theta < \theta_{max}$) bin, where p and θ are the pion momentum and polar angle, respectively. The central value as well as the square root of the diagonal elements of the covariance matrix are given.

θ_{min} (rad)	θ_{max} (rad)	p_{min} (GeV/c)	p_{max} (GeV/c)	$d^2\sigma^{\pi^+}/(dpd\theta)$ [b/(rad GeV/c)]			
				3 GeV/c	5 GeV/c	8 GeV/c	12 GeV/c
0.35	0.55	0.15	0.20	0.28 ± 0.11	0.74 ± 0.14	1.20 ± 0.18	1.55 ± 0.25
		0.20	0.25	0.41 ± 0.10	0.78 ± 0.09	1.42 ± 0.12	1.81 ± 0.16
		0.25	0.30	0.55 ± 0.06	1.05 ± 0.10	1.59 ± 0.11	2.18 ± 0.14
		0.30	0.35	0.53 ± 0.05	1.00 ± 0.05	1.67 ± 0.11	2.14 ± 0.14
		0.35	0.40	0.56 ± 0.05	1.05 ± 0.08	1.64 ± 0.07	2.14 ± 0.07
		0.40	0.45	0.50 ± 0.04	1.10 ± 0.06	1.55 ± 0.08	2.21 ± 0.14
		0.45	0.50	0.47 ± 0.04	1.10 ± 0.05	1.53 ± 0.06	2.15 ± 0.07
		0.50	0.60	0.44 ± 0.04	0.94 ± 0.06	1.45 ± 0.07	2.20 ± 0.12
		0.60	0.70	0.36 ± 0.04	0.80 ± 0.08	1.27 ± 0.13	2.12 ± 0.18
		0.70	0.80	0.26 ± 0.04	0.47 ± 0.08	0.93 ± 0.16	1.78 ± 0.21
0.55	0.75	0.10	0.15	0.33 ± 0.12	0.76 ± 0.17	0.87 ± 0.21	1.26 ± 0.30
		0.15	0.20	0.49 ± 0.08	1.02 ± 0.10	1.53 ± 0.10	1.77 ± 0.14
		0.20	0.25	0.59 ± 0.09	1.23 ± 0.09	1.72 ± 0.12	2.19 ± 0.17
		0.25	0.30	0.60 ± 0.05	1.11 ± 0.07	1.61 ± 0.10	2.15 ± 0.17
		0.30	0.35	0.56 ± 0.05	1.12 ± 0.07	1.54 ± 0.07	2.13 ± 0.10
		0.35	0.40	0.46 ± 0.04	1.03 ± 0.05	1.47 ± 0.07	2.08 ± 0.07
		0.40	0.45	0.46 ± 0.04	0.87 ± 0.04	1.27 ± 0.05	1.98 ± 0.06
		0.45	0.50	0.37 ± 0.04	0.80 ± 0.04	1.21 ± 0.05	1.76 ± 0.07
		0.50	0.60	0.27 ± 0.03	0.61 ± 0.05	1.03 ± 0.06	1.53 ± 0.09
		0.60	0.70	0.17 ± 0.03	0.38 ± 0.05	0.71 ± 0.10	1.21 ± 0.11
		0.70	0.80	0.11 ± 0.02	0.25 ± 0.05	0.43 ± 0.08	0.82 ± 0.12
0.75	0.95	0.10	0.15	0.47 ± 0.10	0.80 ± 0.13	1.07 ± 0.17	1.16 ± 0.20
		0.15	0.20	0.63 ± 0.07	1.17 ± 0.07	1.69 ± 0.11	1.95 ± 0.12
		0.20	0.25	0.76 ± 0.06	1.22 ± 0.07	1.64 ± 0.09	1.94 ± 0.11
		0.25	0.30	0.57 ± 0.05	0.95 ± 0.05	1.45 ± 0.07	1.92 ± 0.11
		0.30	0.35	0.57 ± 0.04	0.93 ± 0.06	1.31 ± 0.06	1.78 ± 0.08
		0.35	0.40	0.46 ± 0.04	0.73 ± 0.04	1.17 ± 0.05	1.40 ± 0.05
		0.40	0.45	0.36 ± 0.03	0.60 ± 0.04	0.99 ± 0.04	1.27 ± 0.05

TABLE XI. (*Continued*).

θ_{min} (rad)	θ_{max} (rad)	p_{min} (GeV/c)	p_{max} (GeV/c)	$d^2\sigma^{\pi^+}/(dpd\theta)$ [b/(rad GeV/c)]			
				3 GeV/c	5 GeV/c	8 GeV/c	12 GeV/c
		0.45	0.50	0.30 ± 0.03	0.50 ± 0.03	0.80 ± 0.05	1.11 ± 0.05
		0.50	0.60	0.19 ± 0.03	0.35 ± 0.03	0.56 ± 0.05	0.85 ± 0.06
		0.60	0.70	0.09 ± 0.02	0.20 ± 0.03	0.32 ± 0.05	0.55 ± 0.06
0.95	1.15	0.10	0.15	0.45 ± 0.09	0.80 ± 0.11	1.13 ± 0.14	1.14 ± 0.17
		0.15	0.20	0.68 ± 0.07	1.12 ± 0.07	1.55 ± 0.09	1.82 ± 0.11
		0.20	0.25	0.51 ± 0.04	1.01 ± 0.06	1.40 ± 0.09	1.72 ± 0.08
		0.25	0.30	0.43 ± 0.04	0.77 ± 0.04	1.16 ± 0.05	1.48 ± 0.07
		0.30	0.35	0.29 ± 0.02	0.59 ± 0.04	0.92 ± 0.07	1.20 ± 0.06
		0.35	0.40	0.27 ± 0.03	0.50 ± 0.03	0.72 ± 0.04	0.97 ± 0.05
		0.40	0.45	0.19 ± 0.03	0.41 ± 0.03	0.65 ± 0.03	0.79 ± 0.05
		0.45	0.50	0.14 ± 0.02	0.30 ± 0.02	0.49 ± 0.04	0.64 ± 0.04
		0.50	0.60	0.08 ± 0.01	0.20 ± 0.02	0.30 ± 0.03	0.46 ± 0.04
1.15	1.35	0.10	0.15	0.57 ± 0.09	0.76 ± 0.10	1.06 ± 0.14	1.10 ± 0.18
		0.15	0.20	0.64 ± 0.05	1.09 ± 0.08	1.39 ± 0.10	1.74 ± 0.11
		0.20	0.25	0.47 ± 0.04	0.85 ± 0.05	1.22 ± 0.07	1.43 ± 0.07
		0.25	0.30	0.40 ± 0.04	0.65 ± 0.04	0.93 ± 0.05	1.09 ± 0.06
		0.30	0.35	0.25 ± 0.03	0.46 ± 0.03	0.67 ± 0.05	0.86 ± 0.05
		0.35	0.40	0.15 ± 0.02	0.32 ± 0.03	0.48 ± 0.02	0.69 ± 0.04
		0.40	0.45	0.10 ± 0.01	0.23 ± 0.02	0.38 ± 0.02	0.51 ± 0.04
		0.45	0.50	0.08 ± 0.01	0.18 ± 0.02	0.28 ± 0.03	0.34 ± 0.03
1.35	1.55	0.10	0.15	0.72 ± 0.12	0.86 ± 0.14	1.26 ± 0.21	1.30 ± 0.23
		0.15	0.20	0.70 ± 0.06	1.11 ± 0.09	1.44 ± 0.10	1.77 ± 0.16
		0.20	0.25	0.44 ± 0.04	0.83 ± 0.06	1.11 ± 0.09	1.29 ± 0.09
		0.25	0.30	0.33 ± 0.03	0.52 ± 0.04	0.74 ± 0.05	0.92 ± 0.06
		0.30	0.35	0.19 ± 0.03	0.37 ± 0.03	0.52 ± 0.03	0.63 ± 0.05
		0.35	0.40	0.11 ± 0.01	0.26 ± 0.02	0.36 ± 0.02	0.48 ± 0.03
		0.40	0.45	0.07 ± 0.01	0.16 ± 0.02	0.24 ± 0.02	0.37 ± 0.03
		0.45	0.50	0.04 ± 0.01	0.09 ± 0.01	0.17 ± 0.02	0.21 ± 0.03
1.55	1.75	0.10	0.15	0.65 ± 0.12	0.99 ± 0.16	1.27 ± 0.20	1.29 ± 0.23
		0.15	0.20	0.71 ± 0.06	1.00 ± 0.08	1.40 ± 0.10	1.57 ± 0.11
		0.20	0.25	0.41 ± 0.04	0.68 ± 0.05	0.95 ± 0.07	1.04 ± 0.08
		0.25	0.30	0.24 ± 0.03	0.45 ± 0.04	0.57 ± 0.04	0.67 ± 0.04
		0.30	0.35	0.13 ± 0.02	0.23 ± 0.02	0.36 ± 0.03	0.46 ± 0.03
		0.35	0.40	0.08 ± 0.01	0.18 ± 0.02	0.24 ± 0.02	0.31 ± 0.02
		0.40	0.45	0.04 ± 0.01	0.09 ± 0.01	0.16 ± 0.02	0.20 ± 0.02
		0.45	0.50	0.03 ± 0.01	0.06 ± 0.01	0.10 ± 0.02	0.12 ± 0.02
1.75	1.95	0.10	0.15	0.60 ± 0.09	0.88 ± 0.10	0.99 ± 0.11	1.01 ± 0.13
		0.15	0.20	0.56 ± 0.05	0.77 ± 0.05	1.00 ± 0.05	1.13 ± 0.06
		0.20	0.25	0.28 ± 0.03	0.48 ± 0.03	0.62 ± 0.05	0.73 ± 0.04
		0.25	0.30	0.15 ± 0.03	0.26 ± 0.03	0.34 ± 0.03	0.40 ± 0.03
		0.30	0.35	0.07 ± 0.01	0.15 ± 0.02	0.22 ± 0.02	0.24 ± 0.02
		0.35	0.40	0.03 ± 0.01	0.08 ± 0.01	0.14 ± 0.02	0.15 ± 0.02
		0.40	0.45	0.01 ± 0.01	0.05 ± 0.01	0.08 ± 0.01	0.10 ± 0.01
		0.45	0.50		0.02 ± 0.01	0.05 ± 0.01	0.06 ± 0.01
1.95	2.15	0.10	0.15	0.51 ± 0.07	0.63 ± 0.07	0.75 ± 0.07	0.73 ± 0.08
		0.15	0.20	0.45 ± 0.04	0.65 ± 0.04	0.72 ± 0.04	0.90 ± 0.04
		0.20	0.25	0.22 ± 0.03	0.36 ± 0.03	0.43 ± 0.03	0.52 ± 0.04
		0.25	0.30	0.11 ± 0.02	0.17 ± 0.02	0.24 ± 0.02	0.24 ± 0.03
		0.30	0.35	0.05 ± 0.01	0.10 ± 0.01	0.14 ± 0.01	0.17 ± 0.01
		0.35	0.40	0.02 ± 0.01	0.05 ± 0.01	0.09 ± 0.01	0.11 ± 0.01
		0.40	0.45	0.01 ± 0.01	0.03 ± 0.01	0.05 ± 0.01	0.06 ± 0.01
		0.45	0.50		0.02 ± 0.01	0.02 ± 0.01	0.04 ± 0.01

TABLE XII. HARP results for the double-differential π^- production cross section in the laboratory system, $d^2\sigma^{\pi^-}/(dpd\theta)$, for p-Sn interactions. Each row refers to a different ($p_{min} \leqslant p < p_{max}$, $\theta_{min} \leqslant \theta < \theta_{max}$) bin, where p and θ are the pion momentum and polar angle, respectively. The central value as well as the square root of the diagonal elements of the covariance matrix are given.

θ_{min} (rad)	θ_{max} (rad)	p_{min} (GeV/c)	p_{max} (GeV/c)	$d^2\sigma^{\pi^-}/(dpd\theta)$ [b/(rad GeV/c)]			
				3 GeV/c	5 GeV/c	8 GeV/c	12 GeV/c
0.35	0.55	0.15	0.20	0.33 ± 0.12	0.74 ± 0.13	1.30 ± 0.19	1.62 ± 0.24
		0.20	0.25	0.39 ± 0.08	0.74 ± 0.09	1.41 ± 0.11	1.75 ± 0.16
		0.25	0.30	0.35 ± 0.06	0.76 ± 0.07	1.36 ± 0.09	1.88 ± 0.12
		0.30	0.35	0.36 ± 0.04	0.78 ± 0.05	1.35 ± 0.07	1.78 ± 0.08
		0.35	0.40	0.25 ± 0.03	0.66 ± 0.04	1.28 ± 0.06	1.65 ± 0.06
		0.40	0.45	0.34 ± 0.04	0.61 ± 0.03	1.16 ± 0.05	1.48 ± 0.05
		0.45	0.50	0.29 ± 0.03	0.56 ± 0.03	1.07 ± 0.04	1.42 ± 0.06
		0.50	0.60	0.23 ± 0.02	0.50 ± 0.03	0.96 ± 0.05	1.34 ± 0.06
		0.60	0.70	0.19 ± 0.03	0.46 ± 0.04	0.86 ± 0.06	1.31 ± 0.09
		0.70	0.80	0.13 ± 0.03	0.36 ± 0.05	0.68 ± 0.08	1.16 ± 0.12
0.55	0.75	0.10	0.15	0.30 ± 0.12	0.58 ± 0.15	1.07 ± 0.22	1.21 ± 0.31
		0.15	0.20	0.38 ± 0.07	0.97 ± 0.10	1.54 ± 0.10	1.67 ± 0.14
		0.20	0.25	0.43 ± 0.06	0.92 ± 0.06	1.35 ± 0.08	1.76 ± 0.13
		0.25	0.30	0.39 ± 0.04	0.78 ± 0.05	1.32 ± 0.08	1.66 ± 0.07
		0.30	0.35	0.32 ± 0.03	0.67 ± 0.04	1.28 ± 0.06	1.53 ± 0.06
		0.35	0.40	0.29 ± 0.03	0.63 ± 0.03	1.09 ± 0.05	1.38 ± 0.06
		0.40	0.45	0.27 ± 0.03	0.59 ± 0.03	1.00 ± 0.04	1.27 ± 0.05
		0.45	0.50	0.23 ± 0.02	0.52 ± 0.03	0.94 ± 0.04	1.15 ± 0.04
		0.50	0.60	0.17 ± 0.02	0.44 ± 0.03	0.77 ± 0.04	1.05 ± 0.05
		0.60	0.70	0.13 ± 0.02	0.37 ± 0.03	0.61 ± 0.05	0.88 ± 0.07
		0.70	0.80	0.10 ± 0.02	0.25 ± 0.04	0.46 ± 0.07	0.75 ± 0.08
0.75	0.95	0.10	0.15	0.30 ± 0.08	0.70 ± 0.11	1.07 ± 0.14	1.18 ± 0.18
		0.15	0.20	0.51 ± 0.07	1.00 ± 0.07	1.55 ± 0.09	1.83 ± 0.12
		0.20	0.25	0.45 ± 0.05	0.79 ± 0.05	1.36 ± 0.07	1.66 ± 0.08
		0.25	0.30	0.37 ± 0.04	0.78 ± 0.05	1.20 ± 0.06	1.51 ± 0.07
		0.30	0.35	0.31 ± 0.03	0.70 ± 0.04	1.05 ± 0.05	1.32 ± 0.05
		0.35	0.40	0.28 ± 0.03	0.56 ± 0.03	0.88 ± 0.04	1.15 ± 0.04
		0.40	0.45	0.20 ± 0.03	0.47 ± 0.02	0.77 ± 0.03	0.97 ± 0.04
		0.45	0.50	0.16 ± 0.02	0.39 ± 0.02	0.63 ± 0.03	0.88 ± 0.04
		0.50	0.60	0.13 ± 0.02	0.32 ± 0.02	0.54 ± 0.03	0.73 ± 0.04
		0.60	0.70	0.09 ± 0.01	0.24 ± 0.03	0.39 ± 0.04	0.56 ± 0.05
0.95	1.15	0.10	0.15	0.43 ± 0.07	0.69 ± 0.09	1.01 ± 0.12	1.16 ± 0.14
		0.15	0.20	0.50 ± 0.05	0.83 ± 0.05	1.30 ± 0.07	1.63 ± 0.09
		0.20	0.25	0.37 ± 0.04	0.75 ± 0.05	1.20 ± 0.07	1.39 ± 0.08
		0.25	0.30	0.32 ± 0.03	0.70 ± 0.04	1.07 ± 0.05	1.23 ± 0.05
		0.30	0.35	0.28 ± 0.03	0.55 ± 0.03	0.80 ± 0.04	1.04 ± 0.05
		0.35	0.40	0.21 ± 0.02	0.42 ± 0.03	0.66 ± 0.03	0.84 ± 0.04
		0.40	0.45	0.13 ± 0.02	0.31 ± 0.02	0.53 ± 0.03	0.69 ± 0.03
		0.45	0.50	0.08 ± 0.01	0.27 ± 0.02	0.44 ± 0.02	0.57 ± 0.03
		0.50	0.60	0.05 ± 0.01	0.21 ± 0.02	0.32 ± 0.02	0.44 ± 0.03
1.15	1.35	0.10	0.15	0.48 ± 0.08	0.68 ± 0.09	1.00 ± 0.12	1.21 ± 0.19
		0.15	0.20	0.37 ± 0.04	0.89 ± 0.06	1.26 ± 0.07	1.59 ± 0.10
		0.20	0.25	0.37 ± 0.04	0.76 ± 0.04	1.00 ± 0.05	1.23 ± 0.06
		0.25	0.30	0.29 ± 0.03	0.56 ± 0.04	0.83 ± 0.05	0.97 ± 0.05
		0.30	0.35	0.19 ± 0.02	0.39 ± 0.03	0.62 ± 0.04	0.76 ± 0.04
		0.35	0.40	0.16 ± 0.02	0.31 ± 0.02	0.48 ± 0.03	0.65 ± 0.03
		0.40	0.45	0.10 ± 0.02	0.24 ± 0.02	0.38 ± 0.02	0.49 ± 0.03
		0.45	0.50	0.07 ± 0.01	0.18 ± 0.02	0.28 ± 0.02	0.36 ± 0.02
1.35	1.55	0.10	0.15	0.45 ± 0.08	0.81 ± 0.13	1.06 ± 0.17	1.45 ± 0.26
		0.15	0.20	0.50 ± 0.05	0.98 ± 0.07	1.33 ± 0.09	1.64 ± 0.11
		0.20	0.25	0.38 ± 0.04	0.68 ± 0.05	0.93 ± 0.06	1.20 ± 0.07

TABLE XII. *(Continued.)*

θ_{min} (rad)	θ_{max} (rad)	p_{min} (GeV/c)	p_{max} (GeV/c)	$d^2\sigma^{\pi^-}/(dpd\theta)$ [b/(rad GeV/c)]			
				3 GeV/c	5 GeV/c	8 GeV/c	12 GeV/c
		0.25	0.30	0.24 ± 0.03	0.48 ± 0.04	0.76 ± 0.05	0.86 ± 0.06
		0.30	0.35	0.18 ± 0.02	0.32 ± 0.02	0.52 ± 0.05	0.60 ± 0.04
		0.35	0.40	0.12 ± 0.02	0.24 ± 0.02	0.34 ± 0.02	0.43 ± 0.03
		0.40	0.45	0.07 ± 0.01	0.15 ± 0.01	0.26 ± 0.02	0.32 ± 0.02
		0.45	0.50	0.04 ± 0.01	0.10 ± 0.01	0.19 ± 0.02	0.24 ± 0.02
1.55	1.75	0.10	0.15	0.46 ± 0.08	0.74 ± 0.11	0.91 ± 0.14	1.37 ± 0.23
		0.15	0.20	0.55 ± 0.05	0.87 ± 0.06	1.28 ± 0.09	1.43 ± 0.10
		0.20	0.25	0.33 ± 0.03	0.56 ± 0.04	0.77 ± 0.06	0.95 ± 0.06
		0.25	0.30	0.17 ± 0.03	0.35 ± 0.03	0.53 ± 0.04	0.64 ± 0.05
		0.30	0.35	0.10 ± 0.01	0.25 ± 0.02	0.37 ± 0.03	0.47 ± 0.04
		0.35	0.40	0.06 ± 0.01	0.16 ± 0.02	0.25 ± 0.02	0.31 ± 0.02
		0.40	0.45	0.04 ± 0.01	0.10 ± 0.01	0.17 ± 0.01	0.22 ± 0.02
		0.45	0.50	0.02 ± 0.01	0.08 ± 0.01	0.12 ± 0.01	0.16 ± 0.01
1.75	1.95	0.10	0.15	0.41 ± 0.05	0.60 ± 0.07	0.81 ± 0.09	0.94 ± 0.12
		0.15	0.20	0.35 ± 0.03	0.58 ± 0.04	0.89 ± 0.04	1.01 ± 0.05
		0.20	0.25	0.22 ± 0.03	0.40 ± 0.03	0.55 ± 0.03	0.62 ± 0.04
		0.25	0.30	0.14 ± 0.02	0.24 ± 0.02	0.36 ± 0.03	0.40 ± 0.03
		0.30	0.35	0.09 ± 0.02	0.16 ± 0.01	0.26 ± 0.02	0.27 ± 0.02
		0.35	0.40	0.06 ± 0.01	0.09 ± 0.01	0.18 ± 0.01	0.18 ± 0.01
		0.40	0.45	0.03 ± 0.01	0.07 ± 0.01	0.12 ± 0.01	0.15 ± 0.01
		0.45	0.50	0.02 ± 0.01	0.05 ± 0.01	0.08 ± 0.01	0.10 ± 0.01
1.95	2.15	0.10	0.15	0.33 ± 0.04	0.58 ± 0.05	0.72 ± 0.05	0.80 ± 0.07
		0.15	0.20	0.32 ± 0.04	0.50 ± 0.04	0.67 ± 0.04	0.73 ± 0.04
		0.20	0.25	0.16 ± 0.02	0.25 ± 0.02	0.39 ± 0.02	0.46 ± 0.02
		0.25	0.30	0.08 ± 0.02	0.15 ± 0.02	0.26 ± 0.02	0.31 ± 0.02
		0.30	0.35	0.04 ± 0.01	0.11 ± 0.01	0.15 ± 0.02	0.19 ± 0.02
		0.35	0.40	0.02 ± 0.01	0.07 ± 0.01	0.10 ± 0.01	0.11 ± 0.01
		0.40	0.45	0.01 ± 0.01	0.04 ± 0.01	0.08 ± 0.01	0.08 ± 0.01
		0.45	0.50		0.03 ± 0.01	0.07 ± 0.01	0.05 ± 0.01

TABLE XIII. HARP results for the double-differential π^+ production cross section in the laboratory system, $d^2\sigma^{\pi^+}/(dpd\theta)$, for p-Ta interactions. Each row refers to a different ($p_{min} \leqslant p < p_{max}$, $\theta_{min} \leqslant \theta < \theta_{max}$) bin, where p and θ are the pion momentum and polar angle, respectively. The central value as well as the square root of the diagonal elements of the covariance matrix are given.

θ_{min} (rad)	θ_{max} (rad)	p_{min} (GeV/c)	p_{max} (GeV/c)	$d^2\sigma^{\pi^+}/(dpd\theta)$ [b/(rad GeV/c)]			
				3 GeV/c	5 GeV/c	8 GeV/c	12 GeV/c
0.35	0.55	0.15	0.20	0.14 ± 0.09	0.60 ± 0.20	1.16 ± 0.30	1.42 ± 0.41
		0.20	0.25	0.39 ± 0.10	0.93 ± 0.15	1.54 ± 0.19	2.06 ± 0.23
		0.25	0.30	0.54 ± 0.06	1.16 ± 0.11	2.00 ± 0.14	2.39 ± 0.18
		0.30	0.35	0.55 ± 0.08	1.27 ± 0.09	2.13 ± 0.16	2.50 ± 0.13
		0.35	0.40	0.69 ± 0.06	1.24 ± 0.08	2.12 ± 0.10	2.72 ± 0.16
		0.40	0.45	0.68 ± 0.06	1.23 ± 0.07	2.03 ± 0.08	2.60 ± 0.10
		0.45	0.50	0.66 ± 0.05	1.22 ± 0.06	2.01 ± 0.13	2.56 ± 0.09
		0.50	0.60	0.55 ± 0.05	1.15 ± 0.06	2.02 ± 0.11	2.42 ± 0.13
		0.60	0.70	0.30 ± 0.06	0.91 ± 0.09	1.78 ± 0.18	2.20 ± 0.21
		0.70	0.80	0.18 ± 0.04	0.57 ± 0.10	1.22 ± 0.20	1.79 ± 0.24
0.55	0.75	0.10	0.15	0.29 ± 0.13	0.73 ± 0.26	0.98 ± 0.37	1.00 ± 0.41
		0.15	0.20	0.51 ± 0.11	0.99 ± 0.16	1.79 ± 0.19	1.91 ± 0.26
		0.20	0.25	0.71 ± 0.08	1.34 ± 0.13	2.10 ± 0.15	2.84 ± 0.21
		0.25	0.30	0.67 ± 0.07	1.35 ± 0.09	2.13 ± 0.13	2.72 ± 0.13

TABLE XIII. (*Continued*).

$\theta_{\min}$ (rad)	$\theta_{\max}$ (rad)	$p_{\min}$ (GeV/c)	$p_{\max}$ (GeV/c)	$d^2\sigma^{\pi^+}/(dpd\theta)$ [b/(rad GeV/c)]			
				3 GeV/c	5 GeV/c	8 GeV/c	12 GeV/c
		0.30	0.35	0.61 ± 0.06	1.30 ± 0.08	2.17 ± 0.09	2.74 ± 0.13
		0.35	0.40	0.67 ± 0.05	1.19 ± 0.06	1.91 ± 0.11	2.64 ± 0.11
		0.40	0.45	0.54 ± 0.05	1.06 ± 0.05	1.87 ± 0.09	2.46 ± 0.09
		0.45	0.50	0.47 ± 0.04	0.96 ± 0.05	1.65 ± 0.09	2.19 ± 0.09
		0.50	0.60	0.28 ± 0.04	0.78 ± 0.06	1.41 ± 0.10	1.82 ± 0.12
		0.60	0.70	0.16 ± 0.03	0.48 ± 0.07	0.95 ± 0.13	1.24 ± 0.14
		0.70	0.80	0.08 ± 0.02	0.30 ± 0.05	0.58 ± 0.11	0.93 ± 0.14
0.75	0.95	0.10	0.15	0.53 ± 0.13	1.05 ± 0.22	1.13 ± 0.30	1.19 ± 0.32
		0.15	0.20	0.75 ± 0.08	1.42 ± 0.11	2.06 ± 0.12	2.31 ± 0.19
		0.20	0.25	0.77 ± 0.06	1.49 ± 0.11	2.15 ± 0.14	2.57 ± 0.14
		0.25	0.30	0.72 ± 0.06	1.31 ± 0.08	1.92 ± 0.09	2.39 ± 0.12
		0.30	0.35	0.61 ± 0.05	1.05 ± 0.06	1.78 ± 0.08	2.16 ± 0.09
		0.35	0.40	0.46 ± 0.04	0.96 ± 0.05	1.53 ± 0.08	1.78 ± 0.08
		0.40	0.45	0.40 ± 0.04	0.82 ± 0.05	1.33 ± 0.06	1.66 ± 0.07
		0.45	0.50	0.31 ± 0.03	0.63 ± 0.04	1.14 ± 0.06	1.45 ± 0.07
		0.50	0.60	0.19 ± 0.03	0.43 ± 0.04	0.82 ± 0.07	1.06 ± 0.08
		0.60	0.70	0.06 ± 0.02	0.25 ± 0.04	0.48 ± 0.07	0.63 ± 0.09
0.95	1.15	0.10	0.15	0.69 ± 0.14	1.08 ± 0.18	1.40 ± 0.27	1.65 ± 0.33
		0.15	0.20	0.81 ± 0.06	1.42 ± 0.10	2.06 ± 0.13	2.53 ± 0.18
		0.20	0.25	0.75 ± 0.06	1.32 ± 0.07	1.98 ± 0.11	2.57 ± 0.11
		0.25	0.30	0.61 ± 0.05	1.06 ± 0.06	1.67 ± 0.08	2.03 ± 0.09
		0.30	0.35	0.40 ± 0.04	0.79 ± 0.05	1.30 ± 0.08	1.66 ± 0.08
		0.35	0.40	0.34 ± 0.03	0.63 ± 0.03	1.02 ± 0.07	1.27 ± 0.07
		0.40	0.45	0.27 ± 0.03	0.49 ± 0.03	0.82 ± 0.05	1.04 ± 0.05
		0.45	0.50	0.17 ± 0.03	0.34 ± 0.03	0.65 ± 0.04	0.81 ± 0.06
		0.50	0.60	0.09 ± 0.02	0.21 ± 0.02	0.38 ± 0.04	0.50 ± 0.05
1.15	1.35	0.10	0.15	0.71 ± 0.15	1.08 ± 0.20	1.64 ± 0.29	2.02 ± 0.39
		0.15	0.20	0.87 ± 0.07	1.35 ± 0.10	2.03 ± 0.17	2.51 ± 0.20
		0.20	0.25	0.68 ± 0.05	1.17 ± 0.07	1.84 ± 0.10	2.19 ± 0.13
		0.25	0.30	0.43 ± 0.04	0.84 ± 0.05	1.29 ± 0.08	1.57 ± 0.10
		0.30	0.35	0.31 ± 0.04	0.65 ± 0.04	0.90 ± 0.06	1.18 ± 0.07
		0.35	0.40	0.22 ± 0.02	0.48 ± 0.03	0.66 ± 0.04	0.94 ± 0.05
		0.40	0.45	0.14 ± 0.02	0.33 ± 0.03	0.49 ± 0.03	0.70 ± 0.04
		0.45	0.50	0.08 ± 0.01	0.23 ± 0.03	0.36 ± 0.03	0.47 ± 0.04
1.35	1.55	0.10	0.15	0.62 ± 0.15	1.15 ± 0.24	1.61 ± 0.35	2.13 ± 0.41
		0.15	0.20	0.86 ± 0.10	1.41 ± 0.13	1.91 ± 0.21	2.47 ± 0.24
		0.20	0.25	0.72 ± 0.06	1.11 ± 0.09	1.64 ± 0.11	1.98 ± 0.13
		0.25	0.30	0.41 ± 0.04	0.67 ± 0.05	1.06 ± 0.07	1.31 ± 0.09
		0.30	0.35	0.26 ± 0.02	0.43 ± 0.03	0.75 ± 0.05	0.83 ± 0.07
		0.35	0.40	0.16 ± 0.02	0.28 ± 0.03	0.50 ± 0.04	0.58 ± 0.04
		0.40	0.45	0.09 ± 0.01	0.18 ± 0.02	0.32 ± 0.03	0.38 ± 0.03
		0.45	0.50	0.05 ± 0.01	0.11 ± 0.01	0.22 ± 0.02	0.25 ± 0.03
1.55	1.75	0.10	0.15	0.68 ± 0.15	1.05 ± 0.22	1.57 ± 0.37	1.85 ± 0.44
		0.15	0.20	0.78 ± 0.08	1.31 ± 0.12	1.69 ± 0.17	2.12 ± 0.21
		0.20	0.25	0.62 ± 0.06	1.00 ± 0.07	1.36 ± 0.09	1.68 ± 0.11
		0.25	0.30	0.33 ± 0.04	0.57 ± 0.05	0.74 ± 0.06	0.97 ± 0.08
		0.30	0.35	0.18 ± 0.02	0.35 ± 0.03	0.48 ± 0.03	0.58 ± 0.06
		0.35	0.40	0.09 ± 0.02	0.19 ± 0.02	0.32 ± 0.03	0.35 ± 0.03
		0.40	0.45	0.05 ± 0.01	0.10 ± 0.01	0.21 ± 0.02	0.22 ± 0.02
		0.45	0.50	0.03 ± 0.01	0.06 ± 0.01	0.14 ± 0.02	0.14 ± 0.02
1.75	1.95	0.10	0.15	0.78 ± 0.12	1.03 ± 0.19	1.28 ± 0.20	1.43 ± 0.25
		0.15	0.20	0.65 ± 0.05	1.09 ± 0.06	1.39 ± 0.08	1.66 ± 0.10
		0.20	0.25	0.44 ± 0.04	0.71 ± 0.05	0.97 ± 0.06	1.08 ± 0.07

TABLE XIII. (*Continued*).

$\theta_{\min}$ (rad)	$\theta_{\max}$ (rad)	$p_{\min}$ (GeV/c)	$p_{\max}$ (GeV/c)	$d^2\sigma^{\pi^+}/(dpd\theta)$ [b/(rad GeV/c)]			
				3 GeV/c	5 GeV/c	8 GeV/c	12 GeV/c
		0.25	0.30	0.20 ± 0.03	0.38 ± 0.04	0.54 ± 0.05	0.66 ± 0.06
		0.30	0.35	0.09 ± 0.01	0.21 ± 0.02	0.32 ± 0.03	0.33 ± 0.03
		0.35	0.40	0.06 ± 0.01	0.12 ± 0.02	0.19 ± 0.02	0.22 ± 0.02
		0.40	0.45	0.06 ± 0.03	0.08 ± 0.01	0.12 ± 0.01	0.16 ± 0.02
		0.45	0.50	0.01 ± 0.01	0.04 ± 0.01	0.07 ± 0.01	0.09 ± 0.02
1.95	2.15	0.10	0.15	0.72 ± 0.12	0.92 ± 0.14	1.04 ± 0.16	1.33 ± 0.21
		0.15	0.20	0.55 ± 0.05	0.80 ± 0.05	1.09 ± 0.05	1.25 ± 0.06
		0.20	0.25	0.28 ± 0.03	0.51 ± 0.03	0.64 ± 0.05	0.76 ± 0.04
		0.25	0.30	0.13 ± 0.02	0.26 ± 0.03	0.34 ± 0.04	0.44 ± 0.05
		0.30	0.35	0.06 ± 0.01	0.13 ± 0.02	0.19 ± 0.02	0.18 ± 0.02
		0.35	0.40	0.03 ± 0.01	0.07 ± 0.01	0.11 ± 0.02	0.11 ± 0.01
		0.40	0.45	0.02 ± 0.01	0.05 ± 0.01	0.05 ± 0.01	0.07 ± 0.01
		0.45	0.50	0.01 ± 0.01	0.02 ± 0.01	0.03 ± 0.01	0.04 ± 0.01

TABLE XIV. HARP results for the double-differential π^- production cross section in the laboratory system, $d^2\sigma^{\pi^-}/(dpd\theta)$, for p-Ta interactions. Each row refers to a different ($p_{\min} \leqslant p < p_{\max}, \theta_{\min} \leqslant \theta < \theta_{\max}$) bin, where p and θ are the pion momentum and polar angle, respectively. The central value as well as the square root of the diagonal elements of the covariance matrix are given.

$\theta_{\min}$ (rad)	$\theta_{\max}$ (rad)	$p_{\min}$ (GeV/c)	$p_{\max}$ (GeV/c)	$d^2\sigma^{\pi^-}/(dpd\theta)$ [b/(rad GeV/c)]			
				3 GeV/c	5 GeV/c	8 GeV/c	12 GeV/c
0.35	0.55	0.15	0.20	0.33 ± 0.12	0.80 ± 0.23	1.31 ± 0.31	1.70 ± 0.41
		0.20	0.25	0.34 ± 0.08	0.89 ± 0.13	1.59 ± 0.16	2.02 ± 0.23
		0.25	0.30	0.41 ± 0.07	1.10 ± 0.12	1.77 ± 0.14	2.26 ± 0.17
		0.30	0.35	0.47 ± 0.05	0.94 ± 0.07	1.88 ± 0.11	2.15 ± 0.10
		0.35	0.40	0.47 ± 0.05	0.88 ± 0.06	1.67 ± 0.08	2.05 ± 0.10
		0.40	0.45	0.38 ± 0.04	0.77 ± 0.04	1.49 ± 0.07	1.83 ± 0.07
		0.45	0.50	0.30 ± 0.03	0.72 ± 0.05	1.42 ± 0.06	1.64 ± 0.08
		0.50	0.60	0.25 ± 0.03	0.74 ± 0.04	1.28 ± 0.07	1.57 ± 0.09
		0.60	0.70	0.22 ± 0.03	0.64 ± 0.05	1.15 ± 0.08	1.47 ± 0.13
		0.70	0.80	0.18 ± 0.03	0.46 ± 0.07	0.92 ± 0.11	1.27 ± 0.15
0.55	0.75	0.10	0.15	0.37 ± 0.16	0.82 ± 0.27	1.18 ± 0.39	1.37 ± 0.45
		0.15	0.20	0.54 ± 0.09	1.27 ± 0.16	1.74 ± 0.18	2.21 ± 0.25
		0.20	0.25	0.46 ± 0.05	1.18 ± 0.09	1.99 ± 0.14	2.48 ± 0.16
		0.25	0.30	0.52 ± 0.06	1.07 ± 0.08	1.91 ± 0.10	2.33 ± 0.09
		0.30	0.35	0.37 ± 0.04	0.97 ± 0.06	1.57 ± 0.08	2.15 ± 0.09
		0.35	0.40	0.30 ± 0.03	0.89 ± 0.05	1.43 ± 0.07	1.89 ± 0.07
		0.40	0.45	0.35 ± 0.05	0.75 ± 0.04	1.33 ± 0.06	1.69 ± 0.06
		0.45	0.50	0.38 ± 0.03	0.65 ± 0.03	1.18 ± 0.05	1.50 ± 0.06
		0.50	0.60	0.25 ± 0.03	0.56 ± 0.03	1.05 ± 0.05	1.31 ± 0.06
		0.60	0.70	0.16 ± 0.02	0.44 ± 0.04	0.84 ± 0.08	1.12 ± 0.10
		0.70	0.80	0.11 ± 0.02	0.33 ± 0.05	0.64 ± 0.08	0.89 ± 0.12
0.75	0.95	0.10	0.15	0.54 ± 0.13	0.99 ± 0.20	1.42 ± 0.32	1.81 ± 0.39
		0.15	0.20	0.71 ± 0.07	1.29 ± 0.10	2.04 ± 0.13	2.32 ± 0.16
		0.20	0.25	0.65 ± 0.06	1.12 ± 0.08	1.87 ± 0.10	2.46 ± 0.16
		0.25	0.30	0.55 ± 0.05	0.99 ± 0.05	1.68 ± 0.08	2.22 ± 0.10
		0.30	0.35	0.38 ± 0.04	0.82 ± 0.05	1.33 ± 0.06	1.90 ± 0.09
		0.35	0.40	0.33 ± 0.03	0.72 ± 0.04	1.22 ± 0.06	1.57 ± 0.07

TABLE XIV. (*Continued*).

θ_{min} (rad)	θ_{max} (rad)	p_{min} (GeV/c)	p_{max} (GeV/c)	$d^2\sigma^{\pi^-}/(dpd\theta)$ [b/(rad GeV/c)]			
				3 GeV/c	5 GeV/c	8 GeV/c	12 GeV/c
		0.40	0.45	0.27 ± 0.03	0.64 ± 0.03	1.01 ± 0.05	1.33 ± 0.05
		0.45	0.50	0.19 ± 0.02	0.57 ± 0.03	0.88 ± 0.04	1.12 ± 0.05
		0.50	0.60	0.14 ± 0.02	0.46 ± 0.03	0.71 ± 0.04	0.92 ± 0.05
		0.60	0.70	0.09 ± 0.01	0.30 ± 0.04	0.56 ± 0.05	0.69 ± 0.07
0.95	1.15	0.10	0.15	0.74 ± 0.12	1.30 ± 0.21	1.86 ± 0.29	2.12 ± 0.36
		0.15	0.20	0.65 ± 0.06	1.39 ± 0.08	2.13 ± 0.13	2.32 ± 0.13
		0.20	0.25	0.55 ± 0.05	1.02 ± 0.07	1.69 ± 0.09	2.11 ± 0.12
		0.25	0.30	0.48 ± 0.04	0.87 ± 0.05	1.42 ± 0.08	1.80 ± 0.08
		0.30	0.35	0.37 ± 0.03	0.69 ± 0.04	1.10 ± 0.06	1.45 ± 0.07
		0.35	0.40	0.29 ± 0.03	0.54 ± 0.03	0.89 ± 0.04	1.13 ± 0.06
		0.40	0.45	0.22 ± 0.02	0.43 ± 0.02	0.75 ± 0.03	0.91 ± 0.05
		0.45	0.50	0.14 ± 0.02	0.35 ± 0.02	0.60 ± 0.03	0.72 ± 0.04
		0.50	0.60	0.08 ± 0.01	0.26 ± 0.02	0.46 ± 0.03	0.53 ± 0.04
1.15	1.35	0.10	0.15	0.86 ± 0.15	1.36 ± 0.23	2.11 ± 0.36	2.66 ± 0.46
		0.15	0.20	0.67 ± 0.06	1.28 ± 0.09	2.07 ± 0.14	2.37 ± 0.17
		0.20	0.25	0.50 ± 0.04	0.96 ± 0.06	1.58 ± 0.09	1.84 ± 0.11
		0.25	0.30	0.36 ± 0.04	0.73 ± 0.05	1.20 ± 0.08	1.44 ± 0.08
		0.30	0.35	0.22 ± 0.02	0.56 ± 0.04	0.85 ± 0.05	1.00 ± 0.06
		0.35	0.40	0.18 ± 0.02	0.43 ± 0.03	0.67 ± 0.04	0.80 ± 0.04
		0.40	0.45	0.12 ± 0.02	0.30 ± 0.02	0.51 ± 0.03	0.68 ± 0.04
		0.45	0.50	0.07 ± 0.01	0.22 ± 0.02	0.41 ± 0.03	0.53 ± 0.04
1.35	1.55	0.10	0.15	0.73 ± 0.15	1.31 ± 0.25	2.37 ± 0.47	3.06 ± 0.66
		0.15	0.20	0.61 ± 0.07	1.14 ± 0.12	1.87 ± 0.18	2.34 ± 0.22
		0.20	0.25	0.42 ± 0.04	0.82 ± 0.07	1.32 ± 0.10	1.74 ± 0.12
		0.25	0.30	0.29 ± 0.03	0.62 ± 0.05	0.90 ± 0.07	1.21 ± 0.08
		0.30	0.35	0.19 ± 0.02	0.42 ± 0.04	0.60 ± 0.04	0.85 ± 0.07
		0.35	0.40	0.12 ± 0.02	0.29 ± 0.02	0.45 ± 0.03	0.61 ± 0.04
		0.40	0.45	0.08 ± 0.01	0.21 ± 0.02	0.34 ± 0.02	0.46 ± 0.03
		0.45	0.50	0.05 ± 0.01	0.14 ± 0.01	0.27 ± 0.02	0.34 ± 0.03
1.55	1.75	0.10	0.15	0.80 ± 0.16	1.34 ± 0.27	1.84 ± 0.38	2.54 ± 0.53
		0.15	0.20	0.56 ± 0.07	1.06 ± 0.10	1.62 ± 0.16	2.10 ± 0.21
		0.20	0.25	0.35 ± 0.04	0.73 ± 0.05	1.11 ± 0.08	1.44 ± 0.10
		0.25	0.30	0.19 ± 0.02	0.49 ± 0.04	0.67 ± 0.05	0.86 ± 0.07
		0.30	0.35	0.13 ± 0.02	0.31 ± 0.03	0.43 ± 0.04	0.61 ± 0.05
		0.35	0.40	0.09 ± 0.01	0.22 ± 0.02	0.30 ± 0.02	0.41 ± 0.03
		0.40	0.45	0.05 ± 0.01	0.14 ± 0.01	0.21 ± 0.01	0.30 ± 0.02
		0.45	0.50	0.04 ± 0.01	0.10 ± 0.01	0.15 ± 0.01	0.21 ± 0.02
1.75	1.95	0.10	0.15	0.79 ± 0.11	1.28 ± 0.20	1.54 ± 0.23	2.07 ± 0.31
		0.15	0.20	0.48 ± 0.05	0.95 ± 0.06	1.27 ± 0.08	1.58 ± 0.11
		0.20	0.25	0.25 ± 0.03	0.53 ± 0.04	0.81 ± 0.05	0.99 ± 0.07
		0.25	0.30	0.14 ± 0.02	0.32 ± 0.03	0.51 ± 0.04	0.58 ± 0.04
		0.30	0.35	0.11 ± 0.02	0.22 ± 0.02	0.28 ± 0.03	0.41 ± 0.03
		0.35	0.40	0.08 ± 0.01	0.14 ± 0.02	0.21 ± 0.01	0.26 ± 0.02
		0.40	0.45	0.05 ± 0.01	0.09 ± 0.01	0.18 ± 0.01	0.20 ± 0.02
		0.45	0.50	0.03 ± 0.01	0.06 ± 0.01	0.12 ± 0.01	0.12 ± 0.01
1.95	2.15	0.10	0.15	0.59 ± 0.11	1.12 ± 0.16	1.43 ± 0.17	1.85 ± 0.29
		0.15	0.20	0.50 ± 0.05	0.80 ± 0.06	0.99 ± 0.05	1.24 ± 0.07
		0.20	0.25	0.21 ± 0.03	0.39 ± 0.03	0.57 ± 0.03	0.73 ± 0.05
		0.25	0.30	0.09 ± 0.02	0.23 ± 0.02	0.36 ± 0.03	0.42 ± 0.04
		0.30	0.35	0.04 ± 0.01	0.14 ± 0.02	0.19 ± 0.02	0.25 ± 0.02
		0.35	0.40	0.03 ± 0.01	0.09 ± 0.01	0.15 ± 0.01	0.15 ± 0.02
		0.40	0.45	0.02 ± 0.01	0.05 ± 0.01	0.11 ± 0.01	0.11 ± 0.01
		0.45	0.50	0.02 ± 0.01	0.03 ± 0.01	0.07 ± 0.01	0.09 ± 0.01

TABLE XV. HARP results for the double-differential π^+ production cross section in the laboratory system, $d^2\sigma^{\pi^+}/(dpd\theta)$, for p-Pb interactions. Each row refers to a different ($p_{min} \leqslant p < p_{max}, \theta_{min} \leqslant \theta < \theta_{max}$) bin, where p and θ are the pion momentum and polar angle, respectively. The central value as well as the square root of the diagonal elements of the covariance matrix are given.

θ_{min} (rad)	θ_{max} (rad)	p_{min} (GeV/c)	p_{max} (GeV/c)	$d^2\sigma^{\pi^+}/(dpd\theta)$ [b/(rad GeV/c)]			
				3 GeV/c	5 GeV/c	8 GeV/c	12 GeV/c
0.35	0.55	0.15	0.20	0.31 ± 0.11	0.85 ± 0.22	1.15 ± 0.32	1.38 ± 0.41
		0.20	0.25	0.29 ± 0.08	0.87 ± 0.15	1.75 ± 0.20	2.04 ± 0.26
		0.25	0.30	0.49 ± 0.10	1.18 ± 0.13	2.13 ± 0.15	2.66 ± 0.25
		0.30	0.35	0.76 ± 0.08	1.27 ± 0.11	2.19 ± 0.13	2.61 ± 0.17
		0.35	0.40	0.67 ± 0.07	1.34 ± 0.09	2.21 ± 0.10	2.84 ± 0.18
		0.40	0.45	0.76 ± 0.07	1.38 ± 0.10	2.20 ± 0.09	2.53 ± 0.13
		0.45	0.50	0.65 ± 0.06	1.42 ± 0.08	1.99 ± 0.08	2.40 ± 0.12
		0.50	0.60	0.48 ± 0.06	1.27 ± 0.08	1.96 ± 0.09	2.53 ± 0.16
		0.60	0.70	0.26 ± 0.04	0.99 ± 0.10	1.71 ± 0.16	2.19 ± 0.22
		0.70	0.80	0.18 ± 0.03	0.67 ± 0.12	1.12 ± 0.18	1.76 ± 0.23
0.55	0.75	0.10	0.15	0.35 ± 0.15	0.69 ± 0.25	0.84 ± 0.35	1.02 ± 0.46
		0.15	0.20	0.56 ± 0.09	1.31 ± 0.17	1.75 ± 0.22	2.19 ± 0.29
		0.20	0.25	0.70 ± 0.09	1.46 ± 0.11	2.31 ± 0.15	2.87 ± 0.22
		0.25	0.30	0.73 ± 0.07	1.46 ± 0.11	2.21 ± 0.13	3.13 ± 0.20
		0.30	0.35	0.60 ± 0.05	1.31 ± 0.09	2.16 ± 0.12	2.79 ± 0.14
		0.35	0.40	0.61 ± 0.07	1.08 ± 0.08	2.07 ± 0.11	2.65 ± 0.13
		0.40	0.45	0.62 ± 0.06	1.16 ± 0.09	1.87 ± 0.08	2.58 ± 0.14
		0.45	0.50	0.44 ± 0.05	1.17 ± 0.07	1.63 ± 0.08	2.41 ± 0.12
		0.50	0.60	0.31 ± 0.04	0.86 ± 0.08	1.33 ± 0.08	1.96 ± 0.14
		0.60	0.70	0.18 ± 0.03	0.48 ± 0.08	0.93 ± 0.11	1.39 ± 0.14
		0.70	0.80	0.10 ± 0.02	0.27 ± 0.06	0.59 ± 0.11	0.98 ± 0.16
0.75	0.95	0.10	0.15	0.52 ± 0.13	0.83 ± 0.21	1.20 ± 0.31	1.29 ± 0.39
		0.15	0.20	0.87 ± 0.09	1.54 ± 0.14	2.25 ± 0.14	2.78 ± 0.20
		0.20	0.25	0.86 ± 0.08	1.40 ± 0.10	2.25 ± 0.14	2.91 ± 0.19
		0.25	0.30	0.67 ± 0.06	1.20 ± 0.12	1.98 ± 0.11	2.69 ± 0.15
		0.30	0.35	0.59 ± 0.05	1.14 ± 0.07	1.83 ± 0.08	2.39 ± 0.13
		0.35	0.40	0.47 ± 0.05	0.97 ± 0.06	1.65 ± 0.07	2.06 ± 0.11
		0.40	0.45	0.37 ± 0.04	0.79 ± 0.05	1.38 ± 0.06	1.92 ± 0.10
		0.45	0.50	0.29 ± 0.03	0.66 ± 0.04	1.17 ± 0.05	1.61 ± 0.10
		0.50	0.60	0.19 ± 0.03	0.44 ± 0.05	0.81 ± 0.07	1.10 ± 0.10
		0.60	0.70	0.11 ± 0.02	0.25 ± 0.04	0.47 ± 0.07	0.70 ± 0.09
0.95	1.15	0.10	0.15	0.55 ± 0.13	1.02 ± 0.20	1.40 ± 0.25	1.55 ± 0.36
		0.15	0.20	0.92 ± 0.08	1.56 ± 0.11	2.31 ± 0.17	3.00 ± 0.20
		0.20	0.25	0.68 ± 0.07	1.43 ± 0.09	2.01 ± 0.13	2.68 ± 0.16
		0.25	0.30	0.71 ± 0.07	1.12 ± 0.10	1.56 ± 0.10	2.07 ± 0.13
		0.30	0.35	0.48 ± 0.05	0.84 ± 0.07	1.31 ± 0.09	1.74 ± 0.11
		0.35	0.40	0.32 ± 0.04	0.72 ± 0.05	1.07 ± 0.06	1.62 ± 0.10
		0.40	0.45	0.25 ± 0.03	0.55 ± 0.04	0.85 ± 0.05	1.33 ± 0.08
		0.45	0.50	0.16 ± 0.02	0.45 ± 0.04	0.65 ± 0.04	0.96 ± 0.08
		0.50	0.60	0.09 ± 0.02	0.24 ± 0.03	0.44 ± 0.05	0.59 ± 0.07
1.15	1.35	0.10	0.15	0.67 ± 0.14	1.27 ± 0.21	1.68 ± 0.28	1.75 ± 0.35
		0.15	0.20	0.90 ± 0.08	1.49 ± 0.10	2.32 ± 0.15	2.88 ± 0.23
		0.20	0.25	0.64 ± 0.06	1.17 ± 0.08	1.96 ± 0.10	2.53 ± 0.15
		0.25	0.30	0.51 ± 0.05	0.92 ± 0.06	1.32 ± 0.07	1.87 ± 0.13
		0.30	0.35	0.32 ± 0.04	0.64 ± 0.05	0.91 ± 0.07	1.27 ± 0.09
		0.35	0.40	0.21 ± 0.03	0.45 ± 0.04	0.74 ± 0.04	0.89 ± 0.06
		0.40	0.45	0.15 ± 0.02	0.32 ± 0.03	0.55 ± 0.04	0.65 ± 0.05
		0.45	0.50	0.10 ± 0.02	0.22 ± 0.03	0.37 ± 0.03	0.43 ± 0.05

TABLE XV. (*Continued*).

θ_{min} (rad)	θ_{max} (rad)	p_{min} (GeV/c)	p_{max} (GeV/c)	$d^2\sigma^{\pi^+}/(dpd\theta)$ [b/(rad GeV/c)]			
				3 GeV/c	5 GeV/c	8 GeV/c	12 GeV/c
1.35	1.55	0.10	0.15	0.79 ± 0.15	1.39 ± 0.27	1.74 ± 0.35	1.83 ± 0.40
		0.15	0.20	0.90 ± 0.08	1.46 ± 0.11	2.08 ± 0.17	2.51 ± 0.20
		0.20	0.25	0.72 ± 0.06	1.02 ± 0.07	1.68 ± 0.09	2.01 ± 0.14
		0.25	0.30	0.36 ± 0.05	0.66 ± 0.05	1.01 ± 0.06	1.53 ± 0.11
		0.30	0.35	0.21 ± 0.03	0.47 ± 0.05	0.71 ± 0.05	0.89 ± 0.08
		0.35	0.40	0.13 ± 0.02	0.32 ± 0.03	0.53 ± 0.04	0.63 ± 0.06
		0.40	0.45	0.07 ± 0.01	0.21 ± 0.02	0.40 ± 0.03	0.43 ± 0.04
		0.45	0.50	0.05 ± 0.01	0.14 ± 0.02	0.23 ± 0.03	0.27 ± 0.03
1.55	1.75	0.10	0.15	0.80 ± 0.17	1.21 ± 0.23	1.62 ± 0.32	1.93 ± 0.42
		0.15	0.20	0.73 ± 0.07	1.38 ± 0.11	1.83 ± 0.12	2.28 ± 0.16
		0.20	0.25	0.52 ± 0.05	0.96 ± 0.07	1.38 ± 0.09	1.71 ± 0.12
		0.25	0.30	0.29 ± 0.04	0.56 ± 0.05	0.81 ± 0.05	1.00 ± 0.09
		0.30	0.35	0.17 ± 0.02	0.38 ± 0.04	0.54 ± 0.04	0.65 ± 0.06
		0.35	0.40	0.11 ± 0.02	0.25 ± 0.02	0.37 ± 0.03	0.46 ± 0.04
		0.40	0.45	0.06 ± 0.01	0.16 ± 0.02	0.23 ± 0.02	0.31 ± 0.04
		0.45	0.50	0.04 ± 0.01	0.11 ± 0.01	0.15 ± 0.02	0.18 ± 0.03
1.75	1.95	0.10	0.15	0.81 ± 0.13	1.02 ± 0.17	1.47 ± 0.21	1.64 ± 0.28
		0.15	0.20	0.67 ± 0.06	1.23 ± 0.08	1.60 ± 0.08	1.97 ± 0.12
		0.20	0.25	0.36 ± 0.04	0.75 ± 0.07	1.03 ± 0.07	1.29 ± 0.10
		0.25	0.30	0.16 ± 0.03	0.36 ± 0.04	0.56 ± 0.04	0.62 ± 0.07
		0.30	0.35	0.09 ± 0.02	0.22 ± 0.03	0.32 ± 0.03	0.40 ± 0.04
		0.35	0.40	0.07 ± 0.02	0.14 ± 0.02	0.20 ± 0.02	0.21 ± 0.03
		0.40	0.45	0.04 ± 0.01	0.09 ± 0.01	0.13 ± 0.02	0.12 ± 0.02
		0.45	0.50	0.02 ± 0.01	0.06 ± 0.01	0.06 ± 0.01	0.07 ± 0.01
1.95	2.15	0.10	0.15	0.88 ± 0.13	0.81 ± 0.12	1.13 ± 0.17	1.41 ± 0.22
		0.15	0.20	0.64 ± 0.06	0.93 ± 0.06	1.19 ± 0.06	1.40 ± 0.11
		0.20	0.25	0.36 ± 0.05	0.56 ± 0.05	0.74 ± 0.06	1.04 ± 0.09
		0.25	0.30	0.15 ± 0.03	0.25 ± 0.05	0.39 ± 0.04	0.44 ± 0.06
		0.30	0.35	0.07 ± 0.02	0.13 ± 0.02	0.19 ± 0.02	0.24 ± 0.03
		0.35	0.40	0.03 ± 0.01	0.10 ± 0.01	0.11 ± 0.01	0.16 ± 0.02
		0.40	0.45	0.02 ± 0.01	0.06 ± 0.01	0.06 ± 0.01	0.09 ± 0.02
		0.45	0.50	0.02 ± 0.01	0.03 ± 0.01	0.04 ± 0.01	0.06 ± 0.02

TABLE XVI. HARP results for the double-differential π^- production cross section in the laboratory system, $d^2\sigma^{\pi^-}/(dpd\theta)$, for p-Pb interactions. Each row refers to a different ($p_{min} \leqslant p < p_{max}$, $\theta_{min} \leqslant \theta < \theta_{max}$) bin, where p and θ are the pion momentum and polar angle, respectively. The central value as well as the square root of the diagonal elements of the covariance matrix are given.

θ_{min} (rad)	θ_{max} (rad)	p_{min} (GeV/c)	p_{max} (GeV/c)	$d^2\sigma^{\pi^-}/(dpd\theta)$ [b/(rad GeV/c)]			
				3 GeV/c	5 GeV/c	8 GeV/c	12 GeV/c
0.35	0.55	0.15	0.20	0.20 ± 0.10	0.72 ± 0.24	1.47 ± 0.32	1.90 ± 0.46
		0.20	0.25	0.33 ± 0.09	0.78 ± 0.16	1.85 ± 0.21	2.36 ± 0.26
		0.25	0.30	0.37 ± 0.06	0.94 ± 0.10	2.02 ± 0.12	2.67 ± 0.23
		0.30	0.35	0.34 ± 0.05	1.01 ± 0.11	1.87 ± 0.10	2.40 ± 0.14
		0.35	0.40	0.39 ± 0.05	1.07 ± 0.07	1.67 ± 0.08	2.04 ± 0.12
		0.40	0.45	0.34 ± 0.04	0.80 ± 0.06	1.58 ± 0.07	1.74 ± 0.09
		0.45	0.50	0.35 ± 0.04	0.72 ± 0.05	1.42 ± 0.06	1.66 ± 0.12
		0.50	0.60	0.30 ± 0.04	0.75 ± 0.05	1.34 ± 0.06	1.58 ± 0.11

TABLE XVI. (*Continued*).

$\theta_{\min}$ (rad)	$\theta_{\max}$ (rad)	$p_{\min}$ (GeV/c)	$p_{\max}$ (GeV/c)	$d^2\sigma^{\pi^-}/(dpd\theta)$ [b/(rad GeV/c)]			
				3 GeV/c	5 GeV/c	8 GeV/c	12 GeV/c
		0.60	0.70	0.18 ± 0.03	0.67 ± 0.07	1.22 ± 0.09	1.45 ± 0.13
		0.70	0.80	0.15 ± 0.03	0.46 ± 0.08	1.03 ± 0.11	1.51 ± 0.17
0.55	0.75	0.10	0.15	0.43 ± 0.15	0.93 ± 0.32	1.26 ± 0.41	1.72 ± 0.54
		0.15	0.20	0.39 ± 0.09	1.37 ± 0.16	1.91 ± 0.20	2.38 ± 0.30
		0.20	0.25	0.49 ± 0.08	1.19 ± 0.10	2.14 ± 0.13	2.36 ± 0.15
		0.25	0.30	0.53 ± 0.06	1.20 ± 0.08	2.06 ± 0.11	2.55 ± 0.21
		0.30	0.35	0.44 ± 0.05	1.00 ± 0.08	1.87 ± 0.10	2.26 ± 0.11
		0.35	0.40	0.42 ± 0.05	1.02 ± 0.07	1.52 ± 0.08	2.01 ± 0.10
		0.40	0.45	0.32 ± 0.04	0.84 ± 0.06	1.33 ± 0.06	1.81 ± 0.09
		0.45	0.50	0.30 ± 0.03	0.68 ± 0.05	1.25 ± 0.06	1.57 ± 0.08
		0.50	0.60	0.25 ± 0.03	0.58 ± 0.04	1.10 ± 0.05	1.42 ± 0.08
		0.60	0.70	0.16 ± 0.03	0.47 ± 0.05	0.88 ± 0.07	1.17 ± 0.10
		0.70	0.80	0.10 ± 0.02	0.35 ± 0.06	0.67 ± 0.08	0.92 ± 0.12
0.75	0.95	0.10	0.15	0.64 ± 0.14	1.19 ± 0.23	1.77 ± 0.36	1.78 ± 0.40
		0.15	0.20	0.62 ± 0.07	1.45 ± 0.10	2.24 ± 0.13	2.83 ± 0.24
		0.20	0.25	0.55 ± 0.07	1.15 ± 0.08	2.07 ± 0.10	2.69 ± 0.15
		0.25	0.30	0.47 ± 0.05	1.11 ± 0.09	1.79 ± 0.09	2.20 ± 0.15
		0.30	0.35	0.35 ± 0.04	0.98 ± 0.07	1.52 ± 0.07	2.14 ± 0.11
		0.35	0.40	0.34 ± 0.04	0.76 ± 0.05	1.21 ± 0.06	1.74 ± 0.09
		0.40	0.45	0.23 ± 0.03	0.59 ± 0.05	1.08 ± 0.05	1.48 ± 0.08
		0.45	0.50	0.19 ± 0.02	0.47 ± 0.03	0.93 ± 0.04	1.27 ± 0.07
		0.50	0.60	0.16 ± 0.02	0.40 ± 0.03	0.76 ± 0.04	0.99 ± 0.07
		0.60	0.70	0.11 ± 0.02	0.32 ± 0.03	0.59 ± 0.06	0.70 ± 0.09
0.95	1.15	0.10	0.15	0.62 ± 0.12	1.40 ± 0.22	2.14 ± 0.32	2.43 ± 0.39
		0.15	0.20	0.70 ± 0.07	1.46 ± 0.11	2.29 ± 0.13	3.02 ± 0.20
		0.20	0.25	0.56 ± 0.06	1.09 ± 0.08	1.85 ± 0.10	2.66 ± 0.16
		0.25	0.30	0.40 ± 0.04	0.96 ± 0.08	1.49 ± 0.07	2.10 ± 0.12
		0.30	0.35	0.30 ± 0.03	0.83 ± 0.06	1.15 ± 0.06	1.73 ± 0.10
		0.35	0.40	0.29 ± 0.03	0.63 ± 0.05	0.96 ± 0.05	1.38 ± 0.08
		0.40	0.45	0.28 ± 0.03	0.47 ± 0.04	0.78 ± 0.04	1.06 ± 0.07
		0.45	0.50	0.20 ± 0.03	0.36 ± 0.03	0.66 ± 0.03	0.81 ± 0.06
		0.50	0.60	0.10 ± 0.02	0.25 ± 0.02	0.50 ± 0.03	0.60 ± 0.04
1.15	1.35	0.10	0.15	0.63 ± 0.12	1.51 ± 0.24	2.39 ± 0.37	3.18 ± 0.51
		0.15	0.20	0.68 ± 0.07	1.47 ± 0.09	2.20 ± 0.15	2.97 ± 0.21
		0.20	0.25	0.54 ± 0.05	1.01 ± 0.08	1.70 ± 0.10	2.28 ± 0.14
		0.25	0.30	0.33 ± 0.04	0.77 ± 0.06	1.25 ± 0.07	1.61 ± 0.11
		0.30	0.35	0.21 ± 0.03	0.58 ± 0.05	0.94 ± 0.06	1.12 ± 0.08
		0.35	0.40	0.15 ± 0.02	0.42 ± 0.03	0.70 ± 0.04	0.89 ± 0.05
		0.40	0.45	0.13 ± 0.02	0.33 ± 0.03	0.55 ± 0.03	0.74 ± 0.05
		0.45	0.50	0.09 ± 0.02	0.27 ± 0.02	0.45 ± 0.03	0.60 ± 0.05
1.35	1.55	0.10	0.15	0.95 ± 0.20	1.51 ± 0.27	2.36 ± 0.46	3.78 ± 0.67
		0.15	0.20	0.68 ± 0.06	1.29 ± 0.10	2.09 ± 0.13	2.84 ± 0.18
		0.20	0.25	0.44 ± 0.05	0.89 ± 0.07	1.50 ± 0.09	1.89 ± 0.13
		0.25	0.30	0.27 ± 0.04	0.54 ± 0.05	1.03 ± 0.07	1.27 ± 0.09
		0.30	0.35	0.15 ± 0.02	0.37 ± 0.03	0.68 ± 0.05	0.89 ± 0.07
		0.35	0.40	0.15 ± 0.02	0.30 ± 0.02	0.50 ± 0.03	0.72 ± 0.05
		0.40	0.45	0.09 ± 0.02	0.25 ± 0.02	0.37 ± 0.03	0.57 ± 0.05
		0.45	0.50	0.05 ± 0.01	0.19 ± 0.02	0.26 ± 0.02	0.40 ± 0.04
1.55	1.75	0.10	0.15	1.05 ± 0.16	1.36 ± 0.25	2.14 ± 0.39	3.43 ± 0.65
		0.15	0.20	0.57 ± 0.06	1.17 ± 0.09	1.78 ± 0.10	2.48 ± 0.15
		0.20	0.25	0.41 ± 0.05	0.75 ± 0.06	1.13 ± 0.07	1.38 ± 0.10

TABLE XVI. (*Continued*).

θ_{min} (rad)	θ_{max} (rad)	p_{min} (GeV/c)	p_{max} (GeV/c)	$d^2\sigma^{\pi^-}/(dpd\theta)$ [b/(rad GeV/c)]			
				3 GeV/c	5 GeV/c	8 GeV/c	12 GeV/c
		0.25	0.30	0.28 ± 0.04	0.44 ± 0.04	0.81 ± 0.06	0.93 ± 0.07
		0.30	0.35	0.14 ± 0.03	0.34 ± 0.03	0.51 ± 0.04	0.67 ± 0.05
		0.35	0.40	0.09 ± 0.01	0.24 ± 0.03	0.35 ± 0.03	0.48 ± 0.04
		0.40	0.45	0.07 ± 0.01	0.15 ± 0.02	0.25 ± 0.02	0.33 ± 0.03
		0.45	0.50	0.05 ± 0.01	0.10 ± 0.01	0.19 ± 0.01	0.23 ± 0.03
1.75	1.95	0.10	0.15	0.85 ± 0.13	1.19 ± 0.19	1.78 ± 0.25	2.61 ± 0.45
		0.15	0.20	0.48 ± 0.05	1.06 ± 0.06	1.42 ± 0.07	1.89 ± 0.12
		0.20	0.25	0.32 ± 0.04	0.64 ± 0.06	0.83 ± 0.05	1.15 ± 0.08
		0.25	0.30	0.18 ± 0.03	0.30 ± 0.03	0.56 ± 0.04	0.67 ± 0.06
		0.30	0.35	0.09 ± 0.02	0.23 ± 0.02	0.33 ± 0.03	0.39 ± 0.05
		0.35	0.40	0.09 ± 0.02	0.17 ± 0.02	0.24 ± 0.01	0.28 ± 0.03
		0.40	0.45	0.06 ± 0.02	0.12 ± 0.02	0.20 ± 0.01	0.23 ± 0.02
		0.45	0.50	0.03 ± 0.01	0.08 ± 0.01	0.14 ± 0.01	0.17 ± 0.02
1.95	2.15	0.10	0.15	0.74 ± 0.13	0.97 ± 0.17	1.56 ± 0.21	2.02 ± 0.31
		0.15	0.20	0.44 ± 0.05	0.74 ± 0.05	1.16 ± 0.05	1.37 ± 0.09
		0.20	0.25	0.18 ± 0.03	0.40 ± 0.05	0.65 ± 0.04	0.93 ± 0.08
		0.25	0.30	0.10 ± 0.02	0.23 ± 0.03	0.39 ± 0.03	0.53 ± 0.06
		0.30	0.35	0.07 ± 0.02	0.14 ± 0.03	0.22 ± 0.03	0.30 ± 0.04
		0.35	0.40	0.03 ± 0.01	0.08 ± 0.01	0.14 ± 0.01	0.23 ± 0.03
		0.40	0.45	0.02 ± 0.01	0.09 ± 0.01	0.10 ± 0.01	0.15 ± 0.02
		0.45	0.50	0.01 ± 0.01	0.08 ± 0.01	0.08 ± 0.01	0.09 ± 0.02

[1] M. G. Catanesi *et al.* (HARP Collaboration), CERN-SPSC/99-35, 1999.

[2] G. Ambrosini *et al.*, (NA56 Collaboration), Eur. Phys. J. C **10**, 605 (1999); G. Ambrosini *et al.* (NA56 Collaboration), Phys. Lett. **B420**, 225 (1998); G. Ambrosini *et al.* (NA56 Collaboration), Phys. Lett. **B425**, 208 (1998).

[3] H. W. Atherton *et al.*, CERN 80-07, August 1980.

[4] A. Blondel *et al.* CERN-2004-002, ECFA/04/230; M. M. Alsharoa *et al.*, Phys. Rev. ST Accel. Beams **6**, 081001 (2003).

[5] G. Battistoni, Nucl. Phys. B, Proc. Suppl. **100**, 101 (2001).

[6] T. Stanev, AIP Conf. Proc, **516**, 247 (2000).

[7] T. K. Gaisser, Nucl. Phys. B, Proc. Suppl. **87**, 145 (2000).

[8] R. Engel, T. K. Gaisser, and T. Stanev, Phys. Lett. **B472**, 113 (2000).

[9] M. Honda, Nucl. Phys. **B77**, 140 (1999).

[10] M. Bonesini and A. Guglielmi, Phys. Rep. **433**, 66 (2006).

[11] M. H. Ahn *et al.* (K2K Collaboration), Phys. Rev. Lett. **90**, 041801 (2003).

[12] M. H. Ahn *et al.* (K2K Collaboration), Phys. Rev. D **74**, 072003 (2006).

[13] A. A. Aguilar-Arevalo *et al.*, Phys. Rev. Lett. **98**, 231801 (2007).

[14] A. A. Aguilar-Arevalo *et al.* (SciBooNE Collaboration), FERMILAB-PROPOSAL-0954, 2006, arXiv:hep-ex/0601022.

[15] M. G. Catanesi *et al.* (HARP Collaboration), Eur. Phys. J. C **51**, 787 (2007).

[16] M. G. Catanesi *et al.* (HARP Collaboration), Eur. Phys. J. C **53**, 177 (2008).

[17] M. G. Catanesi *et al.* (HARP Collaboration), Eur. Phys. J. C **54**, 37 (2008).

[18] M. G. Catanesi *et al.* (HARP Collaboration), 2008 JINST 3 P04007.

[19] M. G. Catanesi *et al.* (HARP Collaboration), Nucl. Phys. **B732**, 1 (2006).

[20] M. G. Catanesi *et al.* (HARP Collaboration), Astr. Phys. **29**, 257 (2008).

[21] M. G. Catanesi *et al.* (HARP Collaboration), Eur. Phys. J. C **52**, 29 (2007).

[22] M. G. Catanesi *et al.* (HARP Collaboration), Nucl. Instrum. Methods A **571**, 527 (2007); **571**, 564 (2007).

[23] M. Anfreville *et al.*, Nucl. Instrum. Methods A **481**, 339 (2002).

[24] M. Baldo-Ceolin *et al.*, Nucl. Instrum. Methods A **532**, 548 (2004); M. Bonesini *et al.*, IEEE Trans. Nucl. Sci. **50**, 1053 (2003).

[25] E. Radicioni, IEEE Trans. Nucl. Sci. **52**, 2986 (2005).

[26] M. Bogomilov *et al.*, Nucl. Instrum. Methods A **508**, 152 (2003); G. Barr *et al.*, *ibid.* **533**, 214 (2004); M. Bogomilov *et al.*, IEEE Trans. Nucl. Sci. **54**, 342 (2007).

[27] L. Durieu, A. Mueller, and M. Martini, PAC-2001-TPAH142, presented at IEEE Particle Accelerator Conference (PAC2001), Chicago, Illinois, 18–22 Jun 2001; L. Durieu *et al.*, Proceedings of PAC'97, Vancouver (1997); L. Durieu and O. Fernando, CERN PS/PA Note 96-38.

[28] G. D'Agostini, Nucl. Instrum. Methods A **362**, 487 (1995).

[29] S. Agostinelli *et al.* (GEANT4 Collaboration), Nucl. Instrum. Methods A **506**, 250 (2003).

[30] I. Chemakin *et al.* (E910 Collaboration), Phys. Rev. C **65**, 024904 (2002).

[31] K. Long, Nucl. Phys. B, Proc. Suppl. **154**, 111 (2006); ISS/2005/01, http://www.hep.ph.ic.ac.uk/iss/issnotes/ISS_Doc1_v02_13-7-2005.pdf.

[32] R. C. Fernow and J. Gallardo (private communication); S. J. Brooks (private communication).

[33] S. J. Brooks and K. A. Walaron, Nucl. Phys. B, Proc. Suppl. **155**, 295 (2006).

[34] N. V. Mokhov and S. I. Striganov, FERMILAB-CONF-07-008-AD, 2007.

[35] D. H. Wright *et al.*, AIP Conf. Proc. **896**, 11 (2007).

[36] A. Heikkinen *et al.*, e-print physics/0306008.

[37] G. Folger, V. Ivanchenko, and H. P. Wellisch, Eur. Phys. J. A **21**, 407 (2004).

[38] H. W. Bertini and P. Guthrie, Nucl. Phys. **A169**, (1971).

[39] G. Folger and H. P. Wellisch, e-print physics/0306007.

[40] H. Fesefeld, Technical Report PITHA 85-02, Aachen, 1985.

[41] D. H. Wright *et al.*, AIP Conf. Proc. **867**, 479 (2006).

[42] S. G. Mashnik *et al.*, LANL Report LA-UR-05-7321, 2005.